UNIVERSITÀ DEGLI STUDI DI MILANO

Dipartimento di

Scienze Agrarie e Ambientali - Produzione, Territorio e Agroenergia

Ph.D. in Agriculture, Environment and Bioenergy – XXX cycle

FUNCTIONAL ANALYSIS OF MAIZE GENES INVOLVED IN SEEDLING DEVELOPMENT AND IN PLANT – ENVIRONMENT INTERACTION

SUPERVISOR. Prof. Gabriella Consonni

CO-SUPERVISOR. Dott. Fabio Francesco Nocito

Massimo Zilio

MATRICOLA R10855

INDEX

ABSTRACT

Maize is one of the most important cultivated plants on a world scale, with a total production which exceeds one billion tonnes per year (FAOSTAT 2017). It is an important human food source in many parts of the world, but is also intensely exploited for biofuel and feed production. Furthermore, maize is also a model plant for research studies in the field of biology and genetics. For these reasons, maize is one of the most intensively studied crops, with the aim of improving its productivity, which in the USA has increased nearly five times since the 1940s. This dramatic yield improvement is due to the development and widespread use of new farming technologies. An important role was played by genetic improvement, with the use of highly productive maize hybrids and, more recently, biotechnology.

However, the increases in annual productivity of maize and the other main crops exploited for food production seem to have reached a stall phase in recent years.

It has been estimated that the world population will increase from 7.5 to 9.7 billion people by 2050. To meet the food needs of the increasing population, and to satisfy diets that will include more meat, according to the Food and Agricultural Organization (FAO), worldwide crop production will have to increase by 70%. It is a tough task, made even more difficult by the fact that the worldwide area of cultivable soil is decreasing as a consequence of increasing urbanization and climate change.

To reach the target, new strategies are required, which will include multiple and integrated approaches, among them genetic improvement. One of the main challenges will be to develop new plant ideotypes that will combine the capability to tolerate biotic and abiotic stress with no reduction in yield.

Within this perspective, the work carried out in this thesis project was aimed at understanding the molecular mechanisms involved in plant response to environmental factors.

The work was organized in two parts, which are presented here in two different chapters. Both chapters are focused on genes that control plant development as well as plant-environment interactions.

The first chapter deals with the study of the genetic regulation of cuticle deposition in maize. The cuticle is an important plant organ and constitutes the first barrier against many environmental stresses, including water deprivation and pathogen interaction. The cuticle is produced by epidermal cells and is composed of a complex array of long chain hydrocarbons, constantly deposed on the aerial surface for all the plant's life.

To investigate the cuticle biosynthesis process in maize, our strategy was based on the functional characterization of *ZmMYB94*, also known as *fused leaves 1* (*fdl1*). This gene encodes a transcription factor of the R2R3-MYB subfamily, expressed in embryo, seedling and silk tissues. A mutant in this gene, referred to as *fdl1-1,* was available for this study. It originated from the insertion of an *Enhancer*/*Suppressor* (*En*/*Spm*) element in the third exon of the *ZmMYB94* gene. The mutation has a pleiotropic effect on seedling development. The main features of *fdl1-1* mutant plants are irregular coleoptile opening and the presence of regions of adhesion between the coleoptile and the first leaf and between the first and second leaves.

Deeper studies of the *fdl1-1* mutant, performed by electron microscopy analysis, showed that, in regions of organ adhesion, cuticle was absent and, on the epidermal surface, epicuticular wax deposition occurred irregularly. These observations led to the hypothesis that phenotypic alterations observed in the mutant seedlings may be attributable to defects in the cuticle-related biosynthetic pathways.

To gain insight into the role of *fdl1* in controlling cuticle formation, a large-scale RNA sequencing analysis was carried out in this work. By means of this approach, more than one thousand differentially expressed genes (DEGs) were found in the *fdl1-1* mutant compared with the wild type seedling transcriptome.

The analysis of single DEGs confirmed that *fdl1* is involved in the regulation of the biosynthesis of both cuticle components, since genes for the cuticular waxes deposition as well as cutin biosynthesis were detected.

In particular, five genes with a reduced expression level and one with an increased expression level in the *fdl1-1* mutant encoded for enzymes involved in the Fatty acid elongation complex, the main source of basic compounds exploited in cutin and waxes biosynthesis. Furthermore, two genes found with a reduced expression level in the mutant were also involved in the cutin

biosynthesis. Interesting sidelights on these two genes are available from the study of their orthologues in rice (*OsONI3*) and in Arabidopsis (*AtEDA17*). The knock-out mutant of *ONI3* in rice shows a phenotype that is very similar to that of the *fdl1-1* mutant in maize, with defects in cutin deposition and fusions between the coleoptile and the first leaves. Moreover, the knock-out mutant of *EDA17* in Arabidopsis shows defects in cutin deposition and fusions between floral organs.

Other two genes found differentially expressed in *fdl1-1* encode for enzymes involved in epicuticular waxes biosynthesis, thus explaining the defects observed in *fdl1-1* mutants.

On the basis of these observations, we developed a model that explains the mode of action of *fdl1* in controlling cuticle formation.

Furthermore, the large-scale RNA sequencing analysis done in this study revealed a considerable number of genes differentially expressed in the *fdl1-1* mutant that are involved in other important processes, such as plant clock regulation, plant pathogen interaction and hormone signalling. A deeper investigation of the role of these genes will be of help in elucidating the action of *fdl1* in controlling different aspects of plant development.

We also demonstrated in the present study that *fdl1* is actively involved in the drought stress response in maize seedlings. Indeed, an expression analysis showed strong differences in the *fdl1* transcript level in seedlings exposed to drought stress condition compared with seedlings grown in well-watered conditions. Indeed, in normally watered plants, the *fdl1* transcript level constantly increased during leaf expansion, until it reached a high expression level. In plants exposed to drought stress conditions, the *fdl1* transcript level showed a different pattern, with a strong increment in the first day of stress, and then a decrease until the initial level was reached and maintained for the whole duration of drought conditions.

We may speculate that the involvement of *fdl1* in the plant response to drought conditions, consists in promoting a modification of cuticle composition that will reduce water loss.

To further investigate the involvement of *fdl1* in drought stress tolerance, its orthologous gene was identified in *Eragrostis curvula*. This species is particularly interesting for our purposes, because its genome is very similar to the maize genome. Furthermore, unlike maize, in

Eragrostis different ecotypes, characterized by different drought stress tolerance, have been described.

In a preliminary analysis, we observed that the expression pattern of *Ecfdl1* is different among three *Eragrostis* ecotypes. Differently from what was observed in maize, *Ecfdl1* appeared to be expressed in different adult tissues. Moreover, differences in the *Ecfdl1* expression profile were detected in different ecotypes.

Besides in young maize tissues, *fdl1* also appears to have an active role in controlling cuticle deposition in silk tissues. We detected differences between the *fdl1-1* mutant and wild type plants in the composition of the wax layer covering the silks.

Since maize silks constitute the main route of entry for pathogens to reach the seeds, in our opinion the differences found in silk coverage can influence the plant-pathogen interaction.

This hypothesis was confirmed by comparing fusarium ear rot symptoms between wild type and *fdl1-1* mutant ears experimentally inoculated with *Fusarium verticillioides* in a two year experiment. Our results seem to indicate that the *fdl1-1* mutant is less susceptible to fusarium infection compared with the wild type.

In conclusion to this part of the work, our studies provided details about the involvement of *fdl1* in the regulation of cuticle biosynthesis and deposition during two of the most important moments of the plant life cycle: the seedling stage and silk development. Furthermore, in these two delicate moments, we have evidence showing that *fdl1* plays an active role in drought stress response and pathogen interaction.

In the second chapter, the role of brassinosteroids (BRs) in leaf permeability and architecture was further analysed. BRs are a class of steroid hormones essential for plant growth and development. BRs are involved in many developmental traits of agronomic importance such as seed germination, plant architecture, flowering time and seed yield. In addition to having an important role in development, brassinosteroids exert anti-stress effects on plants and are essential for the ability of plants to adapt to abiotic stresses.

This part of the work was focused on the characterization of the maize *lilliputian1-1* (*lil1-1)* mutant, which is impaired in one of the last steps of brassinosteroid biosynthesis. The

subtending gene putatively encodes for a brassinosteroid C-6 oxidase (brC-6 oxidase). The mutant appears severely compromised in height, floral development and overall plant architecture. Leaf primordia are more compressed compared with wild type, and mutant leaves appear thicker than wild type leaves, exhibiting altered shape and the presence of supernumerary cell layers in the mesophyll region between the leaf vessels and the adaxial leaf epidermis.

In this study, alterations in epicuticular waxes deposition were found in the *lil1-1* mutant. Furthermore, it was shown that the leaf epidermis of *lil1-1* shows a significantly lower permeability than wild type. These findings are in accordance with previous observations obtained in our laboratory, which showed that the *lil1-1* mutant shows a better dehydration tolerance.

In our hypothesis, the thicker epidermis observed in *lil1-1* compared with wild type, can explain the lower permeability and the better dehydration tolerance.

Furthermore, in this chapter we used the *lil1-1* mutant to better investigate the BRs biosynthesis pathway. This is a complex pathway and, although it has been the subject of several studies in recent years, some aspects are still to be clarified.

For this purpose, we analysed the interaction between the *lil1-1* mutant, and another well-known maize BRs mutant, i.e. the *nana1-1* (*na1-1*) mutant. Both *nana1* and *lil1* genes have key roles in the BR biosynthesis pathway. The product of *nana1* is involved in two parallel pathways, therefore lack of its action may lead to an interruption of both. The *lil1* gene product, however, is involved in the last steps of the pathway, leading to the formation of castasterone and brassinolide.

Our analysis revealed that *lil1-1* is epistatic to *na1-1*. These data suggest the existence in the maize BR pathway of an additional *na1*-independent branch leading to the production of CS precursors.

In conclusion, this part of the work demonstrated the involvement of brassinosteroids in passive leaf permeability and provided new information that will be useful to unravel the complex BR biosynthetic pathway in plants.

Overall, the work developed in this thesis project provides indications useful to better understanding the genetic mechanisms that regulate plant resistance to drought and pathogens.

A good comprehension of these mechanisms can ultimately be useful to identify new genetic tools of interest, and to develop crops more adapted to the challenges of the future.

Because of the appointment with 2050, only 32 annual production cycles remain.

CHAPTER 1

GENETIC REGULATION OF CUTICLE BIOSYNTHESIS

INTRODUCTION

Genetic and molecular control of cuticular waxes biosynthesis in maize

In all higher plants, a thin and continuous hydrophobic layer covers the outer surfaces of the aerial parts providing a protection against desiccation and constituting a physical barrier to environmental stress. This layer, known as cuticle, consists of two major components, i.e. cutin and cuticular waxes. Cutin is a polymer of C16 to C18 hydroxylated fatty acids, that are directly cross-esterified to each other or via glycerol backbone (Beisson *et al.* 2012), while cuticular waxes are complex mixtures of very-long-chain fatty acid (VLCFA) (Post-Beittenmiller 1996).

Cuticle compounds are synthesized by the epidermis before being secreted to cover the cell wall of epidermal cells facing the exterior environment. Besides vegetative organs, the cuticle covers flowers, fruits, seeds as well as pollen grains. Cuticle synthesis starts during embryogenesis with the formation of a procuticle and proceeds in the early stages of plant development; its deposition is tightly co-regulated with plant growth to provide a constant wax and cutin deposition required during plant growth (Misra, S; Ghosh 1991).

The cuticle is composed of the cuticular layer, a cutin rich domain with embedded polysaccharides, and the cuticle proper. The cuticle proper is constituted by the cutin polymer, which forms the structural matrix, and cuticular waxes, which are embedded in the cutin, and by a layer of waxes that are deposited on the cuticle surface as films or wax crystals. Waxes forming the outer layer of a plant tissue are termed epicuticular waxes (Bernard and Joubès 2013; Yeats and Rose 2013). The protective capacities of the cuticle are based on the physical and biochemical properties of its highly hydrophobic components, which are ultra-structurally assembled in several layers (Jeffree 1996). The cuticle layer provides a primary waterproof barrier and a protection against different environmental stresses, mainly controlling non-stomatal water loss and gas exchange, but also acts as a physical barrier against damages by insects and pollution (Post-Beittenmiller 1996; Lee and Suh 2015).

Besides its major role in stress response and adaptation, the cuticle is also thought to be involved in plant development, mainly through regulation of epidermal cell morphology (Jeffree 1996).

Cuticular wax composition in juvenile and adult organs, comparison between maize and Arabidopsis

Cuticular waxes are a mixture of different compounds, which are derived in most cases from very long-chain fatty acids (VLCFAs) and include primary and secondary alcohols, aldehydes, fatty acids, alkanes, ketones, and wax esters (Jenks *et al.* 2002; Kunst and Samuels 2003; Nawrath 2003).

In both Arabidopsis and maize plants, wax composition changes according to the developmental stage and the organ (Table 1).

Species	Organs	Components (relative %)							
		Fatty acids	Aldehydes	Alkanes	Primary alcohols	Secondary alcohols	Ketones	Wax esters	Alkenes
Arabidopsis	Leaf	1	14	73	8	0	0	4	0
	Stem	1	7	44	12	9	22	5	0
	Silique	1	4	50	14	9	22	0	0
	Flower	0	2	62	5	15	14	2	0
	Seed coat	0	9	51	13	18	9	0	0
	Leaf sheath	43	24	9	23	0	0	2	0
	Anther	11	0	33	2	0	0	0	55
Maize	Young leaf blade	0	25	4	69	0	0	2	0
	Young leaf sheath	0	42	14	39	0	0	5	0
	Silk	0	1	48	0	0	7	0	44

Table 1. Relative percentage of wax compounds present in the cuticle of *Arabidopsis thaliana, Oryza sativa* and *Zea mays* adult plants. Number 0 indicates that trace or undetectable amounts were observed. Data from (Lee and Suh 2015).

In Arabidopsis juvenile leaves, alkanes are the major wax components, representing up to 70% of the total waxes in rosette leaves, followed by secondary alcohols, (23%) and aldehydes (14%) (Bernard and Joubès 2013).
In Arabidopsis, cuticular wax composition of adult plants is different from that of seedlings. In Arabidopsis adult leaves, the major components are still represented by alkanes (73.6%), but the second most represented components aldehydes (14%), instead secondary alcohols (Table 1).

Also in maize cuticular waxes composition is different in juvenile versus adult leaves. Moreover, juvenile leaves have a thin cuticle and are coated with epicuticular waxes, whereas adult leaves have a thick cuticle and lack epicuticular waxes on their surfaces.
In maize **seedlings** cuticular waxes are composed of long-chain alcohols (69%), aldehydes (25%), alkanes (4%) and esters (2%) (Javelle *et al.* 2010). Alcohols and aldehydes are predominantly 32 carbons in length, i.e., n-dotriacontanol (99%of all the alcohols) and dotriancontaldehyde (96% of the aldehydes) and the alkane fraction is mainly 31 carbons in length, i.e. hentriaconate (Bianchi *et al.* 1977)
Instead, approximately 70% of the waxes produced throughout the adult life of a maize plant consist of esters (Bianchi *et al.* 1985).

Cuticular wax biosynthesis

Cuticular wax aliphatic compounds consist of a mixture of very long carbon chain molecules ranging from 22 to 36 carbon atoms.
In all plants, the biosynthesis starts with the production of VLC-acyl-CoAs by the elongase complex.
C16 and C18 fatty acids, resulting from the plastidial de novo synthesis, are esterified to Co-enzyme A (CoA) before entering the ER-bound multi-enzymatic fatty acid elongase (FAE) complex. Each FAE cycle generates an extension of the acyl chain by two carbons, through four successive reactions. The first reaction is catalysed by a b-ketoacyl-CoA synthase (KCS) that condenses malonyl-CoA with an acyl-CoA, producing b-ketoacyl-CoA. The second reaction

is catalysed by a b-ketoacyl-CoA reductase (KCR) that reduces b-ketoacyl-CoA to b-hydroxyacyl-CoA. The third reaction is catalysed by a b-hydroxyacyl-CoA dehydratase (HCD) that dehydrates b-hydroxyacyl-CoA to enoyl-CoA. The fourth and last reaction is catalysed by an enoyl-CoA reductase (ECR) that reduces enoyl-CoA to re-obtain acyl-CoA with the addition of two carbons (Lee and Suh 2015).

Twenty-one *KCS* genes were described in Arabidopsis, of which seven have been characterized for their role and substrate specificity. This finding lead to the hypothesis of the existence of multiple *KCS* genes with distinct chain-length specificity. They perform sequential and parallel reactions to produce VLCFAs with the broad chain-length-range found in plants.

The other three enzymes involved in FAE, i.e. KCR, HCD and ECR are instead shared by all complexes and are ubiquitously expressed in plants (Lee and Suh 2015).

VLC-acyl-CoAs can be transformed into free VLCFAs and/or processed through two distinct pathways, the alcohol-forming pathway or the alkane-forming pathway, leading to the production of the whole variety of aliphatic cuticular wax compounds (Fig. 2) (Bernard and Joubès 2013).

A first demonstration that endogenous VLCFAs, produced through the elongation of C16 and C18 fatty acids, are required for the formation of waxes came from experiments in which exogenous labelled very long-chain fatty acids supplied to maize tissues were shown to be converted to fatty alcohols (Bianchi *et al.* 1978).

Studies conducted in Arabidopsis epidermal cells, showed that loss of activity in single elongation component caused a severe decrease in all wax constituents (Zheng 2005), thus providing an additional indication that all the different wax aliphatic compounds originate from the fatty acid elongation pathway (FAE).

Primary alcohol formation was shown, **in both maize** and Arabidopsis **seedlings,** to result from a two-step reaction: VLCFAs are reduced to aldehydes and subsequently reduced to primary alcohol by an alcohol-forming fatty acyl reductases (FAR) (Schnable *et al.* 1994; Bernard and Joubès 2013). Functional studies in heterologous systems, such as *Escherichia coli*, *Saccharomyces cerevisiae*, and *Nicotiana benthamiana* leaves revealed that alcohol synthesis from VLCFAs can be processed by a single enzyme, and the potential intermediate aldehyde remaining bound to the FAR (Rowland and Domergue 2012).

Primary alcohols formed by the FAR are substrates for subsequent **alkyl ester** formation. As shown in Lai *et al.* 2007, the ester synthase enzyme catalyses the esterification of primary alcohols, exploiting as predominant acyl substrate 16:0 CoA.

Analyses of Arabidopsis CER mutants showed that VLCFAs are used as precursors to form **alkanes** via a putative **intermediate aldehyde** (Samuels *et al.* 2008). The obtainment of the in vitro conversion of radiolabelled C18 aldehydes into C17 alkanes using microsomal fractions from pea leaves and from the green algae *Botryococcus braunii* (Cheesbrough and Kolattukudy 1984; Schneider-Belhaddad and Kolattukudy 2000) provided further support to the hypothesis of a two-step conversion. Alkane chain lengths are consistent with a C1 loss from VLCFAs and/or aldehyde precursors. How even-numbered VLCFAs are transformed into odd-numbered alkanes remains an intriguing question. It was proposed that, in plants, VLCFAs could be reduced by a fatty acid reductase into corresponding even-numbered aldehydes and then an aldehyde decarbonylase (AD) would catalyse the conversion into alkanes with the loss of one carbon. In **Arabidopsis leaves**, alkanes are the end products, while **in stems**, these molecules can be further modified to **secondary alcohols and ketones** (Bernard and Joubès 2013).

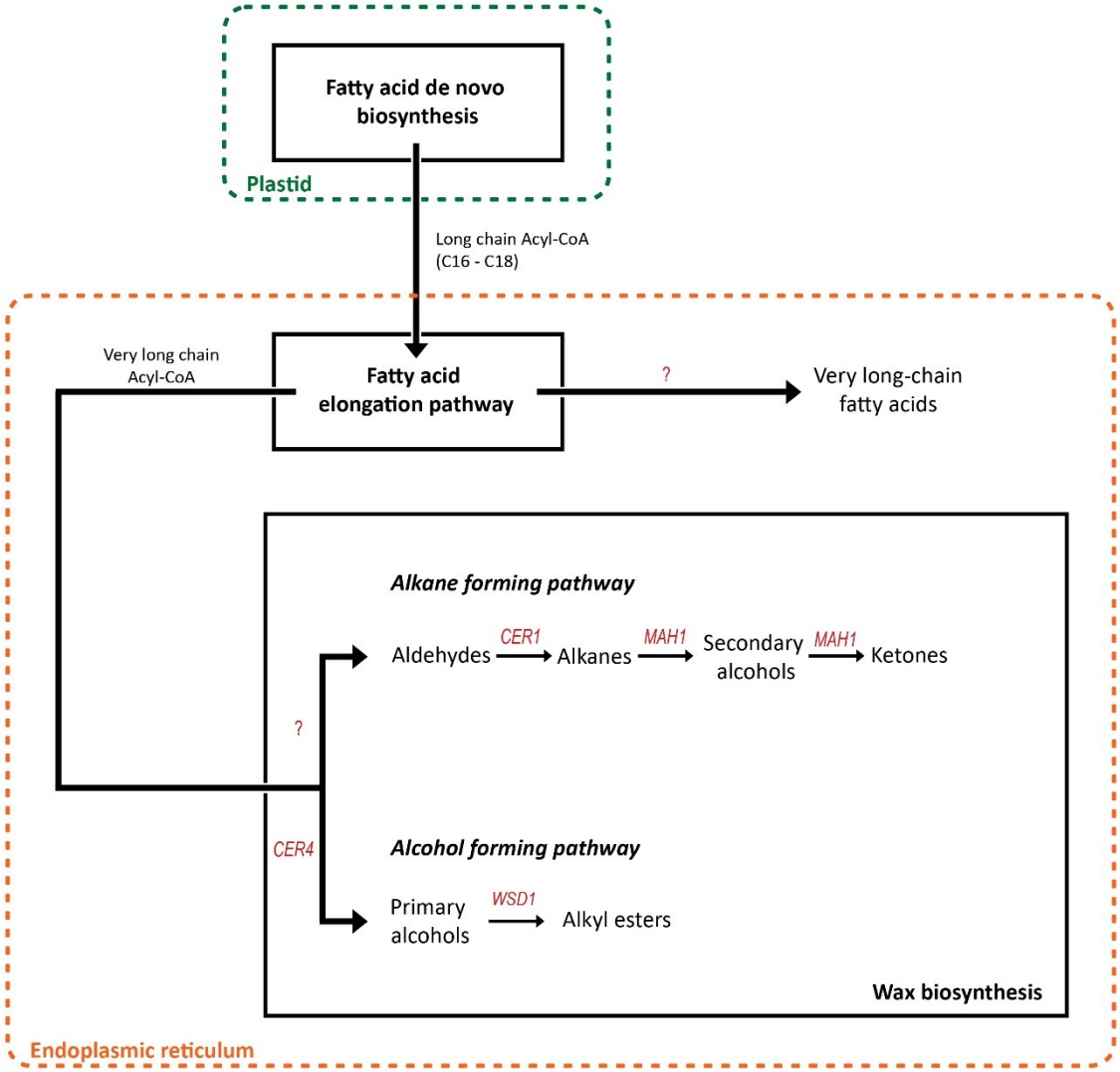

Figure 1. Schematic representation of the main biochemical pathways involved in the formation of wax components in plants. In red are reported the genes of *A. thaliana* involved in the corresponding step.

Genetic control of waxes biosynthesis in maize

In a wild-type maize plant, the first five to six juvenile leaves have a glaucous surface appearance, due to the presence of epicuticular waxes on their surface, whereas all leaves appearing later in plant development have a glossy surface (Poethig R. S. 1990; Lawson and Poethig 1995). Mutant seedlings impaired in juvenile wax synthesis can be easily recognized because of the glossy appearance of the first five to six leaves. On this basis, the phenotype of mutants with altered wax composition has been referred to as glossy. The glossy mutants

show another distinct trait associated with their wax alteration: if juvenile leaves are sprayed with water they form beads on their surface. Differently, the normal seedlings shed water almost completely (Bianchi 1960) (Fig.1).

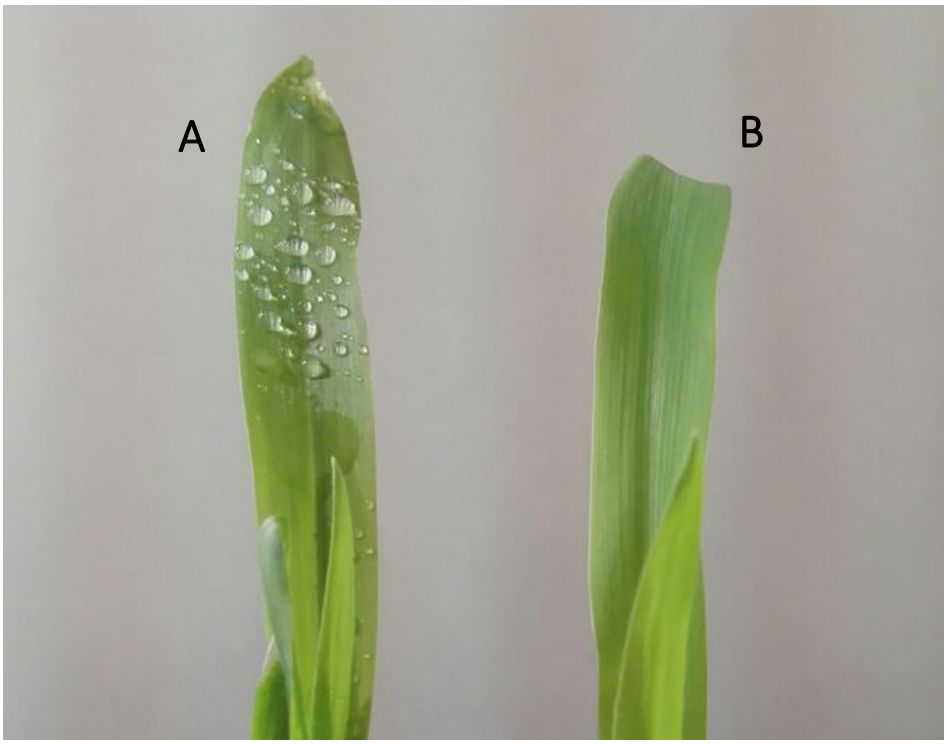

Figure 2. A detail of the second leaf of a *glossy2* mutant seedling (A) compared with a wild type sibling (B) at the same stage of growth. Water droplets are visible only on the leaf surface of the *gl* mutant plant.

It was hypothesized that two different pathways are producing leaf waxes in maize. One pathway is responsible for wax synthesis in the first five or six juvenile leaves, whereas the second pathway produces waxes during later phases (Bianchi *et al.* 1985). At least 26 loci, namely the *GLOSSY* loci, have been detected that affect the quantity and/or the composition of cuticular waxes on the surface of seedling leaves. They all arose from the genetic dissection of the wax biosynthetic process obtained through forward genetic analysis.

Eight glossy genes have been cloned and their functional characterization is available. In the recent years two additional maize genes involved in the regulation of wax deposition have

been described, i.e. *outer cell layer1* (*ocl1)* and *fused leaves 1* (*fdl1)* (Depge-Fargeix *et al.* 2011; La Rocca *et al.* 2015).

Among these, five genes encode for enzymes involved in the wax biosynthesis (*glossy1*, *glossy 2*, *glossy4*, *glossy8a* and *glossy8b*) one is a wax transporter (*glossy13*) and four are regulatory factors (*glossy3*, *glossy15*, *ocl1* and *fdl1*). Main features of these genes and related mutants are reported here below and summarized in Table 2, in which the Arabidopsis and Rice corresponding genes are also reported.

***Glossy1*.** The main effect of the ***glossy1* (*gl1*) mutation** consists in a dramatic **decrease** of the amount of total juvenile waxes, which corresponds to about 27% of the wild type amount. The mutant shows a large reduction of aldehydes and alcohols. Moreover, the predominant chain length of long-chain aldehydes and the corresponding free and esterified alcohols, is **reduced by two carbon atoms, from C32 to C30** (Bianchi et al. 1985). **The predicted GLOSSY1 protein** belongs to the family of membrane-bound desaturases/hydroxylases, however its specific function remains unknown (Sturaro *et al.* 2005).

***Glossy2*.** The ***glossy2* (*gl2*)** mutant phenotype is characterized by the presence of wax crystalloids showing a grain shape, as shown by SEM analysis, instead of the various shapes, such as spikes, rodlets and plates typical of wild type epicuticular waxes. In the first six leaves, the mutant plant has a reduction in the amount of total surface waxes to one-fifth compared with wild type. Chemical composition of *gl2* mutant seedlings is similar to adult wild type leaves, but wax compounds are two carbons shorter than wild type compounds. The *glossy2* transcript was shown to be predominantly expressed in juvenile leaves (Tacke *et al.* 1995). *CER2,* the orthologous gene in Arabidopsis, belongs to the BAHD superfamily of acyl-transferases, and seems to be involved in the fatty acid elongation pathway (Bernard and Joubès 2013).

Glossy4*.** The ***glossy4 (gl4) mutant shows a reduction of star-type particles on the leaf surface. A reduction in both **C32 aldehydes and alcohols**, which are the predominant chain

length groups in the wild seedlings was observed in *gl4* seedlings, which is compensated by an **increase in the C30 chain length** components that become the most abundant fraction. *CUT1*, which **encodes a condensing enzyme** involved in the synthesis of very-long-chain fatty acids, appears to be the corresponding Arabidopsis homolog. Subcellular localization predicts that Gl4 is targeted to the plasma membrane or cytoplasmic reticulum (Avato *et al.* 1987; Liu *et al.* 2009).

Glossy8a* and *Glossy8b*.** The ***glossy8a (gl8a) mutant shows alterations in the epicuticular waxes crystalloids. Indeed, SEM analysis revealed that in the mutant leaves surface are present only crystalloids with a grain shape. The level of cuticular waxes accumulated in the mutant seedlings corresponds to **5% of that of** wild-type and C30–C32 carbon chain components are reduced to 35% of the total. Other shorter component fractions are over represented in the mutant if compared with wild type. It has been proposed that the maize *gl8a* gene **encodes a b-ketoacyl-CoA reductase (KCR)**, which localized in endoplasmic reticulum and is a component of the fatty acid elongase (Xu *et al.* 1997).

The ***glossy8b (gl8b)*** mutant exhibits a very similar phenotype to the glossy8a mutant, although in the gl8b mutant, the level of total waxes is reduced to 50% of the wild type level and C30–C32 carbon chain components are reduced to 83% of the total. *gl8a* and *gl8b* are two paralogous genes and map in syntenic chromosomal regions. Their gene structure is conserved and the encoded proteins are 97% identical. Although the two genes have similar expression pattern, as indicated by the composition of mutant waxes, their roles are not completely overlapping (Xu *et al.* 1997).

Glossy13*.** The ***glossy13 (gl13) mutant seedlings show necrotic glossy leaves and are lethal. Most of the mutant plants die at the three-leaf stage and plants that survive to maturity are sterile and smaller than non-mutant sibs. Epicuticular wax crystals on mutant leaves appear significantly disorganized and, after dissection, leaf sections show a higher water loss rate compared with wild type. The *gl13* gene is a homolog of an ATP-Binding cassette G (ABCG32) family Arabidopsis gene, suggesting that *gl13* is involved in the transport of epicuticular waxes onto the surfaces of epidermal cells (Li *et al.* 2013).

Glossy3*.** The ***glossy3 (gl3) mutant shows dramatic changes in epicuticular waxes, with the presence of amorphous masses of wax and only occasional rodlets and other crystalloids, particularly near the guard cells. The *gl3* gene is predicted to encode an R2R3 type MYB transcription factor that directly or indirectly affects the expression of a number of genes involved in the biosynthesis of very-long-chain fatty acids (Liu *et al.* 2012).

Glossy15*.** The ***glossy15 (gl15) mutant shown a replacement of juvenile leaf phenotype with an adult phenotype observed already at the three-leaf stage. This observation suggests that *gl15* is involved in the determination of juvenile leaves epidermal cell identity. The *gl15* gene putative product is a transcription factor with high similarity to Arabidopsis *APETALA2* gene. *gl15* mRNA is detectable in low abundance in leaves three to six, and it is not present in adult leaves (Moose and Sisco 1996; Lauter *et al.* 2005).

Ocl1*. o*cl1 encodes a transcription factor of the HD-ZIP IV class that is expressed in the epidermis of embryo, endosperm, organ primordia and meristematic tissues. Lack of an obvious phenotype observable in *ocl1* mutant and the transient nature of the trait observed in dominant-negative mutant suggests a functional redundancy with other genes (Khaled *et al.* 2005; Depge-Fargeix *et al.* 2011). However, plants overexpressing *ocl1* show alterations in the wax composition of juvenile leaves. Indeed, in these plants, the C24 to C28 fatty alcohol contents were significantly increased in the leaf blade and ester contents were systemically reduced (Javelle *et al.* 2010).

***Fdl1*.** The ***fused leaves1* (*fdl1*) mutant** shows different developmental defects, such abnormal coleoptile opening, and presence of fusions between the coleoptile and the first leaf or between the first and the second leaf. Electronic microscope analysis show defects in cuticle deposition in epidermal cells, as well as a reduction of epicuticular waxes on the juvenile leaves surface. *fdl1* encodes for a transcription factor of the R2R3-MYB subfamily, that is expressed in embryos, coleoptiles, young leaves and silks (La Rocca *et al.* 2015).

GENE NAME	PHYSICAL POSITION	MAIZEGDB ID	ARABIDOPSIS TAIR ID	RICE GENOME PROJECT ID	FUNCTION
glossy1	Chr7: 118550916..118556690	GRMZM2G114642	AT5G57800	LOC_Os09g25850	Biosynthesis
glossy2	Chr2: 10630672..10633711	GRMZM2G098239	AT4G24510	LOC_Os04g52164	Biosynthesis
glossy3	Chr4: 185828677..185830259	GRMZM2G162434	AT1G08810	LOC_Os11g03440	MYB transcriptional factor
glossy4	Chr4: 166858871..166860792	GRMZM2G003501	AT1G25450	LOC_Os02g49920	Biosynthesis
glossy8a	Chr5: 181248005..181251026	AC205703.4_FG006	AT1G67730	LOC_Os02g38440	Biosynthesis
glossy8b	Chr4: 132787074..132790535	GRMZM2G087323	AT1G67730	LOC_Os02g38440	Biosynthesis
glossy13	Chr3: 10276457..10286585	GRMZM2G118243	AT2G26910	LOC_Os01g42410	ABCG transporter
glossy15	Chr9: 96744684..96748035	GRMZM2G160730	AT4G36920	LOC_Os06g43220	AP-2 family transcriptional factor
ocl1	Chr3: 27552061..27559751	GRMZM2G026643	AT4G00730	LOC_Os02g45250	HD-ZIP class IV transcription factor
fdl1	Chr7: 167647343..167649332	GRMZM2G056407	AT3G28910; AT3G47600; AT5G62470	LOC_Os08g33940; LOC_OS12G03150; LOC_OS12G03150	MYB transcriptional factor

Table 2. List of all the known and characterized maize genes involved in wax accumulation. For each gene is reported the physical map position, in according to the Maize B73 RefGen_V3 genome. Are also reported function, ID for MaizeGDB and the ID of the orthologous genes in Arabidopsis and rice.

Besides the genes characterized and reported in Table 2, in the past years other *glossy* loci were described, but the corresponding genes were never sequenced. However, some information about them are disposable, mainly deriving from the study of the correspondent

mutants. Nevertheless, for almost all of them except *glossy5*, the information disposable are not enough to speculate about their role.

***Glossy5*.** In the ***glossy5* (*gl5*)** mutant the **main wax constituents are aldehydes** while in the wild type plants alcohols are the predominant fraction. In addition, whereas in wild type waxes, both aldehydes and alcohol are made up mainly of C32 chain (99%), in *gl5* mutant waxes, the principal aldehyde is still C32 (90%) but the predominant free alcohol are C24, C26 and C28, with C32 representing only 16% of the total. Since a clear block in free alcohol synthesis is observed, accompanied by a strong accumulation of long-chain aldehydes, the most likely explanation is that the gene product is involved in the alcohol forming pathway, probably **in the reduction of fatty acids to alcohols** (Bianchi *et al.* 1978). The *glossy5* locus maps at 4S.

***Glossy6*.** The ***glossy6* (*gl6*)** mutant shows a great variability in the abundance of crystalline waxes deposed on the surface of near cells groups. Also on the surface of individual cells, the density of waxes change, with zones near the epidermal cells junctions consistently better covered than others (Beattie and Marcell 2002). The mutant waxes **composition is similar to that of *gl2* mutant**, with a high percentage of C26, C28 and C30 alcohols instead of C32. (Bianchi *et al.* 1985). The *glossy6* locus maps at 3L-69, but the protein encoded remains unknown.

***Glossy7*.** The ***glossy7* (*gl7*)** mutant shows a **total wax amount of mutant plants reduced at 40%** of the wild type level. The relative composition of waxes components is similar to wild type (Bianchi *et al.* 1977). Only 20% of the mutant leaf lamina is covered with waxes (Lorenzoni and Salamini 1975). Probably *gl7* gene influence the synthesis of long-chain fatty acid at a **very early stage**, and/or interfere with the supply of precursors (Avato *et al.* 1985). The *glossy7* locus maps at 4L, but the protein encoded and its role remains unknown.

Glossy11*.** The ***glossy11 **(*gl11*)** mutant shows an abnormal seedling morphology, male sterility and is occasionally viviparous. Mutant plants show a 30% reduction of total wax yield compared with wild type and dramatic differences in waxes composition. The dominant class of compounds in the mutant are esters, while in wild type is free alcohols, which are instead strongly reduced in the mutant. The stronger difference with wild type plants is related to the total amount of aldehydes**. Mutant completely lacks aldehydes,** while in wild type waxes the percentage of these compound reach 20% of the total waxes amount. In mutant plants, free fatty acids are represented for 88% by C16 and C18, while in the wild type these two compounds represent only 38% of the total free fatty acids amount. **Esterified alcohol C32**, which account almost 100 % in normal wax, amounts to **only 13%** of the total esterified alcohols in the mutant, where C24 and C30 are the dominant homologues. Indeed, the range of esterified fatty acids in wild type is from C20 to C30, with C24 predominant. In mutant plants, the predominant one is C20, with also consistent amounts of C22, C24 and C30 (Avato *et al.* 1985). The *glossy11* locus maps at 2S, but the protein encoded and its role remains unknown.

Glossy14*.** The ***glossy14 **(*gl14*)** mutant shows a hydrophobicity of the leaves surface higher than others glossy mutants known and similar to wild type plants. The amount of epicuticular waxes produced by *gl14* mutant plants is about **20% lower than in wild type plants**. When observed at the electron microscopy, leaf surface of *gl14* mutants shows the presence of **crystal structures named "wax worms"**: very large, rod-shaped bodies of wax that were typically 4–9 um long. Wax worms appear almost always oriented parallel to the stomatal openings, and sometimes are clustered in regions near the epidermal cell junctions. This is a unique feature, neither observed in wild type plants, nor in other *glossy* mutants. Furthermore, the leaf surface of *gl14* mutant has another unique feature, the presence of **regions that shows an over-accumulation of waxes** that are sufficient to completely cover all the cells surface (Beattie and Marcell 2002). The *glossy14* locus maps at 2S, but the protein encoded and its role remains unknown.

Biosynthesis localization and wax transport

Several studies conducted in different plant species demonstrated that enzymes involved in the formation of VLCFAs are localized in the **endoplasmic reticulum** (**ER**). Subcellular fractionation experiments carried out in *Zea mays* revealed that the β-ketoacyl reductase membrane-embedded enzyme residing in ER (Xu *et al.* 2002). Arabidopsis CER6 condensing enzyme and enoyl-CoA reductase GFP fusion proteins was shown to localize to the ER (Kunst and Samuels 2003). The ER is also the subcellular compartment in which VLCFAs are further metabolized. Experiments conducted in yeast localized the FAR, which is encoded by the Arabidopsis CER4 and catalyses the conversion of acyl-CoA to primary alcohols, in the ER (Ukitsu *et al.* 2007). Similarly, the mid-chain alkane hydroxylase MAH1, which catalyses the oxidation of alkanes to secondary alcohols and ketones in Arabidopsis stems, was localized to the ER of epidermal pavement cells (Greer *et al.* 2007).

The mechanism for transport of wax molecules from the site of biosynthesis to the cuticle is only partially understood.

The first part of the transport mechanism, within epidermal cells, is difficult to investigate through electron microscopy since sample preparation for this analysis implies the extraction of lipophilic compounds. However, by analogy with other intracellular lipid transport processes, it has been suggested that it occurs through direct molecular transfer at ER-plasma membrane (PM) contact sites (Kunst and Samuels 2003). This hypothesis was supported by the observation of membrane contact sites, in which cortical ER is in close proximity (within 10 nm) to the PM (Staehelin 1997). It has also been suggested that the monomolecular exchange of lipids implies mechanism for membrane recycling and/ or wax trafficking (Kunst and Samuels 2003).

After wax molecules have been delivered to the PM, they must be released from the lipid bilayer into the apoplastic environment. The recent discovery of CER5 and WBC11 transporters in Arabidopsis stems constitutes a first progress toward a more detailed understanding of this process. These ATP binding cassette (ABC) transporters from the ABCG/WHITE-BROWN COMPLEX (WBC) subfamily were shown to be involved in cuticle formation. Both *CER5* and *WBC11* mutants show reduced surface wax loads combined with intracellular wax accumulation. Localization of both transporters to the PM was shown in

stem epidermal cells using functional transporter–fluorescent protein fusions and confocal microscopy analysis (Pighin 2004; Bird *et al.* 2007).

Once wax components have been exported from the epidermal cell, they must cross the hydrophilic cell wall to reach the cuticle. Lipid transfer proteins (LTPs) are the most attractive candidates for wax transport across the cell wall (Kader 1996). They are abundantly expressed in the epidermis, secreted into the apoplast (Thoma *et al.* 1993), small enough to traverse the pores of the cell wall and contain a hydrophobic pocket that binds long-chain fatty acids in vitro (Zachowski *et al.* 1998). However, no experimental evidence has been proposed yet to support this hypothesis. Reverse genetic approaches may soon reveal whether these proteins indeed function as cuticular lipid carriers within the epidermal cell wall.

Cuticle and developmental processes

In Arabidopsis, wax related mutants *CER1*, *CER2* and *CER3* show a decreased stomatal index, thus indicating a cross-talk between stomata differentiation and cuticular metabolism (Chen *et al.* 2003). Numerous transgenic plants with an impaired cutin load are characterized by organ fusion phenotypes while conserving an intact epidermal cell layer. This suggests the specific requirement of a proper cuticle to define organ boundaries (Sieber *et al.* 2000; Nawrath 2006).

A role of wax compounds was also found in **pollen** grain physiology. In the Arabidopsis mutants *CER1*, *CER2* and *CER6*, alterations in epicuticular waxes cause an altered pollen grain surface. Furthermore, pollen grains of these mutants were sterile in low humidity but normally fertile in high humidity conditions (Preuss *et al.* 1993; Aarts *et al.* 1995). Pollen grains showed sterility and failed to rehydrate when placed on the stigma but showed a normal growth in vitro. This demonstrated that the lipid defects observed in the mutants are likely to have an effect on the regulation of pollen hydration (Hülskamp *et al.* 1995).

Cuticular waxes in plant response to abiotic and biotic stress

Stomatal conductance plays a major role in plant transpiration, nevertheless leaves deprived of stomata show a residual water loss, suggesting an additional non-stomatal component in plant transpiration. An active role of cuticle in preventing plant desiccation has been proposed in several plants, such as tobacco (*Nicotiana glauca L. Graham*) and sesame (*Sesamum indicum L.*). An increase of cuticular wax synthesis during water deprivation was observed in these species (Bernard and Joubès 2013).

In Arabidopsis a positive correlation between increase of wax amount and tolerance to drought stress was reported (Aharoni *et al.* 2004). Indeed, it was observed that an accumulation of waxes is triggered by water deprivation and osmotic stress treatments, suggesting that induction of cuticle formation could be one of the mechanisms contributing to the acquisition of tolerance to hydric stress (Kosma *et al.* 2009).

Resistance to water deprivation is mainly associated with the regulation of cuticular permeability. In *A. thaliana* plants overexpressing *MYB96* or *CER1* showed an increased wax load associated with lower cuticle permeability and improved resistance to water stress (Bourdenx *et al.* 2011). However, in the Arabidopsis *BDG* mutant for example, increased amounts of both cutin and waxes were associated with a higher cuticular permeability (Kurdyukov 2006). It is therefore clear that cuticle thickness and amount of lipid compounds cannot be the only factors affecting cuticular permeability. It must be related to other factors, such as the specific composition and organization of cuticle components.

Furthermore, a secondary, but not less important role was proposed for epicuticular waxes in the control of water transpiration. As indicated by scanning electron microscopy (SEM) analyses of *Shiny* Arabidopsis mutants, wax crystals can modulate light reflectance, thus acting in temperature regulation by preventing water vaporization in plant cells and therefore limiting transpiration (Shepherd *et al.* 2007). The control of light reflectance by wax crystals is also commonly thought to be of a significant importance in plant physiology by protecting the plant against damaging wavelength such as UV radiation while conserving a satisfactory ratio of light penetrance for photosynthesis activity (Holmes and Keiller 2002).

By comparing the shape of water drops on smooth versus crystalloid leaf surfaces, it was also proposed that wax crystals are involved in a self-cleaning process called the lotus effect. Crystalline microstructures lead to the formation of spherical droplets and thus trigger water repelling on the plant surface, limiting the deposition of dust, pollutants and pathogen spores (Barthlott and Neinhuis 1997).

Moreover, avoidance of water stagnation on the plant surface was shown to have beneficial effects on plant infection caused bacterial pathogens (Marcell and Beattie 2002).

In plant/pathogen and plant/insect interactions, wax compounds were found to act either as chemical attractors in feeding stimulants or as deterrent molecules. In this context, the role exerted by wax compounds is associated with the chemical composition of waxes rather than their physical properties (Eigenbrode and Espelie 1995). Indeed, it has been shown that waxes could contain active components that induce germination and formation of the appressorium by fungal pathogens (Podila *et al.* 1993). As reported in Arabidopsis, waxes chemical composition is also an active signal for pathogens. Egg deposition of Large Cabbage White butterfly *Pieris brassicae* was shown to modify wax composition leading to the arrest of the parasitoids (Blenn *et al.* 2012).

Since the cuticle is a tightly organized structure, it is highly feasible that most of the components act synergistically in the various processes. However, the specific significance of single wax components in cuticle functions during environmental or developmental processes is largely unknown. Nevertheless, alkanes which are the major wax compounds in Arabidopsis, were found to have a specific contribution in cuticle properties, reducing cuticle permeability and water stress sensibility when over-accumulated (Bourdenx *et al.* 2011).

Wax composition in maize silks

Waxes are also present in silks, where constitute a two-way barrier: they prevent excessive moisture loss, and are the first defence against attack by external agents. Maize silks are often a point of first contact, or indeed, a major route of entry for both fungal and insect pests (Misra, S; Ghosh 1991). Silk cuticle contains large quantities of both n-alkanes and n-alkenes

(Perera *et al.* 2010). For these reasons, maize silk tissue may constitute a convenient system for studying hydrocarbon biosynthesis.

Maize silk cuticular waxes differ from those of other plant organs, since they are very rich in long-chain normal hydrocarbons. These hydrocarbons constitute a large portion (>90%) of silk cuticular waxes (Perera *et al.* 2010) and are rare biological molecules, whose biosynthetic origin has yet not been unravelled.

Chemical analysis (Perera and Nikolau 2007) indicated that waxes isolated from maize silks consist of homologous series of compounds ranging from 19 to 33 carbon atoms, constituted of linear alkanes, alkenes, dienes, saturated and unsaturated ketones, and saturated and unsaturated aldehydes. In contrast to the alkanes, alkenes and ketones, which are a homologous series with odd numbers of carbon atoms (ranging from 19 to 33 atoms), the aldehydes are a homologous series of even numbers of carbon atoms (ranging from 26 to 30 atoms). About 44 and 48% of the silk cuticular waxes are unsaturated hydrocarbons (alkenes and dienes) and saturated hydrocarbons (alkanes), respectively. The remainders are mainly ketones (7%), and the aldehydes accounting for about 0.4% of the isolated cuticular waxes.

The majority of the silk wax compounds are present in the portion of the organ that is external to the husks and in which net accumulation occurs rapidly two–three days after emergence. Silks are thin organs particularly susceptible to desiccation. The finding that the cuticle-associated hydrocarbons are concentrated on the silk portion that is exposed to the atmosphere (rather than in that covered by the husks) is consistent with the hypothesis that accumulation of large quantities of hydrocarbons has a role in protecting these organs from excessive water loss (Perera *et al.* 2010).

The *fdl1* gene is involved in the regulation of cuticle deposition in maize

The *fdl1-1* mutant was previously isolated and characterized in our laboratory. Its mutant phenotype is expressed at early stages of seedling development, from germination to the three-four leaves stage, causing a general delay in germination and seedling growth as well as phenotypic abnormalities (Fig. 4). The main features of mutant plants are irregular coleoptile

opening and the presence of regions of adhesion between the coleoptile and the first leaf and between the first and second leaves.

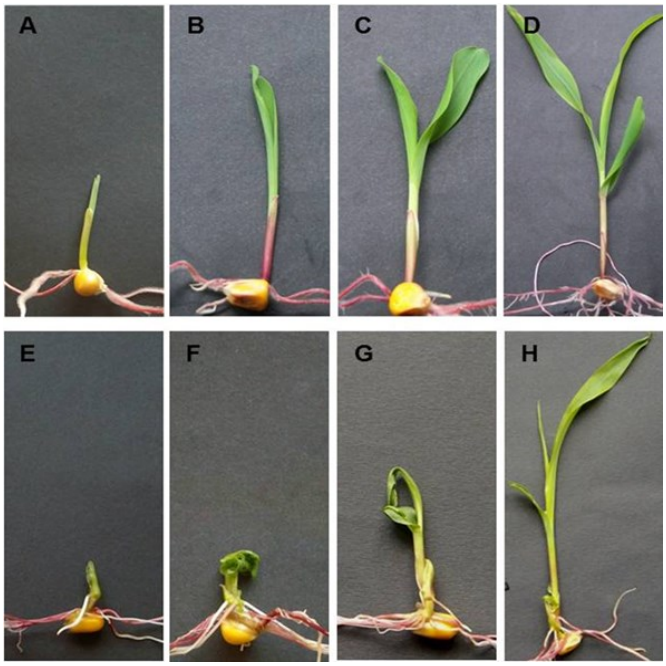

Figure 3. Representative wild-type (A-D) and *fdl1-1* mutant (E-H) seedlings at succeeding stages of development: coleoptile (A,E), first leaf (B,F), second leaf (C,G) and third leaf (D,H)

A previous study suggested that the *fdl1-1* mutation was caused by an *Enhancer*/*Suppressor* (*En*/*Spm*) element insertion, which was located in the third exon of the sequence encoding ZmMYB94, a transcription factor of the R2R3-MYB subfamily (La Rocca *et al.* 2015). Moreover, the spatial and temporal expression profile of the *ZmMYB94* gene, as determined by quantitative RT-PCR, was shown to perfectly overlap the pattern of mutant phenotypic expression. High expression was observed in the embryo, in the seedling coleoptile and in the first two leaves, whereas RNA level decreases at the third leaf stage (La Rocca *et al.* 2015).

Preliminary phylogenetic reconstructions considering 104 unambiguously alignable amino acid residues from the highly conserved MYB domains of all annotated R2R3-MYB proteins from *Z. mays*, *Oryza sativa*, *Brachypodium distachyon*, *A. thaliana* and *Vitis vinifera* has indicated that *ZmMYB94* falls within a well-supported clade containing representatives of all species considered, but did not allow confident assignment of an exact phylogenetic placement. Taking into account only sequences within this clade and performing a subsequent phylogenetic reconstruction that includes 166 aligned amino acid sites that (while failing to

unambiguously) resolves all relationships within the MYB sub-clade, strong support for co-orthology between *ZmMyb94* and *ZmMyb70* with functionally uncharacterized Brachypodium and rice genes as part of a monocot-specific gene family expansion was detected. These analyses recover no support for direct orthology between *ZmMyb94* or *ZmMyb70* and any dicot homolog. Indeed, the most closely related MYBs in dicots were *Vitis vinifera MYB30*, an additional uncharacterized *Vitis vinifera* MYB and a clade of recently duplicated Arabidopsis MYBs (*AtMYB30/94/96*) (La Rocca *et al.* 2015). The absence of direct dicot orthologues of *ZmMYB94* is notwithstanding; it is also interesting to note that *MYB30*, *MYB94* and *MYB96* have all been implicated in the regulation of cuticular wax biosynthesis in Arabidopsis (Sheperd T. and D.W. 2006; Raffaele *et al.* 2008). *AtMYB30*, *AtMYB94* and *AtMYB96* were characterized as positive regulators of wax biosynthesis (Raffaele *et al.* 2008; Seo *et al.* 2011). *AtMYB94* and *AtMYB96* transcription factors, closely located in the phylogenetic tree (Lee and Suh 2015), provided evidence for their function in ABA-dependent regulation of wax synthesis during water stress (Seo *et al.* 2011; Lee and Suh 2015), while *AtMYB30* during biotic stress (Raffaele *et al.* 2008).

A deeper analysis of the *fdl1-1* mutant leaves was performed by SEM analysis and evidenced an alteration in epicuticular wax deposition, which was less homogenous on the mutant than in the wild-type leaf surfaces. Indeed, mutant leaf surfaces exhibited a patchy distribution of epicuticular waxes, with some areas evenly covered and others completely devoid. This trait, similarly to the other *fdl1-1* traits, was confined to the first two leaves since later leaves show a regular distribution of epicuticular waxes that was indistinguishable from that of wild-type leaves. This leads to the hypothesis that phenotypic alterations observed in the mutant seedlings may be attributable to e defect in the wax biosynthetic pathway (La Rocca *et al.* 2015).

MYB genes are important transcriptional regulators

A number of different factors are required for the initiation of the process of transcription, including factors required for chromatin remodelling and DNA unwinding, as well as proteins of the pre-initiation complex and the RNA polymerase II complex. The transcription factors

are proteins that recognize DNA in a sequence-specific manner and that regulate the frequency of initiation of transcription upon binding to specific sites in the promoter of target genes. Transcription factors can be activators, repressors, or both, and display a modular structure. Based on similarities in one of the modules, namely the DNA-binding domain, transcription factors have been classified into families (Pabo 1992). MYB family proteins possess a conserved DNA-binding domain (DBD), which is homologous to the DBD of animal c-Myb (Klempnauer *et al.* 1982) and is composed of up to three imperfect repeats (named sequentially as R1, R2 and R3, respectively) (Dubos *et al.* 2010). The R2R3 sub-class of MYB factors contains two repeats and is the most common type in plants (Du *et al.* 2013). 157 genes encoding R2R3-MYB proteins have been identified in the maize genome and classified into 37 subgroups, according to their structure and phylogenetic relationships (Du *et al.* 2013). However, functional studies have been performed for only a few maize MYB genes that are involved in the control of phenylpropanoid metabolic pathway (Paz-Ares *et al.* 1987; Marocco *et al.* 1989; Grotewold *et al.* 1991; Fornalé *et al.* 2006; Heine *et al.* 2007). In Arabidopsis, up to 126 members belong to the R2R3-type subfamily have been detected (Yanhui *et al.* 2006) and the roles of many of these proteins have been demonstrated in a variety of development process, such as development of meristem, flower and seeds (Schmitz *et al.* 2002; Zhang *et al.* 2007; Petroni *et al.* 2008), cell cycle control (Araki *et al.* 2004) and stomatal closure (Liang *et al.* 2005). Some Arabidopsis MYB members also regulate plant responses to biotic and abiotic stress conditions (Abe *et al.* 2003; Raffaele *et al.* 2008; Van der Ent *et al.* 2008).

Eragrostis curvula as model plant for drought tolerance studies

Eragrostis curvula is a perennial grass, member of the Poaceae family, native to Southern Africa. Generally this species could be utilised for soil conservation and/or as a source of forage (Colom and Vazzana 2002). In the last years, *E. curvula* was largely exploited as model plant to study mechanisms undergoing apomixis in plants. Indeed, *E. curvula* displays a type of apomixis termed pseudogamous diplospory, and the Eragrostis complex includes cytotypes with different ploidy levels (from 2x to 8x) that may undergo sexual reproduction, facultative apomixis, or obligate apomixis (Rodrigo *et al.* 2017).

Most varieties of *E. curvula* are able to sustain high production, are highly persistent, and relatively drought resistant. Besides its importance for the study of apomictic processes, it is an interesting specie for its ability to adapt to drought condition. In the past years several ecotypes were described, characterized by different drought tolerance levels (Colom and Vazzana 2002).

The higher drought resistance showed by some *Eragrostis* ecotypes can probably be attributed to its high capacity to retain water during drought stress.

Studies of waxes covering the cuticle have been performed in plants belonging to the genus *Eragrostis*. A descriptive investigation of wax ultrastructure on leaves of *Eragrostis lehmanniana* demonstrated that drought-tolerant lines were covered with large wax plates in addition to the wax structure found even in drought-susceptible lines. Furthermore, wax analysis showed strong differences in epicuticular wax content between different *E. curvula* ecotypes, relatively high compared with values for other species (Tischler and Voigt 1990).

The positive relationship between wax and water content showed by these studies suggests the possibility that high levels of waxes may have a positive impact on the ability of plants to maintain a high-water content.

Aim of the work

In this work, we performed a functional analysis of the role of *fdl1* in maize.

The study of this MYB gene can represent a useful instrument to understand the genetic mechanisms that regulate the cuticle deposition in maize, during two of the most important moment in plant life: germination and pollination.

The work is divided in three chapters.

- In the first part, we investigated the role of *fdl1* in the regulation of cuticle deposition. We identified genes differentially expressed in *fdl1-1* mutant compared with wild type plants. We tried to correlate the role of these genes with the alterations observed in *fdl1-1* mutant phenotype, also exploiting gas chromatographic analysis of the cuticle compounds.

- In the second part, we investigated the involvement of *fdl1* in drought stress response. Indeed, as reported in the paragraphs above, in drought condition the cuticle constitutes the main plant barrier against the loss of water.
- In the third part, we investigated the role of *fdl1* in cuticle deposition on maize silks, and its involvement in plant-pathogen interaction. For this analysis we exploited the pathogen fungus *Fusarium verticillioides*.

MATERIAL AND METHODS

Plant material

Zea mays

The *fdl1-1* mutant used in this work was originally identified in the selfed progeny of a maize line crossed as female to an En/Spm line (Fig. 3). *The fdl1-1* allele was maintained in homozygosis as well as in heterozygosis. Heterozygous plants were obtained by outcrossing plants homozygous for the mutation to B73, Mo17, ACR and R-scm$_2$ maize inbred lines.

Figure 3. Wild type and *fdl1-1* seedling (B73 inbred line) at second leaf stage of growth.

Wild-type and mutant maize seeds were germinated in a growth chamber at 25°C on wet filter paper. Seeds were kept in the dark for 4–5 d and then transferred to a 14 h light photoperiod and photon fluence of 70 µmol m^{-2} s^{-1}.

For experiments at adult stage plants were sown and growth directly in open field. The field was located in Verderio Superiore (LC), Italy. Plants were sown between April and May.

Figure 4. Zea mays plants growth in open field.

Eragrostis curvula

All experiments were performed using plants from three different genotypes, i.e. Don Eduardo, Don Walter and Don Pablo, chosen because these materials belong to the Robusta type, highly resistant to drought conditions (Voigt et al., 1984; Holt et al., 1979).

Seeds were provided by Professor Viviana C. Echenique (Centro de Recurdos Naturales Renovables de la Zona Semiárida, CERZOS – CCT CONICET, BahÍa Blanca – Argentina). Plants were grown in the greenhouse, both in Bahia Blanca (CERZOS – CONICET), and in Milan (Disaa – Unimi).

Figure 5. Eragrostis curvula plant (cv. Don Walter) growing in the greenhouse at the University of Milan (Italy)

Seeds sterilization

Before sowing, all the seeds (*Z. mays* and *E. curvula*) were sterilized by keeping them in a solution of bleach/water 1:1 for 20 minutes. Then the seeds were washed with deionized water and immediately sown.

Drought stress treatment

Maize plants from the same B73 generation were sown in plastic pots. All the pots were filled exactly with the same amount of soil amount (Vigor Plant®).The drought stress conditions were monitored using the relative water soil content (RWSC) parameter. The RWSC parameter indicates the percentage of water contained in the substrate, relative to the maximum water content that the substrate can hold. Relative water soil content was calculated with the formula:

$$\text{RWSC X \%} = \frac{100 \text{ x WEIGHT OF WATER IN THE SUBSTRATE (g)}}{\text{MAXIMUM OF WATER CONTAINING THE SUBSTRATE (g)}}$$

To calculate the maximum of water containing the substrate, pots containing the substrate were fully soaked and weighed. Afterwards, the same pots were fully dried and weighed again. The difference between the weight of the pot fully soaked and fully dried were considered the maximum of water containing the substrate.

Drought stress treatments were initiated in six old days plants by stop watering. The RWSC of each pot was calculated daily by measuring and adjusting the water amount until reach 80% for the plants of the normal watered (NW) group and 30% for the low watered (LW) group. Once the desired RWSC was reached, it was maintained constant during all the experiment.

The second leaf of each plant were collected every day, at the same time, submerged in liquid nitrogen and stored -80°C. Four or five biological replicas were taken for each treatment, as is shown in Table 6.

DAS	DURATION OF DROUGHT STRESS (HOURS)	NUMBER OF REPLICAS	
		NW	LW
6	0	4	4
7	24	4	4
8	48	5	5
9	72	5	5
10	96	5	5
11	120	5	5
12	144	5	5

Table 6. Scheme of the samples taken during the drought stress experiment. DAS: days after sowing. NW: normal waterer (RWSC 80%). LW: low watered (RWSC 30%).

F_2 progenies segregating for *fdl1-1* and a *glossy* mutant

Fdl1-1/fdl1-1 (B73) heterozygous plants were used as female and crossed with *gl2/gl2* homozygous plants. The F_1 progeny was selfed in the field (year 2016), in order to obtain F_2 populations segregating both for *fdl1-1* and for *gl2*.

Since homozygous *gl13* mutant plants are lethal after the third – fourth leaf stage, plants carrying this mutation were used as heterozygous. *Fdl1-1/fdl1-1* (B73) heterozygous plants

were used as female and crossed with heterozygous *Gl13/gl13* plants. The F_1 progeny was selfed in the field (year 2016), in order to obtain F_2 populations segregating both for *fdl1-1* and for *gl13*.

Experimental inoculation with *F. verticillioides*

A mix of eight *F. verticillioides* strains was used for the inoculations. Strains were isolated from *Zea mays* plants in Lombardia (Italy) in 2011. Their fumonisin production capability was tested *in vitro* (Venturini et al., 2016).

Strains were growth on plates with potato dextrose agar (PDA), and incubated in dark condition for seven days at 25°C.

Twenty-four hours before inoculations, a conidia suspension for each strain was prepared in sterile water and 0.01% Tween®20 on a final concentration of 10^6 conidia/ml. Suspensions were kept overnight at 4°C and mixed just before starting with the inoculations.

Ears prepared for inoculation were self-pollinated 8 – 12 days before inoculation (Schaafsma *et al.* 1997), and covered with a paper bag.

Inoculation was performed by spraying the conidia suspension directly on the ear's silks (Fig. 6). An equal number of ears were inoculated with distilled water and used as control.

Figure 6. A) Inoculation procedure on maize silks. B) Ear covered with plastic bag.

For experiments on silks, immediately after inoculation, ears were covered with a transparent plastic bag, in order to avoid cross contaminations and for promoting the formation of high humidity conditions inside (Fig. 6). Immediately after inoculation and at 72 hours, silks were taken from the entire ear and kept at -80°C. Three biological replies were taken from each treatment.

For experiments involving the use of ripe ears, these structures were covered with a bag made with a tiny net, and subsequently with a paper bag. At maturity, twelve ears inoculated with *F. verticillioides* suspension and twelve inoculated with water were harvested and immediately used for experiments.

Quantitative analysis of Fusarium ear rot

Differences between ears of wild type plants and mutant plants were evaluated from a pathological and mycological point of view. In order to evaluate the differences in response to this pathogen mature ears of wild type and *fdl1-1* homozygous mutant plants were inoculated with a *F. verticillioides* conidia suspension.

Ears were collected at maturity and deprived of bracts. The gravity of infection and the difference of *Fusarium* susceptibility between genotypes was evaluated through visual analysis. Presence/absence of damages caused by *Fusarium* was reported for each ear. The gravity of symptoms was evaluated through the FER severity index (I%I). The presence of ear rot was quantified in seven classes (from 0 to 6), based on the percentage of infected area (Fig. 7), and calculated using the formula proposed by Venturini *et al.* 2015.

$$I\%I = \frac{\sum(class\ number * number\ of\ ears\ in\ the\ class) * 100}{(numeber\ of\ classes - 1) * number\ of\ ears\ observed}$$

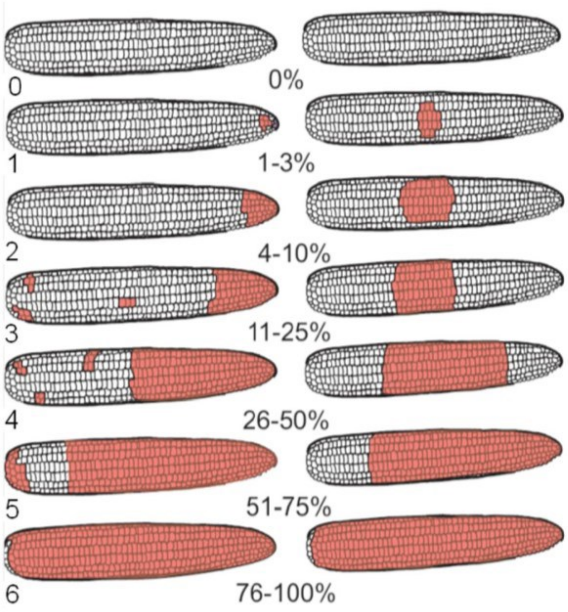

Figure 7. Fusarium ear rot (FER) severity evaluation through I%I index. On the top is reported the formula, in the image the different classes with the percentages of infected surface.

Gas chromatography–Mass spectrometry analysis on maize silks

Analysis of epicuticular wax on maize silks was performed with a combined analysis GC-OCI (gas chromatography - on column injection) and GC/MS (gas chromatography/mass spectrometry). The analysis was performed on 3 technical and 3 biological replicas. After grinding in liquid nitrogen, samples were subjected to extraction dissolving 500 mg of plant material in 2 mL of iso-octane. During extraction, samples were sonicated for 30 minutes at room temperature. At the end of the procedure, the supernatant was analysed in GC/MS injecting 2 µl.

Operative conditions:

- Column: RXI-5ms (Restek), 30 m × 0.25 mm, 0.25 µm film thickness
- Gas carrier (He) = 1mL/min
- Split 1:5
- T injector: 260 °C
- T detector: 280 °C
- T column: 80 °C × 1 min, 7 °C/min until a 320 °C
- Scan 40-500 m/z

Statistical analysis

All the data were statistical analysed and the mean values were tested by one-way analysis of variance (ANOVA) at 5% level of significance using the statistical packages SPSS 22.0 and Prism GraphPad 6.

Genomic databases and in silico analysis

Gene sequences used in this work were obtained from online databases:

- NCBI Genbank (www.ncbi.nlm.nih.gov/genbank)
- MaizeGDB.org (www.maizegdb.org)
- Gramene.org (http://www.gramene.org)
- JGI Phytozome (phytozome.jgi.doe.gov)
- KEGG (http://www.genome.jp/kegg)

DNA extraction

DNA was extracted from plant samples with the procedure here described that employs ethanol precipitation for concentrating and de-salting nucleic acids preparations in aqueous solution.

- Put 20-40 mg of tissue in an 1.5 ml Eppendorf vial
- Add 300 µl of extraction buffer
- Grind the tissue
- Add 100 µl of SDS 2%
- Incubate at 60°C for a time between 30 min and 2 hours
- Spin at maximum speed for 15 min
- Transfer 150 µl of supernatant in another clean Eppendorf vial
- Add 150 µl of 5M ammonium acetate and 300 µl isopropanol. Mix gently
- Incubate at room temperature for 15 min
- Spin at 9000xg for 5 min.
- Waste the supernatant
- Wash the pellet with 500 µl of 70% ethanol (cooled at -20)
- Spin at 9000xg for 5 min
- Waste the supernatant

- Dry at the air or in vacuum condition
- Suspend gently in 50 µl TE pH8
- Incubate at 65°C for 5 min
- Store at -20°C

Extraction buffer: 2M NaCl, 200mM Tris-HCl pH8, 70mM EDTA pH8, 20mM Sodium metabisulfite

RNA extraction and retrotranscription reactions

RNA was extracted from plant tissues using the Invitrogen / Thermo Fisher Scientific "Trizol Plus Purification Kit®". All the extractions were performed following the protocol provided by the manufacturer.

For long-term storage, RNA samples were stored at -80°C.

After extraction, the integrity of RNA was checked on agarose gel. RNA was treated with DNAse (Invitrogen "DNAse I®") to degrade the residual DNA, following the protocol provided by the manufacturer.

RNA was retrotranscripted using the Invitrogen / Thermo Fisher Scientific "Superscript III®" Kit, following the protocol provided by the manufacturer and using PoliT primers for the reaction. The obtained cDNAs were diluted 100 fold and the quality of the cDNA was checked by PCR using ORP or 18s primers.

PCR analysis

PCR analyses, were performed using "GoTaq® G2 Flexy DNA Polymerase" by Promega. The reaction mix was prepared in a total volume of 10 µl, as reported in Table 3.

COMPONENT	VOLUME FOR 10 µl TOTAL	FINAL CONCENTRATION
H_2O	4.25 µl	
5X GoTaq® Flexi Buffer	2 µl	Na^+ 50 mM
$MgCl_2$ 25 mM	1 µl	2.5 mM
Betaine 5 M	0.9 µl	450 mM
dNTPs 10 mM	0.2 µl	0.2 mM
Forward primer 10 mM	0.3 µl	0.3 mM
Reverse primer 10 mM	0.3 µl	0.3 mM
Taq	0.05 µl	0.025 U/µl
DNA		Up to 100 ng/µl

Table 3. Protocol exploited for PCR analysis in this work. For every component are reported the volume used for 10 µl final volume, and the final working concentration.

Reactions were performed following the protocol provided by the manufacturer. Annealing temperatures (T_a) and extension times ($Time_{ext}$) were according to the pair of primers used. Primers were designed using the NCBI "Primer blast" online software. All the primers sequences used in this work are shown in Table 4. PCR conditions for each primer pair set are shown in Table 5.

NAME	GENE NAME	GENE ID (NCBI)	ORGANISM	SEQUENCE (5' – 3')	T_M (°C)
AW-F	*Fdl1*	GRMZM2G056407	*Zea mays*	CCACACAACATGCAACTTGC	58
AW-R				CCACACAACATGCAACTTGC	60
ConsFdl-2				CAAGAACTACTGGAACACGC	58
ORP1F	*Orp1*	GRMZM2G169593		GAGGGCTGTACATTCTGGGA	62
ORP1R				GACAGCGTGACTGATCAGGA	62
18s F	*18s*	AF168884		GGAGCCATCCCTCCGTAGTTAGCTTCTT	68
18s R				CCTGTCGGCCAAGGCTATATACTCGTTG	68
ZmEF1a_qPCR_F1	*Ef1α*	GRMZM2G153541		TGGGCCTACTGGTCTTACTACTG	61
ZmEF1a_qPCR_R1				ACATACCCACGCTTCAGATCCT	62
Mac1-F	*Act1*	GRMZM2G126010		TCCTGACACTGAAGTACCCGATTG	60
Mac1-R				CGTTGTAGAAGGTGTGATGCCAGTT	60
Glossy1F	*Glossy1*	GRMZM2G114642		TTCCTTATATCGGCGCTCAC	57
Glossy1R				CTTGTCGATCTGGTCGAAGT	57
Glossy2NF	*Glossy2*	GRMZM2G098239		AACGAGATGAAGGTCGGGTA	57
Glossy2NR				CACATCACTAGTCACGCCTC	60
Glossy4F	*Glossy4*	GRMZM2G478147		GTTATGGCGAGGAACTGAGG	58
Glossy4R				CCGACCTGGATTTCGTTTCT	57
Glossy8F	*Glossy8a*	Zm00001d017111		CGGACTTTCGTGCTCGACTT	60
Glossy8R				ACGGAGTAGAGCGGATCAGA	59
Glossy13F	*Glossy13*	GRMZM2G118243		CGGCACAGGGATTCTAGGAG	59
Glossy13R				AACCGAAGGCATGCTGAGTA	59
Spm1-R			*Zea mays* transposable element	CGTCGGTTTCATCGGGACC	58
FUM1-F	*Fum1*	XM_018886754	*Fusarium verticillioides*	GGATTGGCTTGATCTTCACAG	65
FUM1-R				GAAGATGGCATTGATTGCCTC	65
UBICEF	*Ubice*	EH186329.1	*Eragrostis curvula*	AAGGAGCTCAAGGACCTGCAGAAA	62
UBICER				TCACTAAGAACACACCACCGGCAT	62
EC_FDL1_F1	*EcFdl1*			GCTTCTCCTCCTGGTCAGTG	60
EC_FDL1_R1				TCACTTTACACGCTCCCACA	60
EC_FDL1_F2				TGAGGTGCGTGTTCCAGTAG	60
EC_FDL1_R2				CGTCCTCGTCTCCTACATCC	60
EC_FDL1_F3				ATCCGCGAGATGTTGTCC	59
EC_FDL1_R3				CTACTGGAACACGCACCTCA	60
EcFDL_IT1F				TCACTTTACACGCTCCCACA	57
EcFDL_IT1R				GCTTCTCCTCCTGGTCAGTG	61
EcFDL_IT3F				CTACTGGAACACGCACCTCA	59
EcFDL_IT3R				ATCCGCGAGATGTTGTCC	56

Table 4. PCR primers used in this work. Primers are shown individually. For every primer is reported the melting temperature (T_m) calculated, the sequence and the correspondent gene.

PRIMERS COUPLE	GENE NAME	ORGANISM	T_A (°C)	PRODUCT LENGTH (BP) (GENOMIC/CDNA)	$TIME_{EXT}$ (S)
AW-F – AW-R	*Fdl1*	*Z. mays*	58	562/414	40
ConsFdl-2F – AW-R	*Fdl1*	*Z. mays*	58	692	40
ConsFdl-2F – Spm1-R	*Fdl1*	*Z. mays*	58	309	30
ORP1F – ORP1R	*Orp1*	*Z. mays*	62	598/525	40
18sF – 18sR	*18s*	*Z. mays*	68	155	20
ZmEF1a_qPCR_F1 – ZmEF1a_qPCR_R1	*Ef1α*	*Z. mays*	60	135	20
FUM1-F – FUM1-R	*Fum1*	*F. verticillioides*	65	355	25
Mac1-F – Mac1-R	*Act1*	*Z. mays*	60	84	15
Glossy1F – Glossy1R	*Glossy1*	*Z. mays*	55	562/414	40
Glossy2NF – Glossy2NR	*Glossy2*	*Z. mays*	55	506	30
Glossy4F – Glossy4R	*Glossy4*	*Z. mays*	55	427	30
Glossy8F – Glossy8R	*Glossy8a*	*Z. mays*	55	305	25
Glossy13F – Glossy13R	*Glossy13*	*Z. mays*	55	839/488	50/30
UBICEF – UBICER	*Ubice*	*E. curvula*	60	136	20
EC_FDL1_F1 – EC_FDL1_R1	*EcFdl1*	*E. curvula*	59	438/305	30/20
EC_FDL1_F2 – EC_FDL1_R2	*EcFdl1*	*E. curvula*	59	528/269	30/15
EC_FDL1_F3 – EC_FDL1_R3	*EcFdl1*	*E. curvula*	59	315	25
EcFDL_IT1F – EcFDL_IT1R	*EcFdl1*	*E. curvula*	62	438/305	30/20
EcFDL_IT3F – EcFDL_IT3R	*EcFdl1*	*E. curvula*	56	315	20

Table 5. Couple of PCR primers used in this work. Primers are shown associated in pairs, as they were used in PCR analysis. For every couple are reported the annealing temperature (T_a) used for reactions, the amplified region length, and the extension time ($Time_{ext}$).

Furthermore, for genes analysed in this work whose sequence is known, the gene model is reported in Figure 8 and Figure 9.

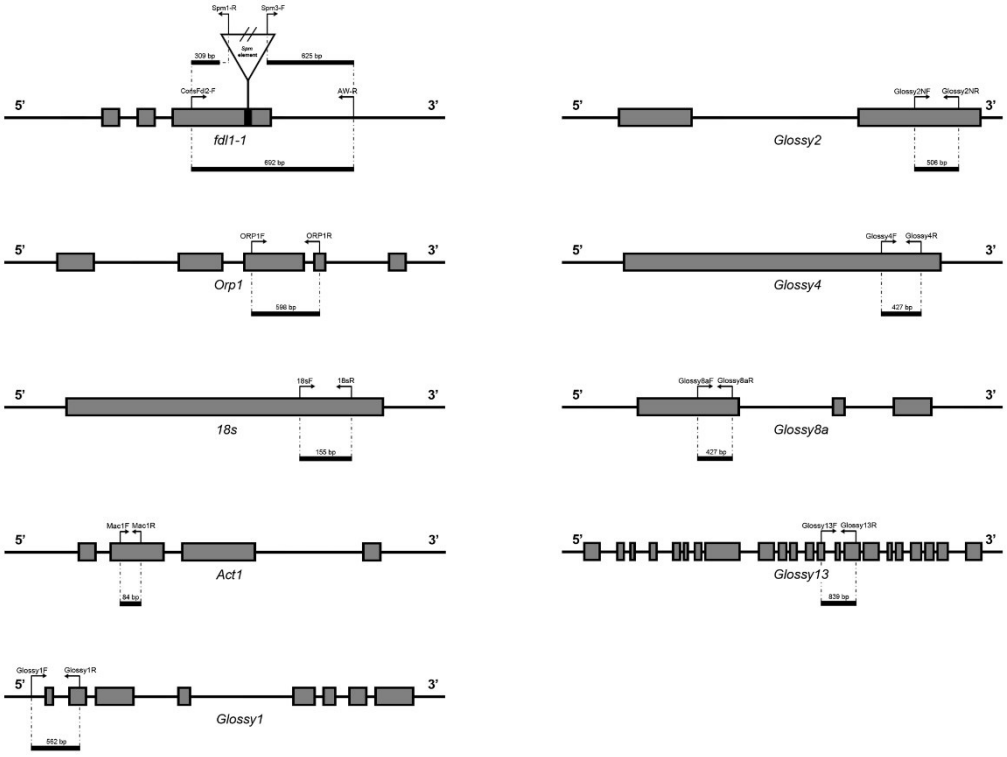

Fig 8. Gene models for all the *Zea mays* genes analysed in this work. All the genes are oriented in 5' – 3' direction. Exons are represented in grey boxes, introns and untranslated parts are represented with a black line.

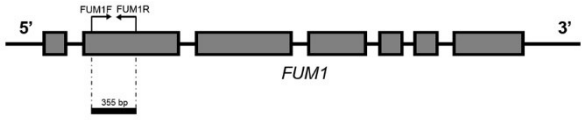

Fig 9. Gene models of *Fusarium verticillioides FUM1* gene analysed in this work. The gene is oriented in 5' – 3' direction. Exons are represented in grey boxes, introns and untranslated parts are represented with a black line.

PCR products were separated by electrophoresis in 1% agarose gels stained with 0.5 µg/ml final concentration of ethidium bromide.

Real-time qPCR reactions

For all the Real-time qPCR, 2 µl of each cDNA samples were used in a final volume of 20 µl containing 10 µl of iQ SYBR Green Supermix and 0.25 µM of each primer. The primers used were AW-F and AW-R, designed on *fdl1* gene. Amplifications were carried out using an iCycler thermocycler equipped with the MyiQ detection system (Bio-Rad, Milano, Italy) in 96-well optical reaction plates sealed with optical tapes (Bio-Rad). The reaction conditions were as follows: 96 °C for 30 s, 40 cycles 96 °C for 30s, 58°C for 30s, 72 °C for 30s.

Data are presented as the mean of two biological replicates and three technical replicates. The absence of nonspecific amplified products was checked with derivative melting curves, obtained by progressive heating at 0.3 °C every 15 s. Raw data were collected and analysed with the iQ5 software (Bio-Rad, Milano, Italy) with the following parameters: baseline from the 2^{nd} to the 10^{th} cycle and threshold calculated automatically by the software for every reaction. Differences in gene expression were calculated by the comparative delta-delta CT method (Schmittgen and Livak 2008) with a dedicated Microsoft Excel macro created by Bio-Rad. All quantifications were normalized to the housekeeping gene *EF1α*.

RNAseq analysis

For the transcriptome sequencing analysis (RNAseq) plants originated from the same segregating ear were used. Plants were grown in growing chamber, and the samples were collected at coleoptile stage of growth. Each plant was genotyped using DNA extracted from the root. Wild type and mutant seedlings selected were homozygous for the *Fdl1* allele, and homozygous for the *fdl1-1* allele respectively.

The experiment comprised three biological replicas from each genotype. Each replica was constituted from a pool of 3 plants.

Sequencing was performed at IGA Technology Services S.r.l. (Udine, Italy) with Illumina Hiseq 2500 (20M reads, depth 50bp).

Data from sequencing were analysed with three different algorithms: Cuffdiff, Limma and DESeq2 (Trapnell *et al.* 2012; Love *et al.* 2014; Ritchie *et al.* 2015).

Cloning of Eragrostis genomic fragment

Ligations of DNA amplified fragments inside T-vector were performed using the Promega "pGEM®-T" ligation kit, following the protocol provided by the manufacturer. Recombinant vectors were transformed into JM109 High-efficiency competent *E. coli* cells (Promega). Transformation procedures were performed following the protocol provided by the manufacturer. *E. coli* cells were growth in solid or liquid medium (0.5% yeast extract, 1% tryptone, 5M NaCl, pH 7, 1.5% agar). For cells selection in Petri dishes, 100µg/ml Ampicillin, 0.5mM IPTG, 80µg/ml x-gal were added to the medium.
Following overnight incubation in Petri dishes, selected colonies were transferred in liquid medium containing ampicillin, and incubated overnight at 37°C.

Plasmid extraction and isolation of insert DNA sequence

T-vector was extracted from *E. coli* cells using the Promega "Wizard® Plus SV Minipreps DNA Purification System" kit, following the protocol provided by the manufacturer.
Insert DNA sequences were extracted from T-vector using the Promega "Assembly of Restriction Enzyme Digestions" kit, following the protocol provided by the manufacturer.

RESULTS

Part 1: *fdl1* regulated genes

Selection and transcriptional analysis of genes putatively regulated by *ZmMYB94/fdl1*

The *ZmMYB94/fdl1* gene belongs to the family of MYB transcription factors (La Rocca *et al.* 2015) and it is presumably involved, directly or indirectly, in the regulation at the transcriptional level of a group of genes. A first strategy adopted in this work for the detection of these genes was based on a "candidate genes approach".

The phylogenetic analysis of *fdl1* (*ZmMYB94*) performed in a previous work (La Rocca *et al.* 2015) indicated that the most closely related genes in *A. thaliana* are *AtMYB30, AtMYB94* and *AtMYB96*.

Arabidopsis genes known to be regulated by these MYB factors were thus selected from studies carried out in this system (Raffaele *et al.* 2008; Seo *et al.* 2011; Lee *et al.* 2016). In addition, since *fdl1-1* shows clear alterations in epicuticular waxes composition and structure, the selection was restricted to genes involved in epicuticular waxes biosynthesis. Each Arabidopsis gene found in this way was used as query for a BLAST search on the *Z. mays* genome, using the BLAST tool from NCBI and MaizeGDB.org.

In this way a total of 17 maize genes, all putative orthologous of genes regulated by *AtMYB30*, *AtMYB94* and *AtMYB96* in Arabidopsis were found (Tab. 9).

Arabidopsis			Maize	
NCBI ID	**NAME**	**ROLE**	**MAIZEGDB ID**	**NAME**
AT1G01120	*KCS1*	β-ketoacyl-CoA synthase 1	GRMZM2G149636	
ATIG01610	*GPAT4*	Glycerol-3P acyl transferase	GRMZM2G083195	
ATIG07720	*KCS2*	β-ketoacyl-COA synthase 2	GRMZM2G022558	*FAE2*
ATIG67730	*KCR1*	β-keto acyl reductase	AC205703.4_FG006	*Glossy8*
AT2G26250	*FDH*	β-ketoacyl-COA synthase	GRMZM2G445602	
AT3G55360	*CER10*	Enoyl-COA reductase	GRMZM2G481843	
AT4G00360	*ATT1*	Cytochrome P450 CYP86A2	GRMZM2G062151	
AT4G14440	*HCD1*	Enoyl-CoA hydratase/isomerase	GRMZM2G101457	
AT4G24510	*CER2*	CoA-dependent acyl transferase	GRMZM2G098239	*Glossy2*
AT5G47330	*PPT1*	Palmitoyl thioesterase	GRMZM2G374779	
AT5G10480	*PAS2*	Tyrosine phosphatase-like protein	GRMZM2G151087	
AT5G57800	*CER3*	Fatty acids reductase putative	GRMZM2G114642	*Glossy1*
AT4G39330	*CAD9*	Cinnamyl alcohol dehydrogenase 9	GRMZM2G090980	
AT1G08810	*ATMYB60*	Myb transcription factor	GRMZM2G162434	*Glossy 3*
AT4G36920	*APETALA 2*	DNA-binding, integrase-type	GRMZM2G160730	*Glossy 15*
AT1G68530	*CER6*	3-ketoacyl-CoA synthase	GRMZM2G478147	*Glossy4*
AT2G26910	*ABCG32*	ABC-2 type transporter	GRMZM2G118243	*Glossy13*

Table 9. List of genes regulated by *AtMYB30*, *AtMYB94*, *AtMYB96* and involved in epicuticular waxes biosynthesis in *A. thaliana*. For every gene is reported NCBI GenBank ID, name in *A. thaliana,* role and the putative orthologous in *Z. mays*. For every orthologous gene is reported MaizeGDB ID and, when exist, the gene name.

From the list of genes shown in Table 9, a sub list of genes was selected, which fulfilled the following two criteria:

- Genes that are involved in specific steps of the cuticle biosynthetic pathway and that appeared to be defective in the homozygous *fdl1-1* mutant (Persico 2015).
- Genes that exhibit a spatial and temporal expression pattern similar to that of *fdl1* (Sekhon *et al.* 2011).

Eight maize genes were selected in this way, which were considered as putatively regulated by *fdl1*. Genes are shown in Table 10.

ARABIDOPSIS ID	ARABIDOPSIS NAME	MAIZE ID	MAIZE NAME	PRODUCT
AT4G24510	*CER2*	GRMZM2G098239	*Glossy2*	CoA-dependent acyl transferase
AT5G57800	*CER3*	GRMZM2G114642	*Glossy1*	Fatty acids reductase putative
AT1G68530	*CER6*	GRMZM2G478147	*Glossy4*	3-ketoacyl-CoA synthase
ATIG67730	*KCR1*	AC205703.4_FG006	*Glossy8*	β-ketoacyl-CoA reductase
AT5G10480	*PAS2*	GRMZM2G151087		Very-long-chain (3R)-3-hydroxyacyl-CoA dehydratase
AT3G55360	*CER10*	GRMZM2G481843		Very-long-chain enoyl-CoA reductase
AT2G26910	*ABCG32*	GRMZM2G118243	*Glossy13*	ABC-2 type transporter
AT1G04220	*KCS2*	GRMZM2G022558	*FAE2*	3-ketoacyl-CoA synthase

Table 10. List of genes regulated by *AtMYB30*, *AtMYB94* and *AtMYB96* that fulfil both the criteria: with an expression pattern similar to *fdl1*, and involved in the cuticle biosynthesis pathway defective in homozygous *fdl1-1* mutant (Persico 2015). Arabidopsis ID (NCBI), Arabidopsis name, Maize ID (NCBI), Maize name and putative role are reported for each gene.

As indicated in Table 10, six maize genes are associated to a specific name and have been characterized. The remaining two, corresponding to Arabidopsis *PAS2* and *CER10* have not been characterized in maize and are described only by the gene ID.

From the genes reported in Table 10, five glossy genes were selected as candidates. This choice was done because these mutants, which were characterized in detail in previous studies, showed similarities to the homozygous *fdl1-1* mutant. Indeed, all these mutants show

an alteration in the epicuticular wax deposition during the juvenile phase. Due to this alteration, both *glossy* and homozygous *fdl1-1* mutants, if sprayed with water retained drops on the leaf surface (Fig. 10).

Figure 10. Leaf phenotype of maize seedlings. At the left is shown the second leaf of a wild type plant. At the right is shown the second leaf of a homozygous *fdl1-1* mutant plant. Retained water beads are visible on the leaf surface of *fdl1-1* mutant. Photo modified from La Rocca *et al*. 2015.

Genetic analysis of the interaction between the *fdl1-1* and *glossy* mutants

A genetic approach can also be adopted to explore the relationship between two different genes involved in the same process. This implies the analysis of phenotypic classes and their segregation ratio in F_2 progenies in which both mutants are segregating. Data obtained allow to verify either their independent action or the presence of interaction between that two genes under study.
In this study, we have planned to test the interaction between *fdl1* and other maize genes involved in wax deposition. In particular we chose *glossy2* (*gl2*) and *glossy13 (gl13)*.

The ***fused leaves 1* (*fdl1*) mutant** shows developmental defects, such abnormal coleoptile opening, and presence of fusions between the coleoptile and the first leaf or between the first and the second leaf. Electronic microscope analysis show defects in cuticle deposition on epidermal cells, as well as a reduction of epicuticular waxes on the juvenile leaves surface (La Rocca *et al.* 2015) (Fig. 11A).

The ***glossy2* (*gl2*)** mutant phenotype is characterized by a reduction in the amount of surface waxes on the first six leaves to one-fifth compared with wild type levels. Wax crystalloids on the surface of the first six leaves show a grain shape instead of the various shapes, such as spikes, rodlets and plates that are visible present in wild type leaf epidermis (Tacke *et al.* 1995). Because of these alterations, the first six leaves of the mutant show a glossy appearance, compared with the dull appearance of the wild type. Furthermore, water beads remain adherent on the surface of the juvenile leaves (Fig. 11B).

The ***glossy13* (*gl13*)** mutant shows epicuticular wax crystals on the leaves significantly disorganized and, after dissection, leaf sections show a higher water loss rate compared with wild type. Because of these alterations also the *gl13* mutant, similarly to *gl2*, shows a glossy appearance on the first six leaves, with water beads that remains adherent on the surface of the juvenile leaves. Furthermore, *gl13* mutant seedlings show necrotic glossy leaves at the third leaf stage, and is lethal (Li *et al.* 2013) (Fig. 11C).

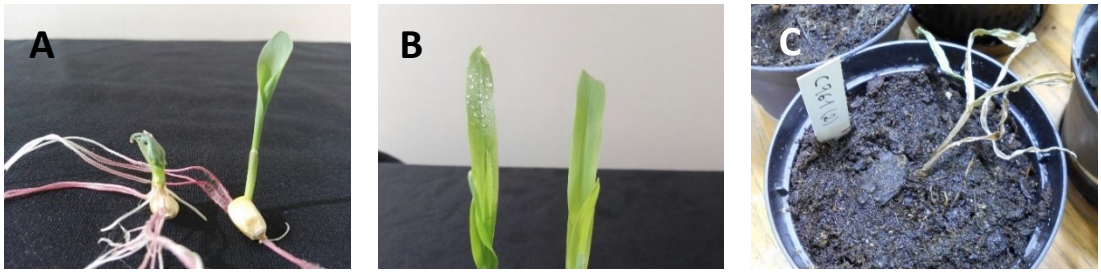

Figure 11. A) *fdl1-1* mutant seedling at the second leaf stage (left) compared with a wild type plant at the same development stage (right). Fusions between leaves and coleoptile are evident in *fdl1-1* mutant. B) *glossy2* mutant seedling at the third leaf stage (left) compared with a wild type plant at the same development stage (right). In the photo is possible to see the water beads retained on the leaf surface of *glossy2* mutant. C) *glossy13* mutant seedling, death at the third leaf stage of growth.

F_1 plants were produced by crossing a heterozygous plant carrying the *fdl1-1* allele (+/*fdl1-1*) and a homozygous *gl2/gl2* plant or a +/*gl13* heterozygous plant. F_1 plants were subsequently self-pollinated to produce F_2 progeny ears. Forty seeds of each F_2 progeny were germinated on filter paper and seedlings were examined by visual scoring to determine their phenotype. Results are reported in Tables 11 and 12.

Eleven F_2 progenies were detected that segregated for both fdl1 and gl2 phenotypes and were therefore produced by selfing +/*gl2* +/*fdl1-1* double heterozygous plants, (Table 11).

		PROGENIES (EXPECTED)		PROGENIES (OBSERVED)	
GENOTYPES CROSSED TO OBTAIN THE F_1 PROGENY	TOTAL	Segregating *fdl1-1* and *glossy*	Segregating only *glossy*	Segregating *fdl1-1* and glossy	Segregating only *glossy*
(+/*fdl* ^3 B73 x *gl2*/*gl2*)	27	13.5	13.5	11	16

Table 11. F_2 progenies, obtained through self-pollination of F_1 plants. F_1 plants were obtained by crossing plants heterozygous for the *fdl1-1* mutation with plants homozygous for *glossy2* mutation. *fdl*: *fdl1-1* allele; *gl2*: *glossy2* allele.

Twelve F_2 progenies were detected that segregated for both fdl1 and gl13 phenotypes and were therefore produced by selfing +/*gl13* +/*fdl1-1* double heterozygous plants (Table 12).

GENOTYPES CROSSED TO OBTAIN THE F_1 PROGENY	TOTAL	PROGENIES SEGREGATING (EXPECTED)				PROGENIES SEGREGATING (OBSERVED)			
		WT	Only *glossy*	Only *fdl1-1*	*fdl1-1* and *glossy*	WT	Only *glossy*	Only *fdl1-1*	*fdl1-1* and *glossy*
(H99/*fdl* x +/*gl13*)	19	4.75	4.75	4.75	4.75	1	5	2	11
(B73/*fdl* 3^ x +/*gl13*^{c})	3	0.75	0.75	0.75	0.75	2	0	0	1

Table 12. Summary of the analysis performed on F_2 progenies obtained through self-pollinating of F_1 progenies. F_1 were obtained crossing heterozygous plants for *fdl1-1* mutation with heterozygous plants for *glossy13* mutation. *fdl*: *fdl1-1* allele; *gl13*: *glossy13* allele.

In F_2 progenies segregating for both fdl1-1 and gl2 mutant phenotypes, a deeper analysis was performed at the seedling developmental stage through visual scoring of F_2 plant phenotypes. Four phenotypic classes were detected, comprising the wild type class and three distinct mutant classes, referred to as *fdl1-1*, *glossy2* and double mutant plants (*fdl1-1*/*fdl1-1 gl2*/*gl2*).

The double mutant phenotypes were selected following the two criteria:

- Plants that showed a clear fdl1-1 phenotype until the third leaf stage
- Plants that maintained a glossy phenotype until the 5 – 6 leaf stage

These plants showed a clear fdl1-1 phenotype at early stage of development and a typical glossy phenotype at later stages (Fig.12).

Figure 12. Comparison between a juvenile leaf of a wild type plant and the equivalent in a double mutant *fdl1-1 - gl2* at the sixth leaf stage. On the leaf surface of the putative double mutant is possible to observe the water beads retained, which are not present on the wild type leaf surface.

To analyse the segregation ratio, data from all the different F_2 families segregating for both *fdl1-1* and *glossy2* mutant phenotypes (Table 11) were pulled together. When tested for fit to a **9** (wt) : **3** (fdl1-1) : **3** (gl2) : **1** (fdl1-1 gl2) segregation, the calculated X^2 value (0.19) confirmed the segregation hypothesis.

Also in F_2 progenies segregating for both fdl1-1 and gl13 mutant phenotypes, the visual scoring identified four phenotypic classes, comprising the wild type class and three distinct mutant classes, referred to as *fdl1-1*, *glossy13* and double mutant plants (*fdl1-1*/*fdl1-1 gl13*/*gl13*).

The double mutant phenotypes were selected following the two criteria criteria:

- Plants that showed a clear *fdl1* phenotype until the third leaf stage
- Plants showing lethality after the third leaf stage

These plants showed a clear fdl1-1 phenotype until the third leaf stage, then started to necrotize and die. The visual analysis of these plant population indicated that both fdl1-1 and glossy13 phenotypes were present (Fig. 13).

Figure 13. Comparison between *fdl1-1 - glossy13* putative double mutant plants and *fdl1-1* mutants. Putative double mutants died after the third leaf stage of growth. *fdl1-1* mutant plants growth at fourth leaf stage show a wild type phenotype.

Also in this case, to analyse the segregation ratio, data from all the different F_2 families segregating for both *fdl1-1* and *glossy13* mutant phenotypes (Table 12) were pulled together. When tested for fit to a **9** (wt) : **3** (fdl1-1) : **3** (gl2) : **1** (fdl1-1 gl2) segregation, the calculated X^2 value (0.71) confirmed the segregation hypothesis.

On the basis of the segregation values observed in the F_2 progenies, we hypothesize that *fdl1* has an independent action from both *glossy2* and *glossy13*. Accordingly, the putative double mutants (*fdl1-1*/*fdl1-1 gl2*/*gl2* and *fdl1-1*/*fdl1-1 gl13*/*gl13*) show both the fdl1 and glossy phenotypes.

Semi quantitative expression analysis on candidate genes

To verify if the expression level of the five candidate genes varies in wild type and homozygous *fdl1* mutant tissues, a semi-quantitative RT-PCR analysis was performed.

cDNA samples were prepared from RNA extracted from wild type and homozygous *fdl1-1* mutant seedlings at coleoptile stage, and *glossy1, glossy2, glossy4, glossy8 and glossy13* transcripts level was assayed in two replicates (Fig. 14). The *orange pericarp 1* (*orp1*) gene was used as internal standard.

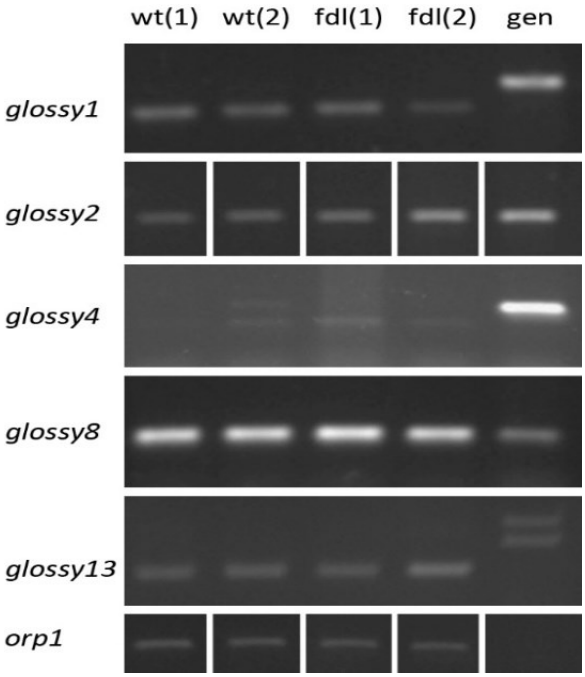

Figure 14. Semi quantitative RT-PCR analysis of the 5 candidate genes selected as putatively regulated by *fdl1*. For every gene, bands referred to two repetitions on wild type cDNA, and two repetitions on homozygous *fdl1-1* mutant cDNA are shown. On the right, the amplification on genomic DNA per each sample is shown. The last lane is referred to *orp1* gene, used as internal standard.

Figure 14 illustrates the obtained amplification products. As is shown, of the five genes analysed no one shows a remarkable change in its transcript level between wild type and homozygous *fdl1-1* mutant plant.

Whole transcriptome analysis

To obtain information about the genes whose activity is either directly or indirectly regulated by the *fdl1* action, an RNAseq analysis was performed. This experiment was conducted using libraries prepared from wild type and homozygous *fdl1-1* mutant seedlings at the coleoptile stage of growth. Indeed, previous expression analysis demonstrated that the expression level of *fdl1* is higher in this phase of growth, and decreases in subsequent stages (La Rocca *et al.* 2015).

A total of 1638 genes was found differentially expressed in the homozygous *fdl1-1* mutant compared with the wild type plant. Only genes with significantly different expression level were considered ($P < 0.05$). Our analysis showed that 990 out of these 1638 genes are up-regulated, while 648 are down regulated in *fdl1-1*.

To obtain functional information about these genes, a database search was done exploiting maizeGDB.org and Gramene.org. In particular, the group of sequences up and down regulated in *fdl1-1* comprise different classes, as is shown in Table 14.

Category	**UP REGULATED**	**DOWN REGULATED**
Genes involved in cuticle biosynthesis and deposition	24	38
Genes involved in plant clock regulation	5	20
Genes involved in plant – pathogen interaction	29	11
Genes involved in hormones metabolism and signalling		
Auxin	10	13
Gibberellin	4	10
Abscisic acid	7	7

Table 14. Genes whose expression was found UP and DOWN regulated in *fdl1-1* compared with wild type plants in the RNAseq analysis were grouped in different categories.

Main defects observed in *fdl1-1* mutant seedlings at the cellular level were cell wall fusion, due to a partial absence of cuticle, and altered epicuticular waxes deposition. On this basis, further analyses were restricted to the group of genes involved in cuticle biosynthesis and

deposition. Indeed, one of the main objectives of this work was to unravel the genetic mechanisms responsible for cuticle deposition and related to the action of *fdl1*.

Figure 15 shows the genes involved in cuticle biosynthesis and deposition detected in this work.

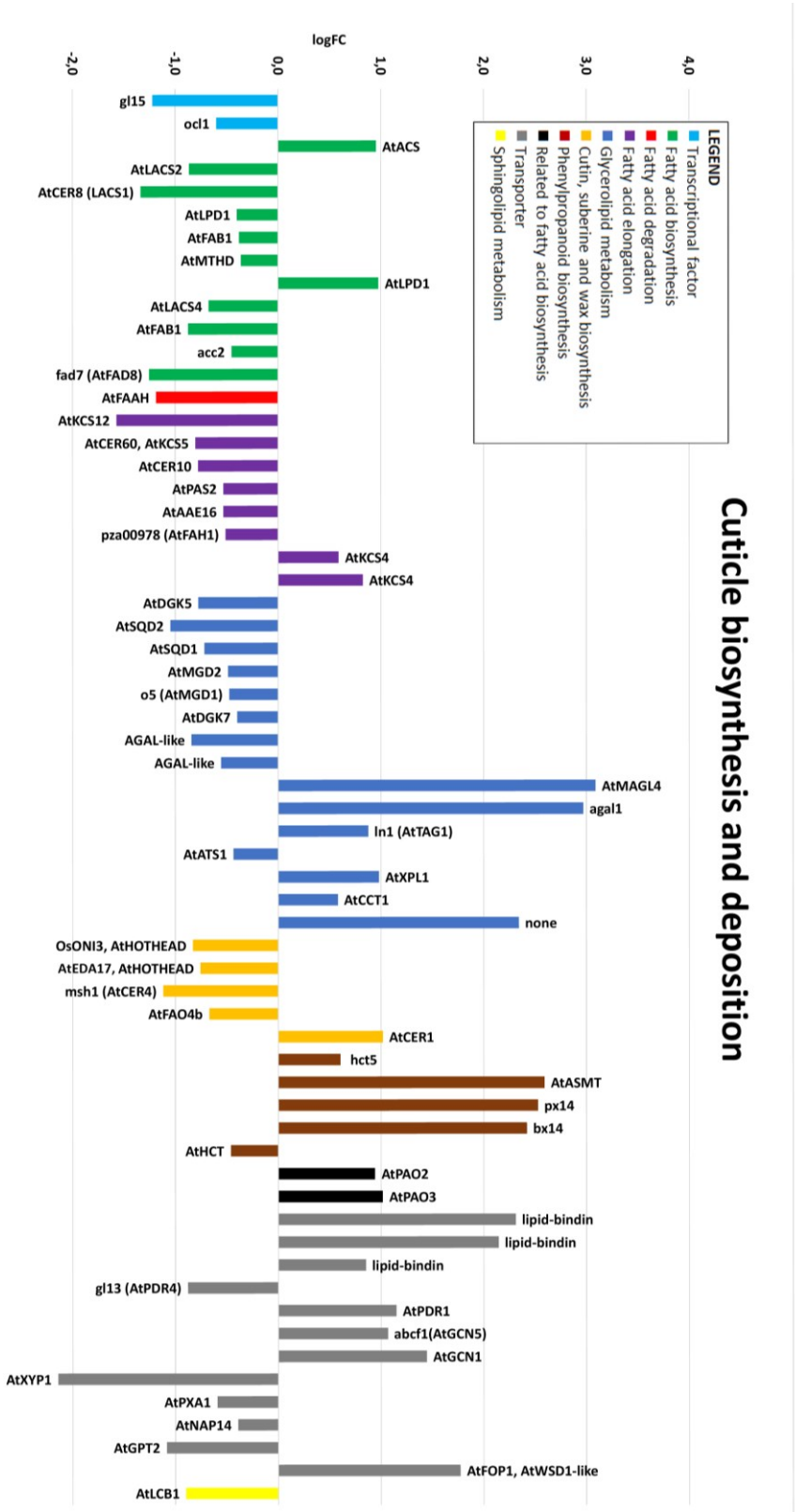

Figure 15. UP and DOWN regulated genes in *fdl1* compared with wild type and involved in processes correlated to cuticle biosynthesis and deposition. The legend shows the colour code used to classify all the genes in functional subgroups. Genes with a logFC parameter upper than zero are considered UP regulated, while genes with a logFC lower than zero are considered DOWN regulated. MaizeGDB ID and the gene name, if available, are reported for each gene. When gene name is not yet present in the maize database, the name of the putative orthologous in *A. thaliana* (prefix At), or *O. sativa* (prefix Os) are reported.

All the genes reported in Figure 15 were used as queries for a search in the KEGG database, in order to find information about the role that they have in the pathway in which they are involved. For nine of them, it was possible to find information on the role in different pathways. Position and role of these genes are described in the next paragraph.

To better understand the effect of the *fdl1-1* mutation on cutin and wax composition, chromatographic analyses were performed in a previous work in collaboration with Dr. Frédéric Domergue, Laboratoire de Biogenese membranaire, University of Bordeaux, France (Persico 2015).

Chemical analyses were performed on wild type and *fdl1-1* mutant plants at different stages of growth, following the protocol described by Bourdenx *et al.* 2011.

In the present work, chemical data were reinterpreted and correlated with transcriptome data. Data are presented in the next paragraphs in which they are referred to specific cuticular components and related pathways.

Fatty acid elongation

The fatty acid elongation pathway (FAE) (Fig. 16), starting from C16 or C18 acyl-CoA and Malonyl-CoA synthesize most of the saturated fatty acid in plants, from arachidic acid (C20 carbon chain length) to hexatriacontanoic acid (C36). In each cycle FAE makes a successive addition of two carbons, derived from malonyl-CoA, and produce VLCFAs.

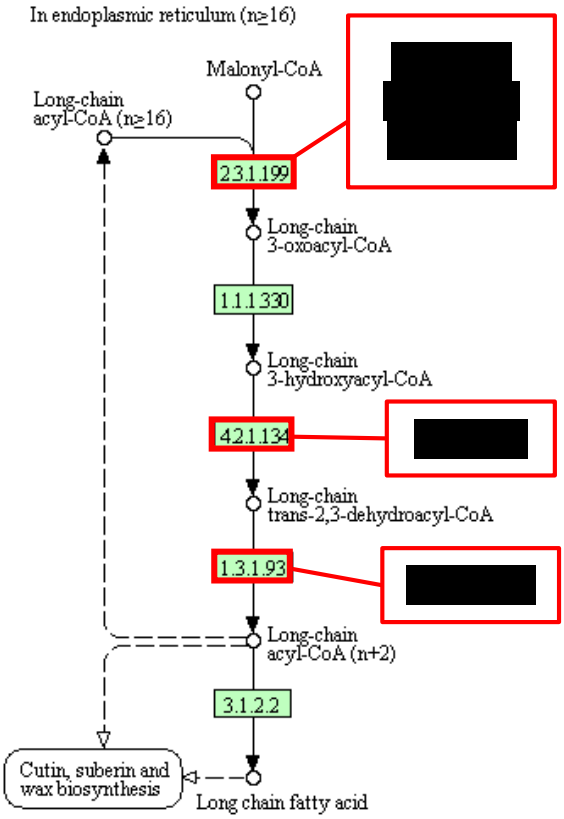

Figure 16. Schematically representation of the *Zea mays* fatty acid elongation pathway, obtained from the KEGG database (http://www.genome.jp/keg; modified). Boxes represent enzymes involved in the pathway. Green boxes are referred to genes described in maize. White boxes are referred to genes already known in other species and predicted in maize. Codes inside boxes are referred to the enzyme family correspondent. Boxes marked in red correspond to enzymes whose expression is altered in *fdl1-1* mutant. Up arrow represents genes upregulated in *fdl1-1*. Down arrow represents genes downregulated in *fdl1-1*.

Five genes encoding enzymes of the FAE complex have an altered expression level in homozygous *fdl1-1* mutant seedlings.

Three differentially expressed genes, *AtKCS4*, *AtKCS12* and *AtCER60*, are involved in the first step, and encode for Acyltransferases enzymes. Multiple forms of Acyltransferases exist with differing preferences for the substrate, and thus the specific form expressed determines the

local composition of very-long-chain fatty acids (Blacklock and Jaworski 2006; Denic and Weissman 2007). The specific substrates of *AtKCS4*, *AtKCS12* and *AtCER60* enzymes have not been characterized. However, it is reported that *AtCER60* is involved in the synthesis of C24:0, C26:0 and C28:0 fatty acids (Haslam and Kunst 2013).

AtPAS2, which appears downregulated in *fdl1-1* seedlings, is involved in the third part of the FAE, and encode for a Hydro-lyase.

The last gene identified in the FAE pathway, *AtCER10*, is involved in the fourth step of elongase and appear downregulated in *fdl1-1*. The enzyme encoded belongs to the class of Oxidoreductase.

In summary, three steps over four of the fatty acid elongation pathway appears to be altered in *fdl1-1*. Four genes were found to be downregulated, and only one upregulated.

The consequences of this general downregulation are visible in the results of chemical analysis of fatty acids, which show a strong quantitative increment of C16:0 in *fdl1-1* mutants and a little increment for C18:0 in *fdl1-1* mutant compared with wild type.

Differently, the analysis does not show an altered amount of C22:0 and C24:0 in mutant versus wild type samples (Fig. 17). In our opinion, the transcriptional downregulation observed can be responsible for the accumulation of substrates (C16 and C18) and may impair the entire biosynthesis of very long-chain fatty acids.

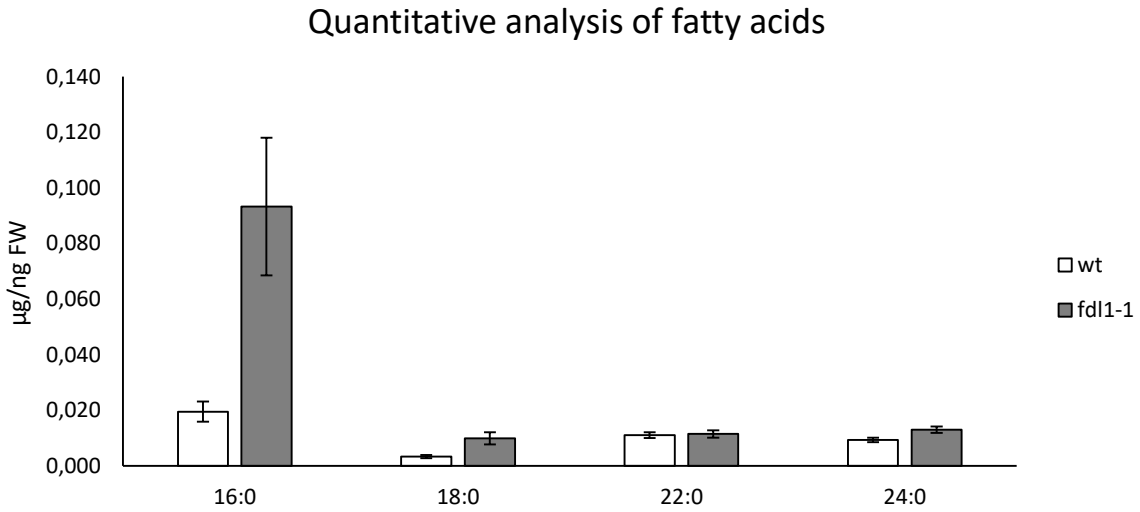

Figure 17. Gas chromatographic analysis of fatty acids extracted from *Zea mays* seedlings at the first developmental stage (coleoptile stage). The analysis was done by Martina Persico Ph.D., and reported in: Persico M., A forward genetics approach to study seed and seedling development in maize, Ph.D. thesis, 2015. For every compound is reported the amount (µg/ng of fresh weight) measured. wt: wild type genotype. fdl1-1: homozygous *fdl1-1* genotype. Error bars show Standard Error.

Cutin and suberin biosynthesis

The biosynthesis of cutin and suberin (Fig. 18) exploit as substrate very long-chain acyl-CoAs from fatty acid elongation and from the biosynthesis of unsaturated fatty acids pathways. Cutin in particular, composed of inter-esterified omega hydroxy acids is quantitatively the major component of plant cuticle.

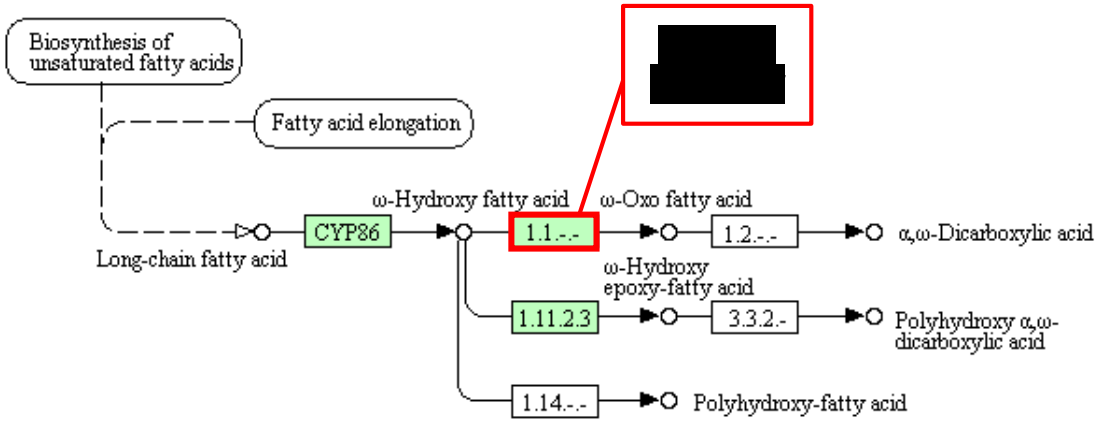

Figure 18. Schematically representation of the *Zea mays* cutin and suberin biosynthesis pathway, obtained from the KEGG database (http://www.genome.jp/kegg). Boxes represent enzymes involved in the pathway. Green boxes are referred to genes described in maize. White boxes are referred to genes already known in other species and predicted in maize. Codes inside boxes are referred to the enzyme family correspondent. Boxes marked in red correspond to enzymes whose expression is altered in *fdl1-1* mutant. Down arrow represents genes downregulated in *fdl1-1*.

Two genes that show an altered expression level in *fdl1-1* are involved in this pathway i.e. *OsONI3* and *AtEDA17*. Both encode for a fatty acid omega-hydroxy dehydrogenase and are involved in the same step of the pathway. The overlap of these two enzymes in the same step has not been investigated. The two enzymes could work with a different preference for the carbon chain length of the substrate.

Also for this pathway, the comparison of these data with gas chromatographic analysis can be useful in order to understand the phenotype of *fdl1-1* (Fig. 19).

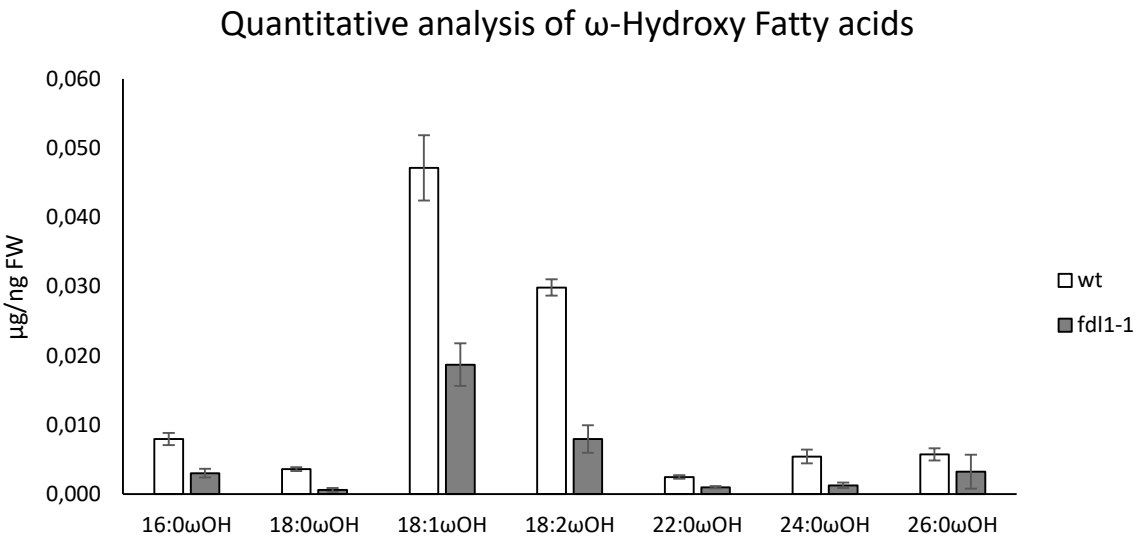

Figure 19. Gas chromatographic analysis of ω-Hydroxy Fatty acids extracted from *Zea mays* seedlings at the first developmental stage (coleoptile stage). The analysis was done by Martina Persico Ph.D., and reported in: Persico M., A forward genetics approach to study seed and seedling development in maize, Ph.D. thesis, 2015. For every compound is reported the amount (µg/ng of fresh weight) measured. wt: wild type genotype. fdl1-1: homozygous *fdl1-1* genotype. Error bars show Standard Error.

ω-Hydroxy Fatty acids, obtained from long chain fatty acids, constitute the first intermediate in cutin and suberin biosynthesis. These compounds are exploited as substrate for all the following reactions of the pathway. Gas chromatographic analysis show a general quantitative decrement for all these compounds analysed.

This decrease could be caused by the alteration observed in the fatty acids elongation pathway. Indeed, FAE synthesises long-chain fatty acids that are exploited as substrate for the biosynthesis of ω-Hydroxy Fatty acids.

Furthermore, in *Oryza sativa ONI3* is required for a correct separation between organs and to avoid organ fusions during seedling development, as shown in the analysis of an *ONI3* knockout that leads to fusions between coleoptile and the first leaves. This mutant also shows severe defects in shoot development and seedling lethality (Akiba *et al.* 2014).

Similarly, a knock-out mutant of *AtEDA17* isolated in *A. thaliana* shows fusions between floral organs and displays reduced fertility (Li-Beisson *et al.* 2013).

In our opinion, both the decreased amount of ω-Hydroxy Fatty acids and the downregulation of *ONI3/EDA17*, can be causative for strong alterations observed in *fdl1-1* mutant cutin.

Wax biosynthesis

The wax biosynthesis pathway (Fig. 20) is divided into two main branches: alkane forming pathway and alcohol forming pathway. Both these branches exploit as substrates fatty acids from fatty acid elongation.

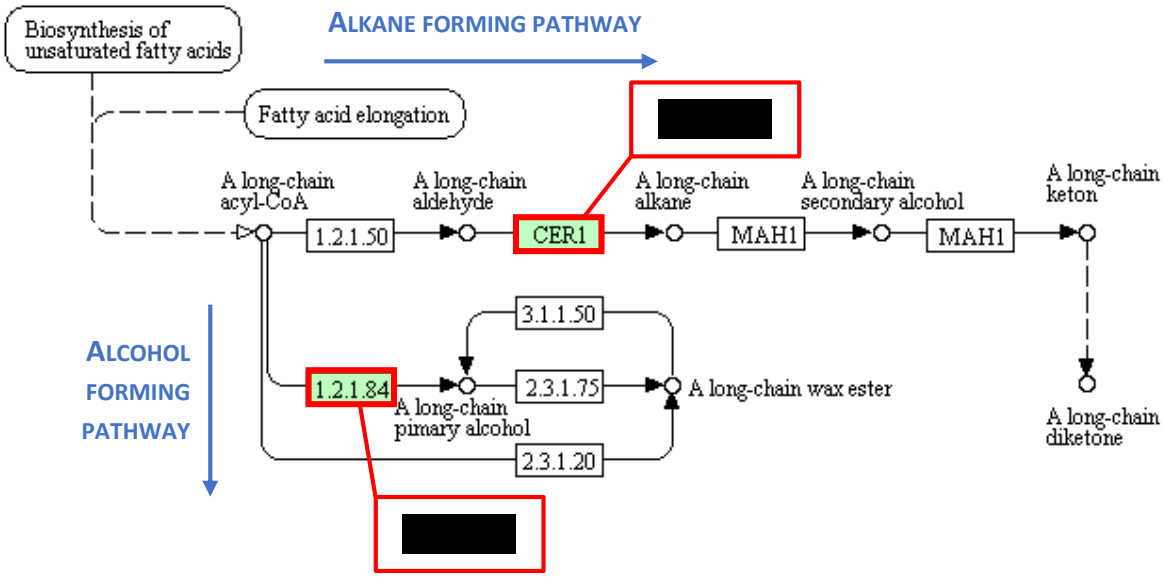

Figure 20. Schematically representation of the *Zea mays* wax biosynthesis pathway, obtained from the KEGG database (http://www.genome.jp/kegg). The image was modified in order to explain the data obtained. Boxes represent enzymes involved in the pathway. Green boxes are referred to genes described in maize. White boxes are referred to genes already known in other species and predicted in maize. Codes inside boxes are referred to the enzyme family correspondent. Boxes marked in red correspond to enzymes whose expression is altered in *fdl1-1* mutant. Up arrow represents genes upregulated in *fdl1-1*. Down arrow represents genes downregulated in *fdl1-1*.

Two genes involved in wax biosynthesis show altered expression in *fdl1-1* compared with wild type.

The first, *AtCER1*, which appears to be upregulated in *fdl1-1*, is involved in the alkane forming pathway. Its product is a long-chain aldehyde alkane-lyase that synthesize a long-chain alkane, using a long-chain aldehyde as substrate. During the reaction, a carbon is removed, transforming even-number aldehydes into odd-number alkanes (Bernard and Joubès 2013).

A gas chromatographic analysis of alkanes and aldehydes done in our laboratory (Fig. 21) show the strong effects that *fdl1-1* mutation has on these classes of compounds.

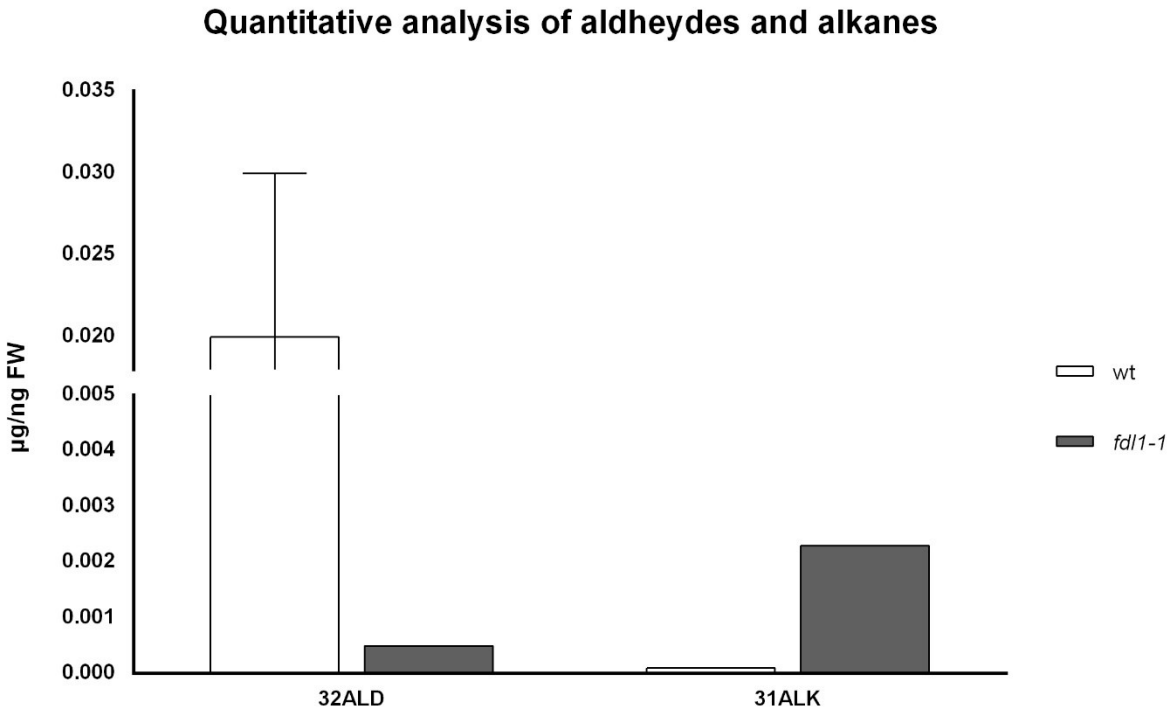

Figure 21. Gas chromatographic analysis of aldehydes and alkanes extracted from *Zea mays* seedlings. The analysis was done by Martina Persico Ph.D., and reported in: Persico M., A forward genetics approach to study seed and seedling development in maize, Ph.D. thesis, 2015. Labels: ALD = aldehydes, ALK = alkane. For every compound is reported the amount (µg/ng of fresh weight) measured. wt: wild type genotype. fdl1-1: homozygous *fdl1-1* genotype. Error bars show Standard Error.

It is possible to see that the total level of 32 aldehyde is strongly lower in the *fdl1-1* mutant compared with the wild type. The level of 31 alkanes, instead, appears higher in the mutant. Indeed, 31 alkanes are produced using 32 aldehydes as substrate, and in particular the aldehyde alkane-lyase encoded by *AtCER1* exploit aldehydes as substrate to synthetize alkanes.

In our opinion, the lower amount of 32 aldehyde and the altered ratio between the two molecules observed in the mutant could be caused by the upregulation of *AtCER1*. A higher expression of this gene can move the chemical equilibrium towards the synthesis of alkanes, consuming almost all the aldehydes in the mutant. This can easily explain also the increment in the amount of 31 alkanes observed in *fdl1-1*.

The second gene, *AtCER4*, is downregulated in *fdl1-1*. *AtCER4* produce a long-chain acyl-CoA reductase, responsible for the first reaction in the alcohol forming pathway. The enzyme produces a long-chain primary alcohol exploiting a long-chain acyl-CoA. Also for this family, multiple forms of reductases exist and each one shows different preferences for the substrate

(Bernard and Joubès 2013). Consequently, the specific form expressed determines the local production of primary alcohols.

Observing data from the gas chromatographic analysis (Fig. 22), is possible to see the strong differences in alcohol found between wild type and homozygous *fdl1-1* mutant plants.

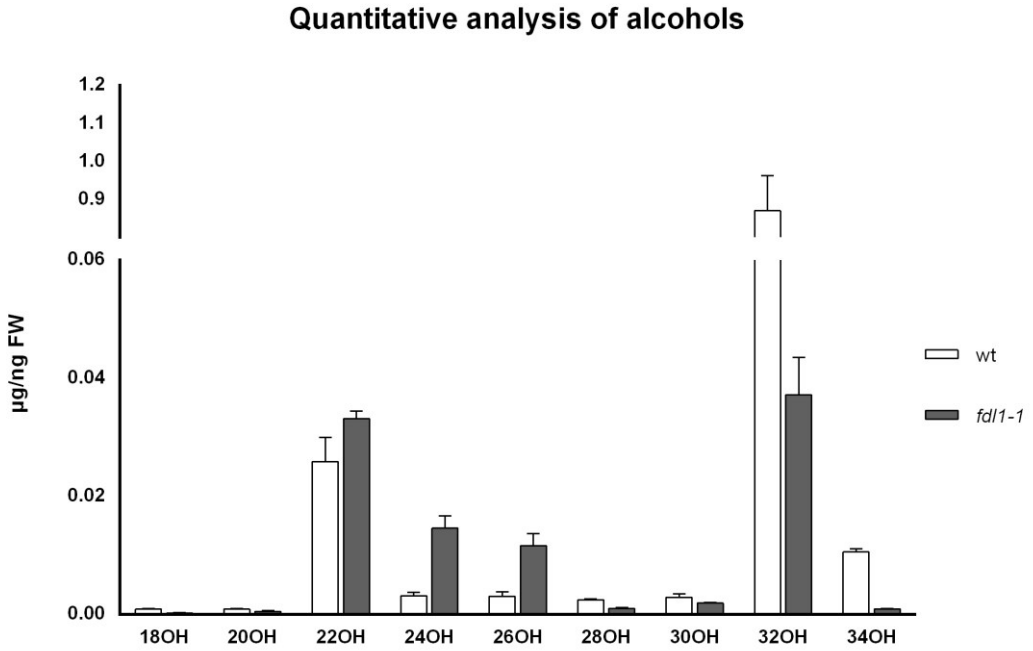

Figure 22. Gas chromatographic analysis of alcohols extracted from *Zea mays* seedlings. The analysis was done by Martina Persico Ph.D., and reported in: Persico M., A forward genetics approach to study seed and seedling development in maize, Ph.D. thesis, 2015. For every compound is reported the amount (µg/ng of fresh weight) measured. wt: wild type genotype. fdl1-1: homozygous *fdl1-1* genotype. Error bars show Standard Error.

The quantity levels of long-chain primary alcohol detected are different between wild type and *fdl1-1* in almost all the compound analysed.

The amount of 18OH and 20OH seems slightly lower in *fdl1-1* compared with wild type. 22OH, 24OH and 26OH level appear instead increased in the mutant, while the amount of 28OH, 30OH, 32OH and 34OH return to being lower in *fdl1-1* compared with wild type.

The highest variation was observed for 32OH, which shows a quantitative decrement of more than one order of magnitude.

In our opinion, the complex pattern of alterations observed can be caused by the defects in the fatty acid elongation pathway, although is difficult to explain it with the data in our possession. The only correlation we detected is the strong decrease in the amount of 32OH that could be caused directly by the downregulation of *AtCER4.*

Part 2: involvement of *fdl1* in drought stress response

Expression analysis on drought stress conditions

Arabidopsis genes *AtMYB94* and *AtMYB96* are known to regulate wax biosynthesis during drought stress (Seo *et al.* 2011). These two genes are phylogenetically closely related to *fdl1* (*ZmMYB96*) (La Rocca *et al.* 2015).

For this reason, the expression level of *fdl1* in drought stress condition was tested through qRT-PCR. The analysis was performed in second leaves, taken from B73 wild type plants.

At the sixth day after sowing, plants were brought at 80% relative water content (RWSC). Afterward, plants were divided into two groups: normal watered and low watered. Normal watered (NW) were kept at 80% RWSC, while low watered (LW) were carry at 30% and kept at constant RWSC for all the duration of the experiment. The relative water content of the soil in every pot was measured every day, as reported in Figure 23.

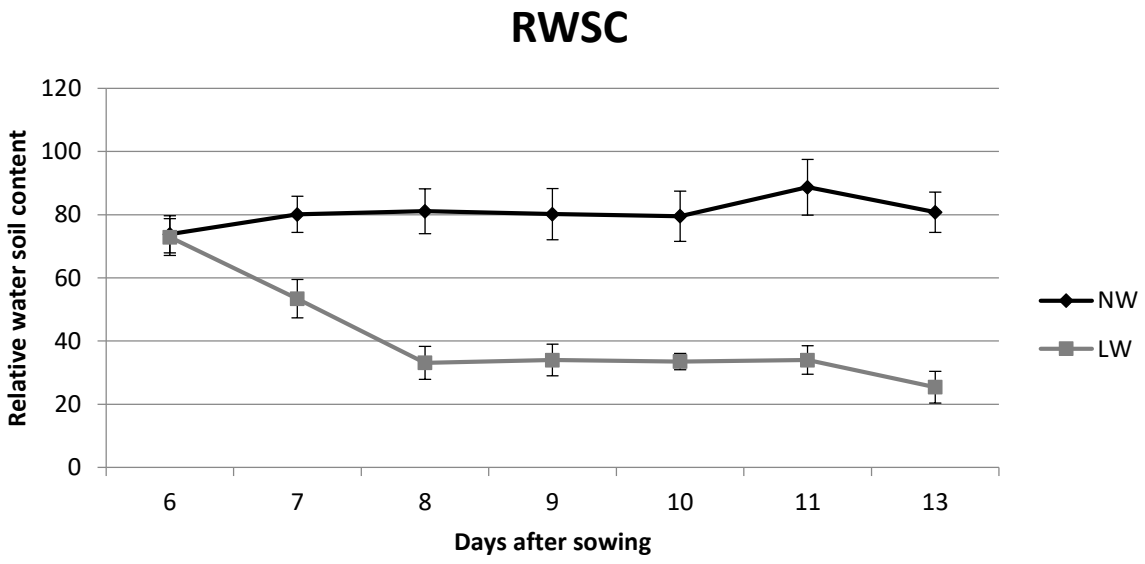

Figure 23. Relative water soil content (RWSC) of the pots containing the plants used for the drought stress experiment. NW: normal watered plants, kept in a constant relative water content in the soil of 80%. LW: low watered plants, kept in a constant relative water content in the soil of 30%. Error bars show Standard Error.

Every day for seven days, samples of second leaf were taken both from normal watered and low watered plants. The results of the RT-qPCR analysis are shown in Figure 24. As internal standard was used the *Elongation factor 1α* (*Ef1α*) gene.

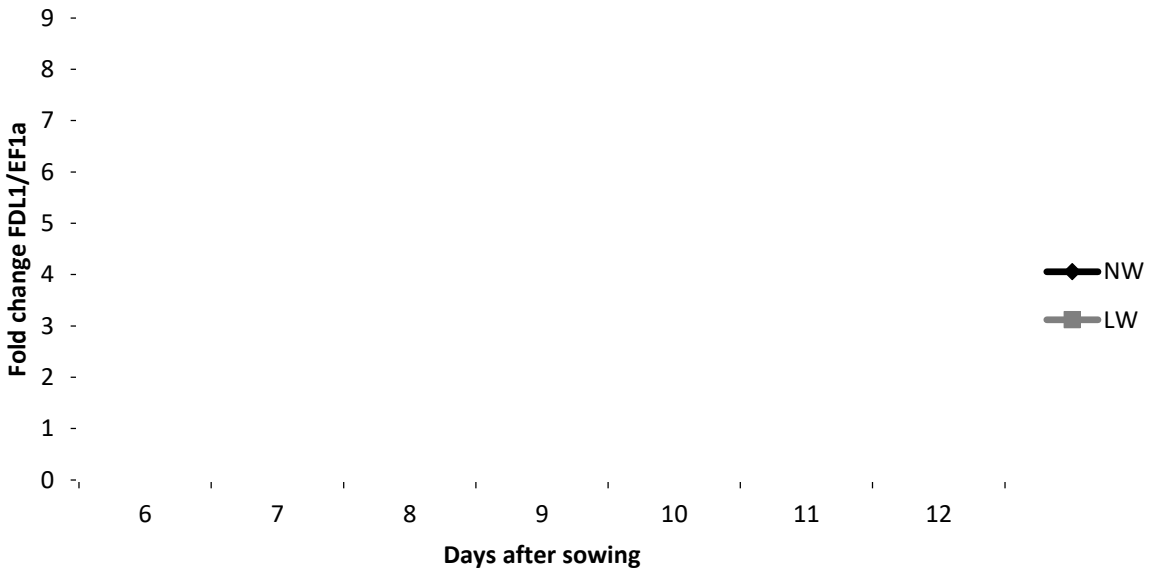

Figure 24. Levels of *fdl1* transcript in maize seedlings from the sixth day after sown, until the thirteenth. NW: normal watered samples, kept in a constant relative water content in the soil of 80%. LW: low watered samples, kept in a constant relative water content in the soil of 30%. As internal standard was used *EF1a* (*Elongation factor 1 alpha*). Error bars show Standard Error. * = P < 0.05, ** = P < 0.01 two tails T Student test.

From the results of this experiment it is possible to make two observations. First, the level of *fdl1* transcript in normal water samples drastically increase during the experiment. This can indicate an increment of *fdl1* expression during the leaf expansion. Indeed, at six days after sowing the second leaf is not fully expanded, and complete the expansion between eleven and thirteen days after sowing.

In low watered samples instead, the level of *fdl1* transcript appears different to the normal watered. Indeed, after an initial strong upregulation at two days of drought stress, the expression level of *fdl1* strongly decreases, returning to the basal level during all the leaf expansion. At twelve days after sowing, *fdl1* transcript level in low watered plants appears to be very lower compared with normal watered samples.

These data show that in plants exposed to a drought stress condition, after an initial upregulation, *fdl1* is strongly downregulated compared with normal watered plants.

Cloning of *fdl1* orthologous gene in *Eragrostis curvula*

E. curvula, a grass species belonging to the Poaceae family, the same family of *Z. mays* comprises different cultivars with different drought stress resistance levels. For this reason, it would be of interest to identify putative *fdl1* orthologous genes in this system and analyse the genetic variants and their expression pattern in different cultivars with different drought stress tolerance.

Cloning of the putative orthologous of *fdl1* in *E. curvula* started from an EST dataset, which originated from the transcriptome analysis of *E. curvula* (Tanganyika cv) flower and that was the only resource available when the project started.

The coding sequence of *fdl1* was used as query for a BLAST search on the EST databank of *E. curvula* and the output corresponded to the isotig42133 sequence, which showed high similarity with *fdl1* (Fig. 25).

Three pairs of PCR primers were designed, in order to amplify and clone three fragments of the EST sequence:

EC_FDL1_F1 – EC_FDL1_R1 (1)

EC_FDL1_F2 – EC_FDL1_R2 (2)

EC_FDL1_F3 – EC_FDL1_R3 (3)

```
>isotig42133
GTCTCGTGGCCGCCGGCGCCGCCGCGCCGCCGAACGACACCTCCGACGCGTCGGAGGACCCGGACGCGCTCT
CCGCGCCGCCGGGCGTGCCCGGCCCGCTACCGCCGCCGCCGCCGCGGCGAGCCTTCCCGGTGGCGGCGCCCC
AGCCGTCGAGCATCCGCGAGATGTTGTCCGCGGTGAGGACGTACGGCCCGGATGGGGAGCTCTGCGACGCGC
CCGACGAGCTCGACGCCGGGCTGTCGGCGCCGCCGGTGGCCGCGGCGGTCGCCGCGTCGGGCTGCTCCGGTG
TCGGCTTGAGGTCGTCGAGCGGCGTGAGGGCCTCGCGCAGCGCGCGGCGCGCCATGTTGATGTCCGTCTGCA
GGCGGCGCTCCCACTGGCCCTTGGAAGACGACGGCGGGCGGTGCGCCGGCGGCTTGGCCGCCGCGTCGCCTC
CGCTCTGCAGCTTCCGCTTGAGGTGCGTGTTCCAGTAGTTCTTGATGTCGTTGTCCGTGCGCTCCGGCAGGT
ACGACGCGATCGCCGCCCACCTGTTGCCGAGGAGAGCCTGGAGGTGGACGATGAGCTTCTCCTCCTGGTCAG
TGAAGTTGCCGCGCTTGATGCCCGGCCGGAGGTAGTTGGTCCACCGGAGCCGGCAGCTCTTGCTGCACCGCA
TCAAGCCGGTTCGGGTCGGGACGGCGCGCCAGTTGCCGGGGCCGTGCTCCTGGATGTAGGAGACGAGGACGA
GGTCCTCCTCCGGCGTCCACGGGCCCTTCTTCACGCCCTCCTTGTCGCAGCACGGCGGCCTCACCATGGTCG
CTCTCGAGCAAGCGGCTGCCCTTCCGGATCTTGCTTCTGGGCAGTGGCGTGTGTGGGAGCGTGTAAAGTGAA
C
```

Figure 25. Genetic sequence of isotig42133 from the EST data bank. The sequence is reported exactly as were found in the data bank, with a 3' – 5' orientation. Primers exploited are reported as coloured sequence. Primers couple 1 is coloured in yellow. Primer couple 2 is coloured in green. Primers couple 3 is coloured in grey.

PCR were conducted on genomic DNA extracted from Tanganyika cv and amplified fragments were cloned in *E. coli* with the pGem T-easy vector. The plasmid DNA was subsequently purified and sequenced.

The analysis of the three sequences obtained shows that the primers pairs 1 and 2 were highly specific, while the number 3 was not specific, and the sequence obtained resulted difficult to be interpreted. Sequences 1 and 2 were aligned to isotig42133, from a reference transcriptome of *E. curvula*, to detect the portion present in genomic DNA, but not in the EST and putatively corresponding to not expressed regions. On this basis, the gene structure was partially assembled and the gene was named *Ecfdl1*.

The obtained sequence comprises an ATG start codon two introns. The ATG position and orientation allows to find the correct 5' – 3' direction of the *Ecfdl1* sequence, which appears reversed and complementary to the isotig42133 sequence.

More recently, a first draft of *E. curvula* genome sequence became available in the group of Prof. Viviana C. Echenique (CERZOS CCT CONICET, Bahía Blanca – Argentina). The partial sequence of *Ecfdl1* previously obtained was used as a query in the genome sequence and the complete sequence of the gene was retrieved (Figure 26).

```
>Ecfdl1
GTTCACTTTACACGCTCCCACACACGCCACTGCCCAGAAGCAAGATCCGGAAGGGCAGCCGCTTG
CTCGAGAGCGACCATGGTGAGGCCGCCGTGCTGCGACAAGGAGGGCGTGAAGAAGGGCCCGTGGA
CGCCGGAGGAGGACCTCGTCCTCGTCTCCTACATCCAGGAGCACGGCCCCGGCAACTGGCGCGCC
GTCCCGACCCGAACCGGTATGTTCAGCACTGGTTGCGTGAGCTTCAATCCATGCACGCATGATTT
TGTTTAGTTTAGTTTAGTTCTTTGTGTACGGCTACGATTCTGTTTTCTGATATGCCTGCCCGCGC
CCGTGTGGATTTTTTTCAGGCTTGATGCGGTGCAGCAAGAGCTGCCGGCTCCGGTGGACCAACTA
CCTCCGGCCGGGCATCAAGCGCGGCAACTTCACTGACCAGGAGGAGAAGCTCATCGTCCACCTCC
AGGCTCTCCTCGGCAACAGGTACATACTACGTCGATTTCAAGATCGATGCATCCTGTTTATTTCT
TGGATTTAGTGGAGGATCTTGCTTGATCTTCGTGGTACACGGTGACTGATCTGGTCGAACACGCG
TGTTGTGTGTTGTAGGTGGGCGGCGATCGCGTCGTACCTGCCGGAGCGCACGGACAACGACATCA
AGAACTACTGGAACACGCACCTCAAGCGGAAGCTGCAGAGCGGAGGCGACGCGGCGGCCAAGCCG
CCGGCGCACCGCCCGCCGTCGTCTTCCAAGGGCCAGTGGGAGCGCCGCCTGCAGACGGACATCAA
CATGGCGCGCCGCGCGCTGCGCGAGGCCCTCACGCCGCTCGACGACCTCAAGCCGACACCGGAGC
AGCCCGACGCGGCGACCGCCGCGGCCACCGGCGGCGCCGACAGCCCGGCGTCGAGCTCGTCGGGC
GCGTCGCAGAGCTCCCCATCCGGGCCGTACGTCCTCACCGCGGACAACATCTCGCGGATGCTCGA
CGGCTGGGGCGCCGCCACCGGGAAGGCTCGCCGCGGCGGCGGCGGCGGTAGCGGGCCGGGCACGC
CCGGCGGCGCGGAGAGCGCGTCCGGGTCCTCCGACGCGTCGGAGGTGTCGTTCGGCGGCGCGGCG
GCGCCGGCGGCCACGAGACCCCTCTTCGAGTACGAGACGAAGCCGGCCGTGGCGGCGCCGCAGAC
GCAGCAGCTGTCGGCGATCGAGTCGTGGCTGTTCGAGGACGACGGCAACTTCCACCACGTCCAGA
ACGGCGGCATGCTTGACGTGGCCATGGATTATCCTTTCTAG
```

Figure 26. Ecfdl1 sequence partially reconstructed. The sequence is reported in 5' – 3' orientation. ATG codon is marked in green. Introns are marked in red. Nucleotides encoding for amino acids of the MYB protein domain are highlighted in yellow.

Semi quantitative analysis of *Ecfdl1* expression

To analyse the expression pattern of *Ecfdl1*, a semi-quantitative RT-PCR analysis was performed (Fig. 27). cDNAs were prepared from total RNAs extracted from different tissues of three *E. curvula* cultivars, which are characterized by different drought stress tolerance:

- Don Eduardo (low drought stress tolerance)
- Don Walter (middle drought stress tolerance)
- Don Pablo (high drought stress tolerance)

cDNAs were then amplified using EcFDL_IT3F – EcFDL_IT3R set of primers. The Eragrostis gene *UBICE* for Ubiquitine (EH186329.1) was used as internal standard.

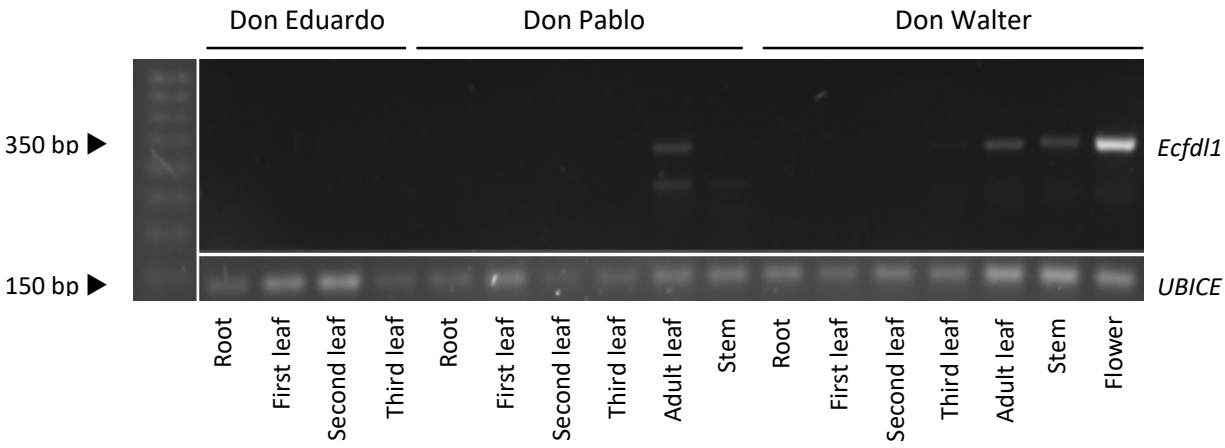

Figure 27. Semi-quantitative RT-PCR analysis on *Ecfdl1*. For *Ecfdl1* was used EcFDL_IT3 primers pairs. For the internal standard primers for *UBICE* gene were used. On the top the name of the cultivar is shown. On the bottom are reported the tissues analysed.

The results show no PCR amplification product in roots and first and second leaves for all the three ecotypes analysed. In the third leaf, is possible to see a very low expression only in Don Walter ecotype. A low but visible level was detected also in the adult leaf of both Don Pablo and Don Walter plants. *Ecfdl1* seems to be expressed also in the stem, but only in Don Walter samples. Furthermore, *Ecfdl1* appears to be expressed in flower samples.

Part3: role of *fdl1* on cuticular wax deposition in maize silks and interaction with *Fusarium verticillioides*

Analysis of lipid profile in maize silks

Maize silks are extremely long structures, being up to 20 cm in length and possess an external surface made of lipids consisting of a complex array of long-chain hydrocarbons. Previous experiments have shown that *fdl1* is expressed not only in the seedlings but also in ear silks, where transcripts accumulate at a very high level (La Rocca *et al.* 2015). Nevertheless, silks produced from homozygous mutant plants did not show any obvious visually detectable phenotypic alteration. Therefore, to characterize the role of *fdl1* in this organ we first analyse the effect of the *fdl1-1* mutation on the chemical composition of the silk cuticle. To this aim, lipids were extracted from cuticles of homozygous mutant and wild type silks and the lipid profile were analysed using GC-OCI (gas chromatography-on column injection) in collaboration with Dr Monica Bonomi (University of Milan). In particular, the analysis was focused on the ratio between straight chain alkane and the sum of alkenes at the same chain length (Fig. 28).

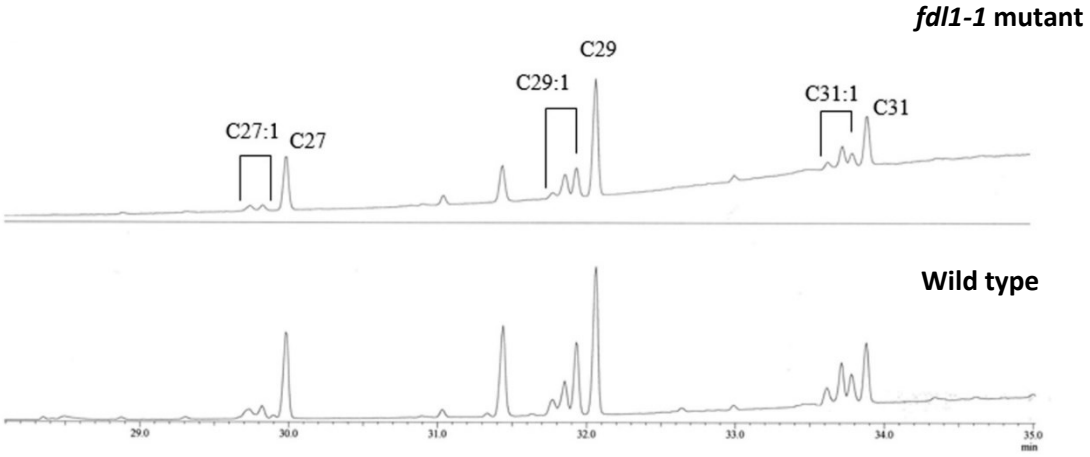

Figure 28. GC/MS analysis of the cuticular waxes in silks. Waxes were extracted with isooctane and the peaks were identified by combination of GC-OCI (gas chromatography - on column injection) and GC/MS (gas chromatography/mass spectrometry). GC/MS operative conditions: Restek RXI-5ms column (30 m x 0.25 mm, 0.25 m i.d.), temp. progr. From 80 °C to 320 °C (rate 7°C/min), scan m/z 40- 500. The ratios between straight chain alkane C 27 and the sum of C27:1, the alkane C29 and the sum of C29:1, the alkane C31 and the sum of C31:1 evidenced marked differences for the two samples considered.

By observing the peaks corresponding to C27, C29 and C31 it is possible to see that the ratio between alkane and the sum of alkene peak values is different between *fdl1-1* and wild type. The *fdl1-1* mutant produces fewer alkenes compared with the alkanes at the same carbon chain length.

These results show that there are differences between *fdl1-1* mutant and wild type lipid profile suggesting a possible role for *fdl1* in regulating lipid deposition in silks.

Quantification of *F. verticillioides* infection on maize ears of wild type and *fdl1-1* mutant plants

In the experimental field (years 2015 and 2016) inoculations with *F. verticillioides* conidia was performed on homozygous *fdl1-1* mutant and wild type silks. Harvested ears were then analysed for the fusarium ear rot (FER) symptoms and *F. verticillioides* kernel infection.

For each genotype, the percentage of infected ears is shown in Figure 29, while the calculated FER severity index is shown in Figure 30.

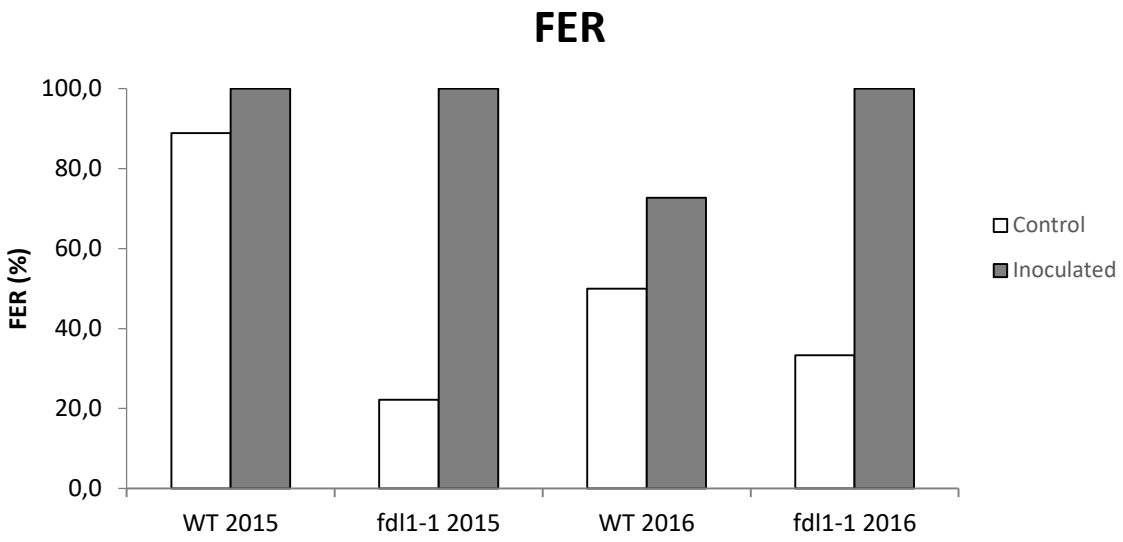

Figure 29. Percentage of ears that shown fusarium ear rot (FER) symptoms over the total analysed. Graphic show data for the years 2015 and 2016. For every genotype (wild type and *fdl1-1*) are shown the FER percentage on control and inoculated group of ears. WT: wild type genotype. fdl1-1: homozygous *fdl1-1* genotype.

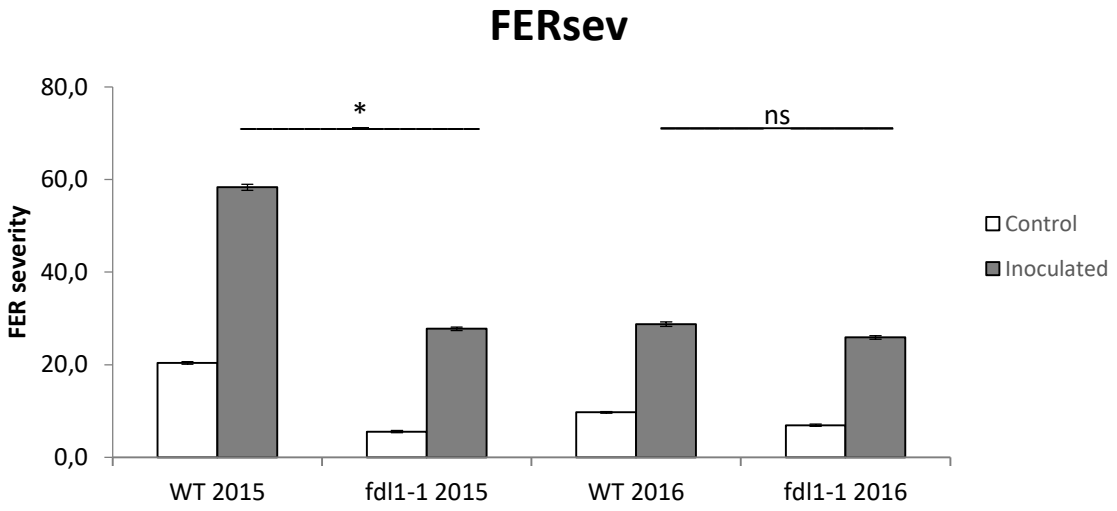

Figure 30. Fusarium ear rot (FER) severity index calculated for each of the genotypes analyzed (wild type and *fdl1-1*). Graphics show data for the years 2015 and 2016. For every genotype the FERsev index was calculated on control and inoculated group of ears. Error bars show Standard Error. WT: wild type genotype. fdl1-1: homozygous *fdl1-1* genotype. Significance symbols are referred to inoculated samples: * = $P < 0.05$, ns = not significant.

FER percentages show an increment of Fusarium infection on the inoculated samples compared with the respective controls both for the years 2015 and 2016. In the control samples, is possible to observe that the percentage of damaged ears is always lower in the mutant parcels compared with wild type.

Analysing FER severity data, also in this case is possible to observe an increment of the severity in all the inoculated samples. In this case is interesting to note that both in years 2015 and 2016, the infection severity was always lower in the *fdl1-1* mutant parcels compared with wild type. For the field year 2015, the differences in severity between wild type and mutant parcels are statistically significant, with a P value of 0.014. Concerning the 2016 data instead, the difference does not appear statistically significant.

This behaviour could be interpreted considering the percentage of damages caused by the European corn borer (ECB). ECB is one of the main carrier exploited by *F. verticillioides* to reach maize kernels. Since each ECB damage can represent a new point of Fusarium infection on the ears, a higher ECB incidence in a parcel could lead to an increment of FER incidence and severity, which is not correlated to the genotype. The percentage of ears that present ECB damages is shown in Figure 31.

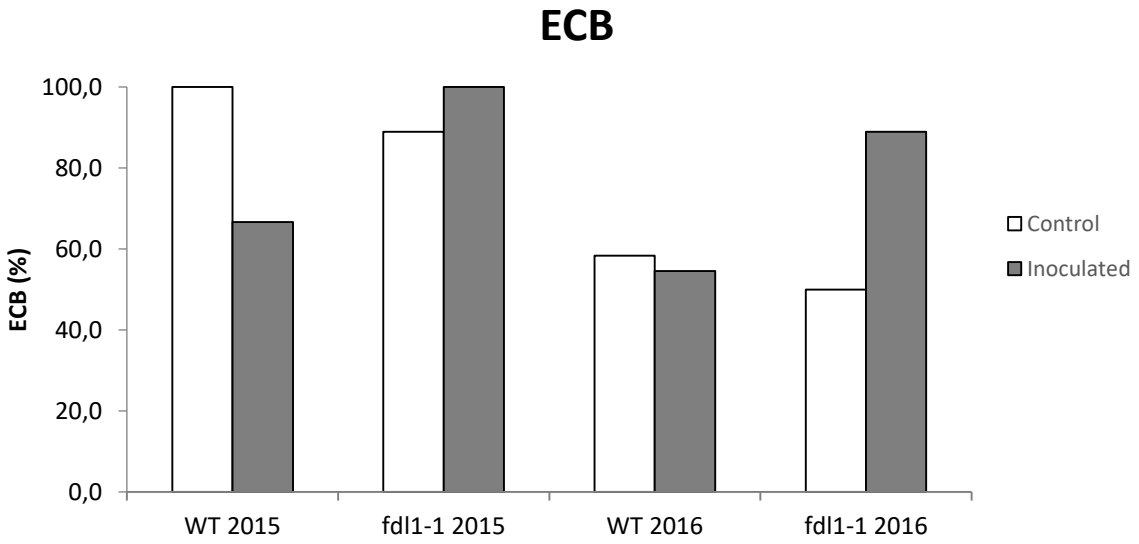

Figure 31. Percentage of ears that shown European corn borer (ECB) symptoms over the total analysed. Graphics show data for the years 2015 and 2016. For every genotype (wild type and *fdl1-1*) are shown the ECB percentage on control and inoculated group of ears. WT: wild type genotype. fdl1-1: homozygous *fdl1-1* genotype.

Analysing data of the year 2015 first, is possible to observe a high percentage of damaged ears in all the parcels. This can explain the presence of Fusarium infection also in control parcels. However, the percentages of damages are similar among parcels, except for the wild type inoculated sample. In this case, the ECB damage percentage is considerably lower compared with the other parcels. Despite this, the wild type inoculated parcel shows a higher Fusarium incidence and severity compared with the *fdl1-1* mutant parcel.

Concerning the data of 2016, the highest ECB incidence was detected in the *fdl1-1* inoculated parcel. In our opinion, this could have caused an increment in the FER incidence and severity for this parcel.

DISCUSSION AND CONCLUSIONS

The experiments presented in this work constitute a part of a bigger project, the final aim of which is to understand the role of *fdl1* in maize. A full understanding of the action of this gene could be very important for both agronomic and scientific purposes.

fdl1 is active during the first phases of the plant life cycle, which are probably the most critical phases. Moreover, the *fdl1* gene is involved in mechanisms underlying plant resistance to biotic and abiotic stress. It could therefore provide a valuable instrument for genetic improvement programs.

fdl1 regulated genes

This part of the work was focused on understanding how the mutation in the *fdl1* gene causes the complex phenotype observed in the *fdl1-1* mutant.

Since *fdl1* is an MYB gene, we assume that its role is to regulate a network of other genes.

To identify these genes, two types of strategies were used.

The first one was based on the selection of candidate genes, which were chosen on the basis of their role in the biosynthesis of cuticle components and their expression profile. Five genes were considered, and their interactions with *fdl1* were tested using two different approaches:

- the analysis of progenies segregating for both *fdl1* and the candidate genes selected,
- a semi-quantitative expression analysis of the selected candidate genes in *fdl1-1* mutant and wild type seedlings.

With the first approach, we produced a good number of populations segregating for both *fdl1-1* and *glossy2* or *glossy13*. These populations can be used in the future to repeat the analysis, with a bigger number of samples.

A visual analysis of the double mutants identified was very complex with the particular genes analysed. This was because the *fdl1-1* mutation shows a pleiotropic effect, with alterations of epicuticular waxes that are also observed in the *glossy* mutants.

However, both for *glossy2* and *glossy13*, the visual analysis of all the F_2 progenies revealed a segregation ratio of 9:3:3:1. This observation suggests that there is no interaction between *fdl1* and the two genes analysed.
In future, using the progenies produced, it will be possible to perform a gas chromatographic analysis of the epicuticular waxes of the double mutants. Analysing seedlings at the early stages, when both *fdl1*, *glossy2* and *glossy13* are expressed, it will be possible to observe whether double mutants show an additive phenotype, compared with the single homozygous mutants *fdl1-1* and *glossy*.

The second approach, the RT-PCR analysis, was not informative. Indeed, for all the candidate genes selected, on the gel was not possible to see differences in the transcript amount between wild type and *fdl1-1* mutant genotypes.

The second strategy, which was based on a large-scale RNA sequencing analysis, produced interesting data.
More than one thousand differentially expressed genes, between *fdl1-1* mutant and wild type RNAs from seedlings, have been identified. They comprise genes involved in cuticle biosynthesis and deposition, along with a considerable number of genes involved in other important processes such as plant clock regulation, plant-pathogen interaction and hormone signalling.
Since this thesis work was specifically focused on genes regulated by *fdl1* and involved in cuticle biosynthesis and deposition, a deeper analysis and characterization was made on this subgroup.

Interestingly, five differentially expressed genes were found to be involved in the fatty acid elongation complex (FAE), four of which appear to be downregulated in the *fdl1-1* mutant. FAE enzymes are responsible for the biosynthesis of even-numbered long-chain fatty acids, starting from C18 up to C32 carbon chain length.
The alterations reported in the expression levels of the five genes involved in the FAE complex can be correlated with the quantitative differences observed in gas chromatographic analysis previously performed in our laboratory. A general downregulation of four FAE genes may

account for the strong increment in C16:0 molecules observed in *fdl1-1* mutant seedlings compared with wild type ones. Fatty acid elongation reactions indeed consume palmitic acid (C16:0) as the first substrate, in order to synthesise very long chain fatty acids.
More importantly, long-chain fatty acids produced by FAE are largely used by almost all the other plant biochemical pathways involved in cuticle biosynthesis and deposition. A severe alteration in the production of these compounds could have an indirect impact on other classes of compounds which are synthesised starting from long-chain fatty acids.

One of the most significant pieces of information given by this analysis concerned the cutin and suberin biosynthesis pathway. Indeed, only one gene of this pathway was found to be downregulated in *fdl1-1* mutant seedlings.
This gene, not yet characterized in maize, showed high similarity to the rice gene *ONI3*, the putative orthologous gene in rice (Akiba *et al.* 2014). For this reason, we provisionally named it *OsONI3.* The downregulation of *OsONI3* in maize *fdl1-1* mutant seedlings might explain almost totally the fusions observed between the coleoptile and the first leaves. In rice, the *ONI3* mutant shows seedling lethality, while *fdl1-1* seedlings manage to survive. In our opinion, this difference can be explained by the only partial downregulation of *OsONI3* observed in the *fdl1-1* mutants. Indeed, in the *fdl1-1* mutant this gene is downregulated but not completely turned off.
Furthermore, gas chromatographic analysis on ω-Hydroxy Fatty acids content in wild type and *fdl1-1* mutant cuticle revealed a general and strong decrease of these compounds in *fdl1-1* compared with wild type. ω-Hydroxy Fatty acids are exploited as the substrate for all the other reactions in the cutin and suberin biosynthesis pathway. The quantitative decrease of these compounds could be ascribable to a strong impairment of the fatty acid elongation complex, which provides all the basic substrates for cutin and suberin biosynthesis.
In our opinion, a reduction of the disposable cutin monomers, coupled with the downregulation of *OsONI3*, can probably cause the defects in cuticle observed in *fdl1-1* mutant seedlings (La Rocca *et al.* 2015).

Two other differentially expressed genes detected were found to be involved in wax biosynthesis. Changes in this pathway are of relevance to explain another trait observed in

fdl1-1 mutant seedlings, namely the presence of altered epicuticular waxes. All *glossy* mutants impaired in epicuticular waxes so far described in maize show notable alterations in the amounts of aldehydes, alkanes, alcohol and esters on their leaf surfaces (Bianchi *et al.* 1979). These compounds are synthesised by the wax biosynthetic pathway, which is divided into two sub-branches, i.e. the alkane-forming pathway and the alcohol-forming pathway (Bernard and Joubès 2013).

One of the two differentially expressed genes involved in wax biosynthesis corresponds to *CER1* from *A. thaliana*. *AtCER1,* which is involved in the alkane forming pathway (Bernard and Joubès 2013), was found to be upregulated in *fdl1-1*. Gas chromatographic analysis showed a strong decrement of 32 aldehydes and an increment of 31 alkanes in the *fdl1-1* mutant compared with wild type seedlings. The amounts of these two compounds are strongly correlated, indeed 31 alkanes are produced using 32 aldehydes as substrate by the aldehyde alkane-lyase encoded by *AtCER1.* The increased expression of *AtCER1* might be responsible for the incremented production of aldehyde alkane-lyase. A higher production of the enzyme can move the reaction equilibrium towards the product, i.e. alkanes, consuming almost all the aldehydes. In our opinion, this can explain the levels of 32 aldehydes and 31 alkanes observed in the *fdl1-1* mutant.

A second gene involved in wax biosynthesis was named *AtCER4*, and corresponds to *CER4* in *A. thaliana* (Bernard and Joubès 2013). This gene is involved in the alcohol-forming pathway and was found to be downregulated in *fdl1-1*. Unfortunately, the specific substrates and products of the reductase encoded by *AtCER4* have never been described, and it is thus impossible to associate the downregulation of its activity with changes in one or more specific long-chain primary alcohols. However, the strong decrement observed for C32OH, and also partially for C34OH levels in *fdl1-1* could be an indication that these two compounds are specific products of the *AtCER4* corresponding reductase in maize.

Another cause of the alterations observed in the amount of primary alcohols could be the alterations observed in the enzymes of the FAE complex. Indeed, as previously mentioned, the fatty acid elongation complex provides the substrates for the production of all the plant primary alcohols.

Overall these data, although they are still to be validated through qRT-PCR, allow us to assemble a model that describes the action of *fdl1* in maize (Fig. 32).

Our hypothesis is that *fdl1* is a positive regulator of four genes involved in the FAE complex (*AtKCS12, AtCER60, AtPAS2 and AtCER10*), one gene (*OsONI3*) in the cutin pathway and one gene (*AtCER4*) in the alcohol-forming pathway. In addition, *fdl1* may act as a repressor of the *AtKCS4* gene, involved in the FAE complex, and for *AtCER1,* involved in wax biosynthesis.

AtMYB30, AtMYB94 and *AtMYB96*, which are the most closely related MYB genes in Arabidopsis, have similar roles. Notably, all of them are involved in the biosynthesis of cuticle compounds, acting principally in the fatty acid elongation pathway (Bernard and Joubès 2013).

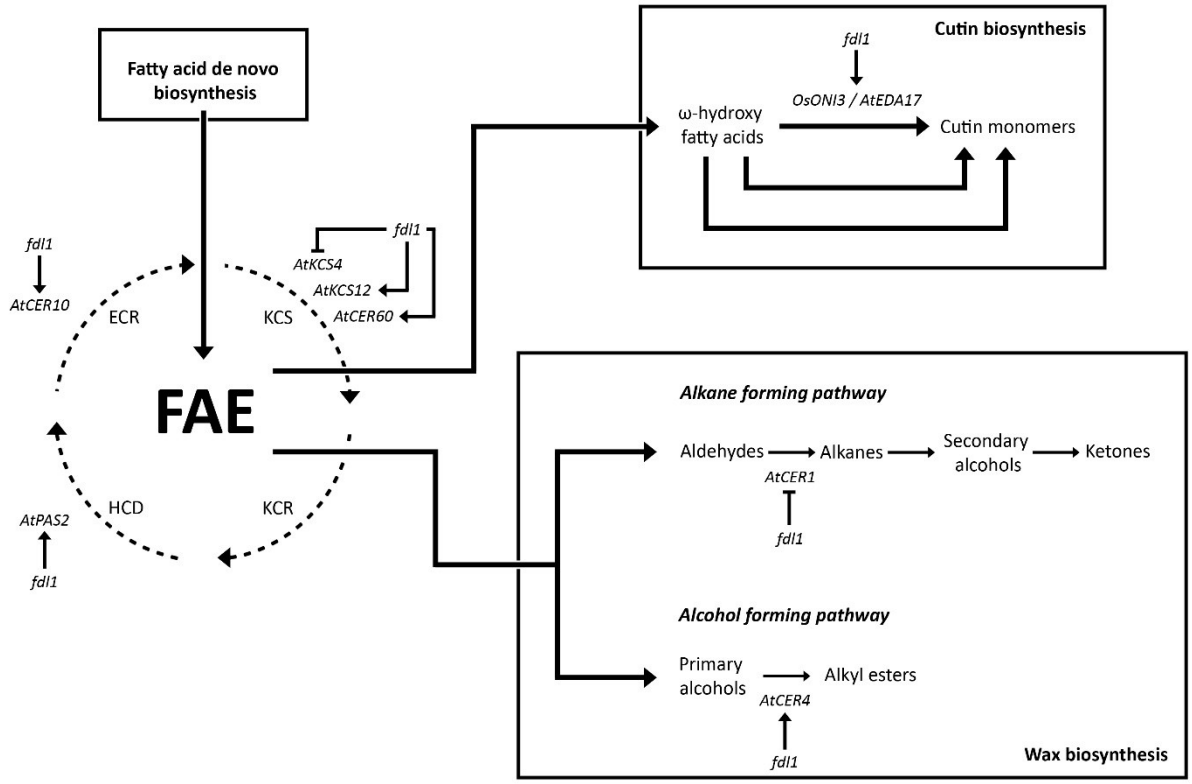

Figure 32. Model assembled to explain the involvement of *fdl1* in the biosynthesis of cuticle compounds.

Involvement of *fdl1* in drought stress response

This part of the work was focused on understanding whether *fdl1* is actively involved in drought stress response.

The analysis of *fdl1* transcript level on the second leaf of plants under drought stress conditions shows a strong alteration in the gene expression profile compared with the normally watered sample.

Indeed, after an initial increase, the transcript level decreased and remained low and stable. In normally watered plants, the *fdl1* transcript level increased during leaf expansion, until it reached a constant level when the leaf was fully expanded.

The decrease in *fdl1* transcript level observed after seven days of drought stress, suggests that *fdl1* is downregulated in low watering conditions. However, the strong and transient upregulation detected between the second and the fourth day of drought stress could represent a response adopted by the plant to tolerate low water conditions. Indeed, as observed in this work, *fdl1* seems to regulate the expression of a large number of genes involved in cuticular deposition and in other processes. The transient upregulation of *fdl1* might have a strong effect on cuticle composition and in other processes that we did not investigate.

Interestingly, expression analysis on *AtMYB94* and *AtMYB96* in Arabidopsis demonstrated that these two genes are overexpressed in drought stress conditions. In these experiments, the transcript levels of *AtMYB94* and *AtMYB96* increased in the first six hours after the start of the drought treatment (Lee *et al.* 2016). No information is however available on the expression level of *AtMYB94* and *AtMYB96* at subsequent times. In future, it may be of interest to make a complete comparison between the expression level of these two genes and *fdl1* during drought stress conditions.

The molecular analysis conducted in *E. curvula* allowed the isolation of the putative orthologous gene of *fdl1*, which was first identified from an EST data bank. The complete coding sequence of this gene was obtained, which includes the ATG codon, two introns and three exons. The structure obtained shows a strong similarity with *fdl1* of maize.

The sequence obtained allowed us to perform a preliminary semi-quantitative analysis of *Ecfdl1* expression in *E. curvula*. Both genes are expressed in the aerial part of the plants and

are not expressed in the root. However, the expression pattern shows some differences between *E. curvula* and maize. *Ecfdl1* does not appear to be expressed in the seedling, with the exception of cv Don Walter third leaf. *Ecfdl1* is instead expressed in adult leaf and stem. *Ecfdl1* is also expressed in the flower. Analogously, *fdl1* is expressed in maize in the silks, which are one of the female reproductive organs.

These data will be confirmed in future analysis employing the more specific real-time qRt-PCR. The availability of the complete *Ecfdl1* sequence will allow us to design more specific and useful primers. Moreover, cultivars of *E. curvula* showing different drought stress resistance, will be analysed to determine whether these differences could be correlated with genetic variants of the *Ecfdl1* gene that might be present in the different varieties.

Role of *fdl1* on deposition of cuticular waxes in maize silks and interaction with *Fusarium verticillioides*

Unlike the previous studies, which were done at the seedling stage of development, the activities of this part of the work were focused on ear silks. In these organs, which are produced by adult plants, the *fdl1* transcript level was the highest detected.

Mutant silks, however, did not display any obviously visible phenotype and therefore, to gain insight into the role of *fdl1* during silk development, gas chromatographic analysis of lipids extracted from the silks' surface was carried out. The results obtained showed some differences between mutant and wild type profiles. In particular, the ratio between straight chain alkanes and the sum of alkenes at the same chain length appeared different for C27, C29 and C31 compounds.

As already mentioned, in plants alkanes are produced from aldehydes through decarbonylation in the alkane-forming pathway. Alkenes however, are obtained directly from the fatty acid elongation pathway through reduction and decarbonylation of long-chain fatty acids (Perera *et al.,* 2010). Consequently, alterations of these biosynthesis pathways in *fdl1-1* due to the lack of *fdl1* regulation can be responsible for the differences detected.

In *fdl1-1* mutant silks, C27, C29 and C31 alkenes production seem to be reduced compared with the wild type sample. This causes a shift of the alkanes/alkenes ratio in favour of alkanes. Unlike in seedling leaves, in maize silks the main components of epicuticular waxes are alkanes and alkenes between C19 and C33, consequently an impairment in the ratio of these two compounds can lead to a severe alteration in the silks' structure.

Results of the quantification of *F. verticillioides* infection on maize ears gave a good indication of the different susceptibility against this fungus between the *fdl1-1* and wild type plants. Indeed, *fdl1-1* mutant ears showed a lower susceptibility to Fusarium ear rot symptoms compared with wild type. However, the high incidence of European corn borer in 2016 made it difficult to draw solid conclusions.

In conclusion, all the experiments presented in this work represent the start of the process aimed towards fully understanding the very complex role of *fdl1* in *Z. mays*.
However, for the first time an MYB gene of the cuticle has been analysed through a whole transcriptome analysis in maize. The results confirm the involvement of *fdl1* in the regulation of cuticle biosynthesis and deposition, and provide information on its involvement in other important plant processes.
The expression analysis also revealed that *fdl1* shows a different expression profile in drought stress conditions. This is the first example of an MYB gene in maize which is responsive to drought stress.
Many known genes involved in cuticle biosynthesis are expressed in maize silks, but their role is unknown. *fdl1* is the first of these genes analysed in silks, and the results of this work demonstrate that it is also involved in the regulation of cuticle biosynthesis in this tissue.

Certainly, in the context of climate changes in progress, lack of water and attacks of new pathogens are two important problems that crops have to face in the future. Interestingly, the experiments presented in this work indicate that *fdl1* is involved in the biosynthesis and regulation of a complex plant organ, the cuticle, which is an important barrier against many stresses, including water loss and pathogen attacks.

A good awareness of this gene and its mechanisms of action can surely help future genetic improvement projects, in order to obtain new maize varieties more adapted to the challenges of the future.

BIBLIOGRAPHY

Aarts M. G. M., Keijzer C. J., Stiekema W. J., Pereira A., 1995 Molecular Characterization of the CER7 Gene of Arabidopsis lnvolved in Epicuticular Wax Biosynthesis and Pollen Fertility. Am. Soc. Plant Physiol. 7: 2115–2127.

Abe H., Urao T., Ito T., Seki M., Shinozaki K., 2003 Transcriptional Activators in Abscisic Acid Signaling. Society 15: 63–78.

Aharoni A., Dixit S., Jetter R., Thoenes E., Arkel G. van, *et al.*, 2004 The SHINE clade of AP2 domain transcription factors activates wax biosynthesis, alters cuticle properties, and confers drought tolerance when overexpressed in Arabidopsis. Plant Cell 16: 2463–2480.

Akiba T., Hibara K. I., Kimura F., Tsuda K., Shibata K., *et al.*, 2014 Organ fusion and defective shoot development in oni3 mutants of rice. Plant Cell Physiol. 55: 42–51.

Araki S., Ito M., Soyano T., Nishihama R., Machida Y., 2004 Mitotic cyclins stimulate the activity of c-Myb-like factors for transactivation of G2/M phase-specific genes in tobacco. J. Biol. Chem. 279: 32979–32988.

Avato P., Bianchi G., Salamini F., 1985 Absence of long chain aldehydes in the wax of the Glossy II mutant of maize. Phytochemistry 24: 1995–1997.

Avato P., Bianchi G., Nayak A., Salamini F., Gentinetta E., 1987 Epicuticular waxes of maize as affected by the interaction of mutant gl8 with gl3, gl4 and gl15. Lipids 22: 11–16.

Barthlott W., Neinhuis C., 1997 Purity of the sacred lotus, or escape from contamination in biological surfaces. Planta 202: 1–8.

Beattie G. A., Marcell L. M., 2002 Effect of alterations in cuticular wax biosynthesis on the physicochemical properties and topography of maize leaf surfaces. Plant, Cell Environ. 25: 1–16.

Beisson F., Li-Beisson Y., Pollard M., 2012 Solving the puzzles of cutin and suberin polymer biosynthesis. Curr. Opin. Plant Biol. 15: 329–337.

Bernard A., Joubès J., 2013 Arabidopsis cuticular waxes: Advances in synthesis, export and regulation. Prog. Lipid Res. 52: 110–129.

Bianchi G., Avato P., Salamini F., 1977 Glossy mutants of maize. VII Chemistry of glossy 1, glossy 3, and glossy 7 epicuticular waxes. Maydica 22: 9–17.

Bianchi G., Avato P., Salamini F., 1978 Glossy mutants of maize. VIII. Accumulation of fatty aldehydes in surface waxes of gl5 maize seedlings. Biochem. Genet. 16: 1015–1021.

Bianchi G., Avato P., Salamini F., 1979 Glossy mutants of maize. Heredity (Edinb). 42: 391–395.

Bianchi A., Bianchi G., Avato P., Salamini F., 1985 Biosynthetic Pathways of Epicuticular Wax of Maize as Assessed by Mutation, Light, Plant-Age and Inhibitor Studies. Maydica 30: 179–198.

Bird D., Beisson F., Brigham A., Shin J., Greer S., *et al.*, 2007 Characterization of Arabidopsis ABCG11/WBC11, an ATP binding cassette (ABC) transporter that is required for cuticular lipid secretion. Plant J. 52: 485–498.

Blacklock B. J., Jaworski J. G., 2006 Substrate specificity of Arabidopsis 3-ketoacyl-CoA synthases. Biochem. Biophys. Res. Commun. 346: 583–590.

Blenn B., Bandoly M., Küffner A., Otte T., Geiselhardt S., *et al.*, 2012 Insect Egg Deposition Induces Indirect Defense and Epicuticular Wax Changes in Arabidopsis thaliana. J. Chem. Ecol. 38: 882–892.

Bourdenx B., Bernard A., Domergue F., Pascal S., Léger A., *et al.*, 2011 Overexpression of Arabidopsis ECERIFERUM1 promotes wax very-long-chain alkane biosynthesis and influences plant response to biotic and abiotic stresses. Plant Physiol. 156: 29–45.

Cheesbrough T. M., Kolattukudy P. E., 1984 Alkane biosynthesis by decarbonylation of aldehydes catalyzed by a particulate preparation from Pisum sativum. Proc. Natl. Acad. Sci. 81: 6613–6617.

Chen X., Goodwin S. M., Boroff V. L., Liu X., Jenks M. a, 2003 Cloning and characterization of the WAX2 gene of Arabidopsis involved in cuticle membrane and wax production. Plant Cell 15: 1170–85.

Colom M. R., Vazzana C., 2002 Water Stress Effects on Three Cultivars of Eragrostis curvula. Ital. J. Agron. 6: 127–132.

Denic V., Weissman J. S., 2007 A Molecular Caliper Mechanism for Determining Very Long-Chain Fatty Acid Length. Cell 130: 663–677.

Depge-Fargeix N., Javelle M., Chambrier P., Frangne N., Gerentes D., *et al.*, 2011 Functional characterization of the HD-ZIP IV transcription factor OCL1 from maize. J. Exp. Bot. 62: 293–305.

Du H., Wang Y. Bin, Xie Y., Liang Z., Jiang S. J., *et al.*, 2013 Genome-wide identification and evolutionary and expression analyses of MYB-related genes in land plants. DNA Res. 20: 437–448.

Dubos C., Stracke R., Grotewold E., Weisshaar B., Martin C., *et al.*, 2010 MYB transcription factors in Arabidopsis. Trends Plant Sci. 15: 573–581.

Eigenbrode S. D., Espelie K., 1995 Effects of Plant Epicuticular Lipids on Insect Herbivores. AtIIlu. Rev. Entomol 40: 171–94.

Ent S. Van der, Verhagen B. W. M., Doorn R. Van, Bakker D., Verlaan M. G., *et al.*, 2008 MYB72 Is Required in Early Signaling Steps of Rhizobacteria-Induced Systemic Resistance in Arabidopsis. Plant Physiol. 146: 1293–1304.

Fornalé S., Sonbol F. M., Maes T., Capellades M., Puigdomènech P., *et al.*, 2006 Down-regulation of the maize and Arabidopsis thaliana caffeic acid O-methyl-transferase genes by two new maize R2R3-MYB transcription factors. Plant Mol. Biol. 62: 809–823.

Greer S., Wen M., Bird D., Wu X., Samuels L., *et al.*, 2007 The cytochrome P450 enzyme CYP96A15 is the midchain alkane hydroxylase responsible for formation of secondary alcohols and ketones in stem cuticular wax of Arabidopsis. Plant Physiol. 145: 653–667.

Grotewold E., Athma P., Peterson T., 1991 Alternatively spliced products of the maize P gene encode proteins with homology to the DNA-binding domain of myb-like transcription factors. Proc. Natl. Acad. Sci. U. S. A. 88: 4587–4591.

Haslam T. M., Kunst L., 2013 Extending The Story Of Very-Long-Chain Fatty Acid Elongation. Plant Sci. 210: 93–107.

Heine G. F., Malik V., Dias A. P., Grotewold E., 2007 Expression and molecular characterization of ZmMYB-IF35 and related R2R3-MYB transcription factors. Mol. Biotechnol. 37: 155–164.

Holmes M. G., Keiller D. R., 2002 Effects of pubescence and waxes on the reflectance of leaves in the ultraviolet and photosynthetic wavebands: A comparison of a range of species. Plant, Cell Environ. 25: 85–93.

Hülskamp M., Kopczak S. D., Horejsi T. F., Kihl B. K., Pruitt R. E., 1995 Identification of genes required for polen-stigma recognition in Arabidopsis thaliana. Plant J. 8: 703–714.

Javelle M., Vernoud V., Depege-Fargeix N., Arnould C., Oursel D., *et al.*, 2010 Overexpression of the Epidermis-Specific Homeodomain-Leucine Zipper IV Transcription Factor OUTER CELL LAYER1 in Maize Identifies Target Genes Involved in Lipid Metabolism and Cuticle Biosynthesis. Plant Physiol. 154: 273–286.

Jeffree C., 1996 Structure and ontogeny of plant cuticles. J. Exp. Bot.: 33–82.

Jenks M. a., Eigenbrode S. D., Lemieux B., 2002 Cuticular Waxes of Arabidopsis. Arab. B. 29: 1.

Kader J.-C., 1996 Lipid-Transfer Proteins in Plants. Annu. Rev. Plant Physiol. Plant Mol. Biol. 47: 627–654.

Khaled A. S., Vernoud V., Ingram G. C., Perez P., Sarda X., *et al.*, 2005 Engrailed-ZmOCL1 fusions cause a transient reduction of kernel size in maize. Plant Mol. Biol. 58: 123–139.

Klempnauer K. H., Gonda T. J., Michael Bishop J., 1982 Nucleotide sequence of the retroviral leukemia gene v-myb and its cellular progenitor c-myb: The architecture of a transduced oncogene. Cell 31: 453–463.

Kosma D. K., Bourdenx B., Bernard A., Parsons E. P., Lü S., *et al.*, 2009 The impact of water deficiency on leaf cuticle lipids of Arabidopsis. Plant Physiol. 151: 1918–29.

Kunst L., Samuels A. L., 2003 Biosynthesis and secretion of plant cuticular wax. Prog. Lipid Res. 42: 51–80.

Kurdyukov S., 2006 The Epidermis-Specific Extracellular BODYGUARD Controls Cuticle Development and Morphogenesis in Arabidopsis. Plant Cell Online 18: 321–339.

Lai C., Kunst L., Jetter R., 2007 Composition of alkyl esters in the cuticular wax on inflorescence stems of Arabidopsis thaliana cer mutants. Plant J. 50: 189–196.

Lauter N., Kampani A., Carlson S., Goebel M., Moose S. P., 2005 microRNA172 down-regulates glossy15 to promote vegetative phase change in maize. Proc. Natl. Acad. Sci. U. S. A. 102: 9412–7.

Lawson E. J. R., Poethig R. S., 1995 Shoot development in plants: time for a change. Trends Genet. 11: 263–268.

Lee S. B., Suh M. C., 2015 Advances in the understanding of cuticular waxes in Arabidopsis thaliana and crop species. Plant Cell Rep. 34: 557–572.

Lee S. B., Kim H. U., Suh M. C., 2016 MYB94 and MYB96 Additively Activate Cuticular Wax Biosynthesis in Arabidopsis. Plant Cell Physiol. 57: 2300–2311.

Li L., Li D., Liu S., Ma X., Dietrich C. R., *et al.*, 2013 The Maize glossy13 gene, cloned via BSR-Seq and Seq-Walking encodes a putative ABC transporter required for the normal accumulation of epicuticular waxes. PLoS One 8: 1–13.

Li-Beisson Y., Shorrosh B., Beisson F., Andersson M. X., Arondel V., *et al.*, 2013 Acyl-Lipid Metabolism. Arab. B. 11: e0161.

Liang Y. K., Dubos C., Dodd I. C., Holroyd G. H., Hetherington A. M., *et al.*, 2005 AtMYB61, an R2R3-MYB transcription factor controlling stomatal aperture in Arabidopsis thaliana. Curr. Biol. 15: 1201–1206.

Liu S., Dietrich C. R., Schnable P. S., 2009 DLA-based strategies for cloning insertion mutants: Cloning the gl4 locus of maize using Mu transposon tagged alleles. Genetics 183: 1215–1225.

Liu S., Yeh C. T., Tang H. M., Nettleton D., Schnable P. S., 2012 Gene mapping via bulked segregant RNA-Seq (BSR-Seq). PLoS One 7: 1–8.

Lorenzoni C., Salamini F., 1975 Glossy mutants of maize. V. Morphology of the epicuticular waxes. Maydica XX: 5–19.

Love M. I., Huber W., Anders S., 2014 Moderated estimation of fold change and dispersion for RNA-seq data with DESeq2. Genome Biol. 15: 550.

Marcell L. M., Beattie G. a, 2002 Effect of leaf surface waxes on leaf colonization by Pantoea agglomerans and Clavibacter michiganensis. Mol. Plant. Microbe. Interact. 15: 1236–1244.

Marocco A., Wissenbach M., Becker D., Paz-Ares J., Saedler H., *et al.*, 1989 Multiple genes are transcribed in Hordeum vulgare and Zea mays that carry the DNA binding domain of the myb oncoproteins. MGG Mol. Gen. Genet. 216: 183–187.

Misra, S; Ghosh A., 1991 Analysis of Epicuticular Waxes. In: Linskens HF., Jackson JF (Eds.), *Essential Oils and Waxes*, Springer- Verlag, Berlin, pp. 205–229.

Moose S. P., Sisco P. H., 1996 Glossy15, an APETALA2-like gene from maize that regulates leaf epidermal cell identity. Genes Dev. 10: 3018–3027.

Nawrath C., 2003 The Biopolymers Cutin and Suberin. Arab. B. 34: 1.

Nawrath C., 2006 Unraveling the complex network of cuticular structure and function. Curr. Opin. Plant Biol. 9: 281–287.

Pabo C., 1992 Transcription Factors: Structural Families and Principles of DNA Recognition. Annu. Rev. Biochem. 61: 1053–1095.

Paz-Ares J., Ghosal D., Wienand U., Peterson P. A., Saedler H., 1987 The regulatory c1 locus of *Zea mays* encodes a protein with homology to myb proto-oncogene products and with structural similarities to transcriptional activators. EMBO J. 6: 3553–3558.

Perera M. A. D. N., Nikolau B. J., 2007 Metabolomics of Cuticular Waxes: A System for Metabolomics Analysis of a Single Tissue-Type in a Multicellular Organism. Concepts in Plant Metabolomics: 111–123.

Perera M. A. D. N., Qin W., Yandeau-Nelson M., Fan L., Dixon P., *et al.*, 2010 Biological origins of normal-chain hydrocarbons: A pathway model based on cuticular wax analyses of maize silks. Plant J. 64: 618–632.

Persico M., 2015 A forward genetic approach to study seed and seedling development in maize.

Petroni K., Falasca G., Calvenzani V., Allegra D., Stolfi C., *et al.*, 2008 The AtMYB11 gene from Arabidopsis is expressed in meristematic cells and modulates growth in planta and organogenesis in vitro. J. Exp. Bot. 59: 1201–1213.

Pighin J. A., 2004 Plant Cuticular Lipid Export Requires an ABC Transporter. Science (80-.). 306: 702–704.

Podila G. K., Rogers M., Kolattukudy P. E., 1993 Chemical Signals from Avocado Surface Wax Trigger Germination and Appressorium Formation in Colletotrichum gloeosporioides ’. Plant Physiol. 103: 267–272.

Poethig R. S., 1990 Phase change and the regulation of shoot morphogenesis in plants. Science 250: 923–30.

Post-Beittenmiller D., 1996 Biochemistry and Molecular Biology of Wax Production in Plants. Annu Rev Plant Physiol Plant Mol Biol 47: 405–430.

Preuss D., Lemieux B., Yen G., Davis R. W., 1993 A conditional sterile mutation eliminates surface components from Arabidopsis pollen and disrupts cell signaling during fertilization. Genes Dev. 7: 974–985.

Raffaele S., Vailleau F., Leger A., Joubes J., Miersch O., *et al.*, 2008 A MYB transcription factor regulates very-long-chain fatty acid biosynthesis for activation of the hypersensitive cell death response in Arabidopsis. Plant Cell 20: 752–767.

Ritchie M. E., Phipson B., Wu D., Hu Y., Law C. W., *et al.*, 2015 limma powers differential expression analyses for RNA-sequencing and microarray studies. Nucleic Acids Res. 43: e47.

Rocca N. La, Manzotti P. S., Cavaiuolo M., Barbante A., Vecchia F. D., *et al.*, 2015 The maize fused leaves1 (fdl1) gene controls organ separation in the embryo and seedling shoot and promotes coleoptile opening. J. Exp. Bot. 66: 5753–5767.

Rodrigo J. M., Zappacosta D. C., Selva J. P., Garbus I., Albertini E., *et al.*, 2017 Apomixis frequency under stress conditions in weeping lovegrass (Eragrostis curvula). PLoS One 12: 1–17.

Rowland O., Domergue F., 2012 Plant fatty acyl reductases: Enzymes generating fatty alcohols for protective layers with potential for industrial applications. Plant Sci. 193–194: 28–38.

Samuels L., Kunst L., Jetter R., 2008 Sealing plant surfaces: cuticular wax formation by epidermal cells. Annu. Rev. Plant Biol. 59: 683–707.

Schaafsma A. W., Nicol R. W., Reid L. M., 1997 Evaluating commercial maize hybrids for resistance to gibberella ear rot. Eur. J. Plant Pathol. 103: 737–746.

Schmittgen T. D., Livak K. J., 2008 Analyzing real-time PCR data by the comparative CT method. Nat. Protoc. 3: 1101–1108.

Schmitz G., Tillmann E., Carriero F., Fiore C., Cellini F., *et al.*, 2002 The tomato Blind gene encodes a MYB transcription factor that controls the formation of lateral meristems. Proc. Natl. Acad. Sci. 99: 1064–1069.

Schnable P. S., Stinard P. S., Wen T. J., Heinen S., Weber D., *et al.*, 1994 The genetics of cuticular wax biosynthesis. Maydica 39: 279–287.

Schneider-Belhaddad F., Kolattukudy P., 2000 Solubilization, partial purification, and characterization of a fatty aldehyde decarbonylase from a higher plant, Pisum sativum. Arch. Biochem. Biophys. 377: 341–349.

Sekhon R. S., Lin H., Childs K. L., Hansey C. N., Robin Buell C., *et al.*, 2011 Genome-wide atlas of transcription during maize development. Plant J. 66: 553–563.

Seo P. J., Lee S. B., Suh M. C., Park M.-J., Go Y. S., *et al.*, 2011 The MYB96 transcription factor regulates cuticular wax biosynthesis under drought conditions in Arabidopsis. Plant Cell 23: 1138–1152.

Sheperd T., D.W. G., 2006 The effects of stress on plant cuticular\rwaxes. New Phytol. 171: 469–499.

Shepherd T., Dobson G., Marshall R., Verrall S. R., Conner S., *et al.*, 2007 *Concepts in Plant Metabolomics* (BJ Nikolau and E. Wurtele, Eds.). Springer.

Sieber P., Schorderet M., Ryser U., Buchala A., Kolattukudy P., *et al.*, 2000 Transgenic Arabidopsis Plants Expressing a Fungal Cutinase Show Alterations in the Structure and Properties of the Cuticle and Postgenital Organ Fusions. Plant Cell 12: 721–737.

Staehelin L. A., 1997 The plant ER: A dynamic organelle composed of a large number of discrete functional domains. Plant J. 11: 1151–1165.

Sturaro M., Hartings H., Schmelzer E., Velasco R., Salamini F., *et al.*, 2005 Cloning and characterization of GLOSSY1, a maize gene involved in cuticle membrane and wax production. Plant Physiol. 138: 478–489.

Tacke E., Korfhage C., Michel D., Maddaloni M., Motto M., *et al.*, 1995 Transposon tagging of the maize Glossy2 locus with the transposable element En/Spm. Plant J. 8: 907–17.

Thoma S., Kaneko Y., Somerville C., 1993 A non-specific lipid transfer protein from Arabidopsis is a cell wall protein. Plant J 3: 427–436.

Tischler C. R., Voigt P. W., 1990 Variability in Leaf Characteristics and Water Loss in the Weeping Lovegrass Complex. Crop Sci. 30: 111–117.

Trapnell C., Roberts A., Goff L., Pertea G., Kim D., *et al.*, 2012 Differential gene and transcript expression analysis of RNA-seq experiments with TopHat and Cufflinks. Nat. Protoc. 7: 562–578.

Ukitsu H., Kuromori T., Toyooka K., Goto Y., Matsuoka K., *et al.*, 2007 Cytological and biochemical analysis of COF1, an Arabidopsis mutant of an ABC transporter gene. Plant Cell Physiol. 48: 1524–1533.

Venturini G., Toffolatti S. L., Assante G., Babazadeh L., Campia P., *et al.*, 2015 The influence of flavonoids in maize pericarp on fusarium ear rot symptoms and fumonisin accumulation under field conditions. Plant Pathol. 64: 671–679.

Xu X., Dietrich C. R., Delledonne M., Xia Y., Wen T. J., *et al.*, 1997 Sequence analysis of the cloned glossy8 gene of maize suggests that it may code for a beta-ketoacyl reductase required for the biosynthesis of cuticular waxes. Plant Physiol. 115: 501–10.

Xu X., Dietrich C. R., Lessire R., Nikolau B. J., Schnable P. S., 2002 The Endoplasmic reticulum-associated maize GL8 protein is a component of the acyl-coenzyme A elongase ivolved in the production of cuticular waxes. Plant Physiol. 128: 924–34.

Yanhui C., Xiaoyuan Y., Kun H., Meihua L., Jigang L., *et al.*, 2006 The MYB transcription factor superfamily of Arabidopsis: Expression analysis and phylogenetic comparison with the rice MYB family. Plant Mol. Biol. 60: 107–124.

Yeats T. H., Rose J. K. C., 2013 The formation and function of plant cuticles. Plant Physiol. 163: 5–20.

Zachowski A., Guerbette F., Grosbois M., Jolliot-Croquin A., Kader J. C., 1998 Characterisation of acyl binding by a plant lipid-transfer protein. Eur. J. Biochem. 257: 443–448.

Zhang Y., Yang C., Li Y., Zheng N., Chen H., *et al.*, 2007 SDIR1 Is a RING Finger E3 Ligase That Positively Regulates Stress-Responsive Abscisic Acid Signaling in *Arabidopsis*. Plant Cell 19: 1912–1929.

Zheng H., 2005 Disruptions of the Arabidopsis Enoyl-CoA Reductase Gene Reveal an Essential Role for Very-Long-Chain Fatty Acid Synthesis in Cell Expansion during Plant Morphogenesis. Plant Cell Online 17: 1467–1481.

CHAPTER 2

INVOLVEMENT OF BRASSINOSTEROIDS IN PLANT GROWTH AND DROUGHT RESPONSE

INTRODUCTION

Hormones strictly regulates plant development

During plant growth, an important number of process, comprising cell division and expansion, are regulated by specific plant hormones. The most known and studied are auxin (IAA), cytokinins (CKs), gibberellins (GAs), brassinosteroids (BRs) and abscisic acid (ABA). It is well known that cytokinins promote cell proliferation, while gibberellins stimulate cell elongation. Auxin and brassinosteroids are involved in both processes. In the last years, different approaches, including mutant phenotype analysis and in vitro assays, were exploited to study the effect of these hormones on plant development.

Auxin, the first plant hormone characterized, is a multi-functional phytohormone that modulates nearly all aspects of plant growth and development. Asymmetric auxin distribution patterns (so-called auxin gradients) provide positional cues for establishing cell polarity and plays a crucial role in the generation of diverse polarity systems, such as polar positioning of root hairs in the trichoblast (Pan *et al.* 2015).

Besides auxin, also gibberellins are involved in promoting the elongation of young stems during seedling growth. GAs promotes the relaxation of the cell walls in the intermodal regions, causing the elongation of internodes (Cosgrove and Sovonick-Dunford 1989). The action of BRs in promoting cell elongation was first observed in a 'bean second internode test' (Mitchell J. W. 1970) and the structure of the stimulating molecule was determined and named brassinolide (Grove *et al.* 1979).

For all these hormones, the biosynthetic pathways, as well as the genetic control underlying them along with the molecular mechanism related to their perception and responses have been extensively analysed. A comprehensive description of the data so far obtained and eventually of the models formulated on their bases is available in the literature (Choi *et al.* 1996; Hedden and Kamiya 1997). From all these studies, emerged the hypothesis that these hormones don't act in isolation but are interrelated by synergistic or antagonistic cross talks so that they modulate each other's biosynthesis or responses. This aspect of hormone action was shown in particular for cell elongation, probably because it is experimentally easy to work with.

Importance of brassinosteroids throughout the plant life cycle

Brassinosteroids (BRs) are a class of steroid hormones essential for plant growth and development. In the last decade, important advances have been made in elucidating their metabolism and signalling pathways, as well as their importance for plant growth and development, in both model plants and crops (Schaller 2004; Clouse 2011). They control cell elongation, division and differentiation (Clouse 2011). BRs are also involved in many developmental traits of agronomic importance such as seed germination, plant architecture, flowering time and seed yield, and in the control of stress tolerance (Divi and Krishna 2009). BRs promote the biosynthesis of ethylene (Shi *et al.* 2006) and guide the distribution of IAA (Li *et al.* 2005). To date, more than 50 BRs have been identified from the entire plant kingdom (Bajguz and Tretyn 2003). Among these, castasterone (CS) and brassinolide (BL) have been identified in plant materials and are considered the active BR molecules.

In addition to have a role in development, brassinosteroids exert anti-stress effects on plants and are essential for the ability of plants to adapt to abiotic stresses. Their action promotes a wide range of adaptive responses, including the control of density and opening of stomata (Argueso *et al.* 2009; Santner and Estelle 2009; Wang *et al.* 2009; Messing *et al.* 2010). Several studies, most of them based on exogenous application of BRs on plants, have demonstrated "anti-stress" effects of BRs.

They have proven the involvement of these hormones in a variety of environmental stresses, including high and low temperatures, drought, salinity and pathogen attack (Krishna 2003; Divi and Krishna 2009). *Brassica napus* and tomato seedlings, grown in the presence of 24-epibrassinolide (EBR), show a significantly increased tolerance to a lethal heat treatment than control seedlings grown in the absence of the compound (Dhaubhadel Chaudhary S. 1999). The application of BRs to two susceptible varieties of sorghum resulted in alleviation of the negative impact of osmotic stress on seed germination and seedling growth. BR application caused a decrease in the activities of the enzymes peroxidase and ascorbic acid oxidase. Moreover, they enhance the levels of soluble proteins and free proline, which are an important manifestation of stress tolerance in many plant species (Anuradha and Rao 2001; Wahid and Ghazanfar 2006; Wahid 2007) and promote the seedling growth under osmotic stress condition (Vardhini and Rao 2003). Enhanced levels of soluble proteins and free proline

were found also in rice (*Oryza sativa L*.) cultivar Super-Basmati foliar sprayed with BRs at five-leaf stage under drought stress condition. Exogenous application of BR also improved carbon assimilation and maintenance of tissue water status, thus improving seedling growth (Farooq *et al.* 2010).

However, their biosynthesis remained unknown until recent years. Studies of the biosynthetic pathway of BRs using cultured cells of *Catharanthus roseus* have revealed that BL is biosynthesized from campesterol by two parallel branched pathways, named early and late C-6 oxidation pathways (Fujioka and Yokota 2003).

As reported in Figure 1, campesterol is first converted to campestanol, which in turn is converted to castasterone (CS) through either the early C-6 oxidation or the late C-6 oxidation pathway. In the last steps, CS is converted to BL.

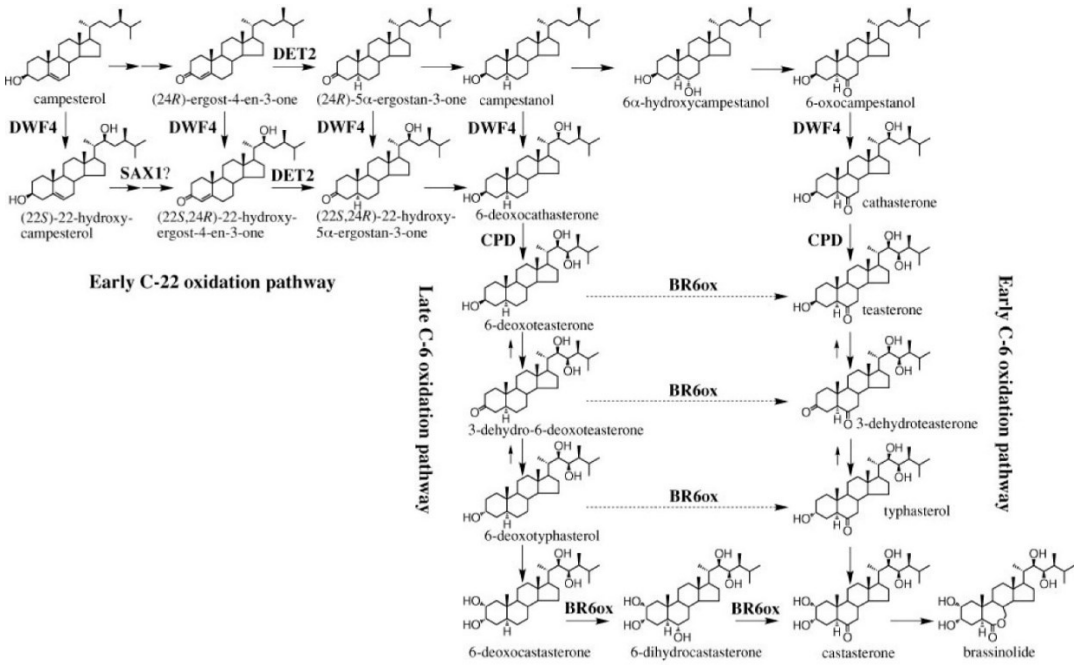

Figure 1. Brassinolide biosynthesis from campesterol. All the enzymes identified in Arabidopsis are shown. Image from: Fujioka, S., & Yokota, T. (2003). BIOSYNTHESIS AND METABOLISM OF BRASSINOSTEROIDS. Annual Review of Plant Biology, 54(1), 137–164.

A number of studies report that both the early and late C-6 oxidation pathways are common in plants, as seen for example in rice and pea (Nomura *et al.* 1999; Hong *et al.* 2002). However, in some species like Tomato, one of the two pathways appears to be predominant over the other (Yokota *et al.* 2001).

Deficient mutants for brassinosteroids: *nana1-1* and *lilliputian1-1*

A number of mutants with lesions in BR biosynthesis and perception/signal transduction have been isolated in different species such as *Arabidopsis thaliana* (Choe *et al.* 2000), *Pisum sativum* (Nomura *et al.* 1997; Schultz *et al.* 2001), *Lycopersicon esculentum* (Bishop *et al.* 1999), *O. sativa* (Yamamuro 2000) and maize (Hartwig *et al.* 2011b; Makarevitch *et al.* 2012). In *Zea mays*, two Br-deficient mutants were recently characterized. The first one was named *nana plant1-1* (*na1-1*), carries a loss-of-function mutation in a *DET2* homolog, a gene in the BR biosynthesis pathway encoding for a 5 α-steroid reductase (Hartwig *et al.* 2011b) (Fig. 2). The second one is *brd1-m1*, impaired in one of the genes involved in the last steps of brassinosteroid biosynthesis that encodes for a brassinosteroid C-6 oxidase (brC-6 oxidase) (Makarevitch *et al.* 2012) (Fig. 2). Recently in our laboratory, we demonstrated that the recessive mutant *lilliputian1-1*, isolated from an active Mutator (Mu) stock (Dolfini et al., 1999), is allelic to *brd1-1* mutant (Persico et al. 2017, submitted). Moreover, the maize BR receptor BRASSINOSTEROID INSENSITIVE1 (BRI1) has been more recently characterized using a transgenic RNA interference (RNAi) approach that knocked down the expression of all five maize *BRI1* homologs (Kir et al., 2015). The resulting phenotype, like that of mutants in structural genes, includes dwarf stature, due to shortened internodes, dark green, upright, and twisted leaves with decreased auricle formation, and feminized male flowers.

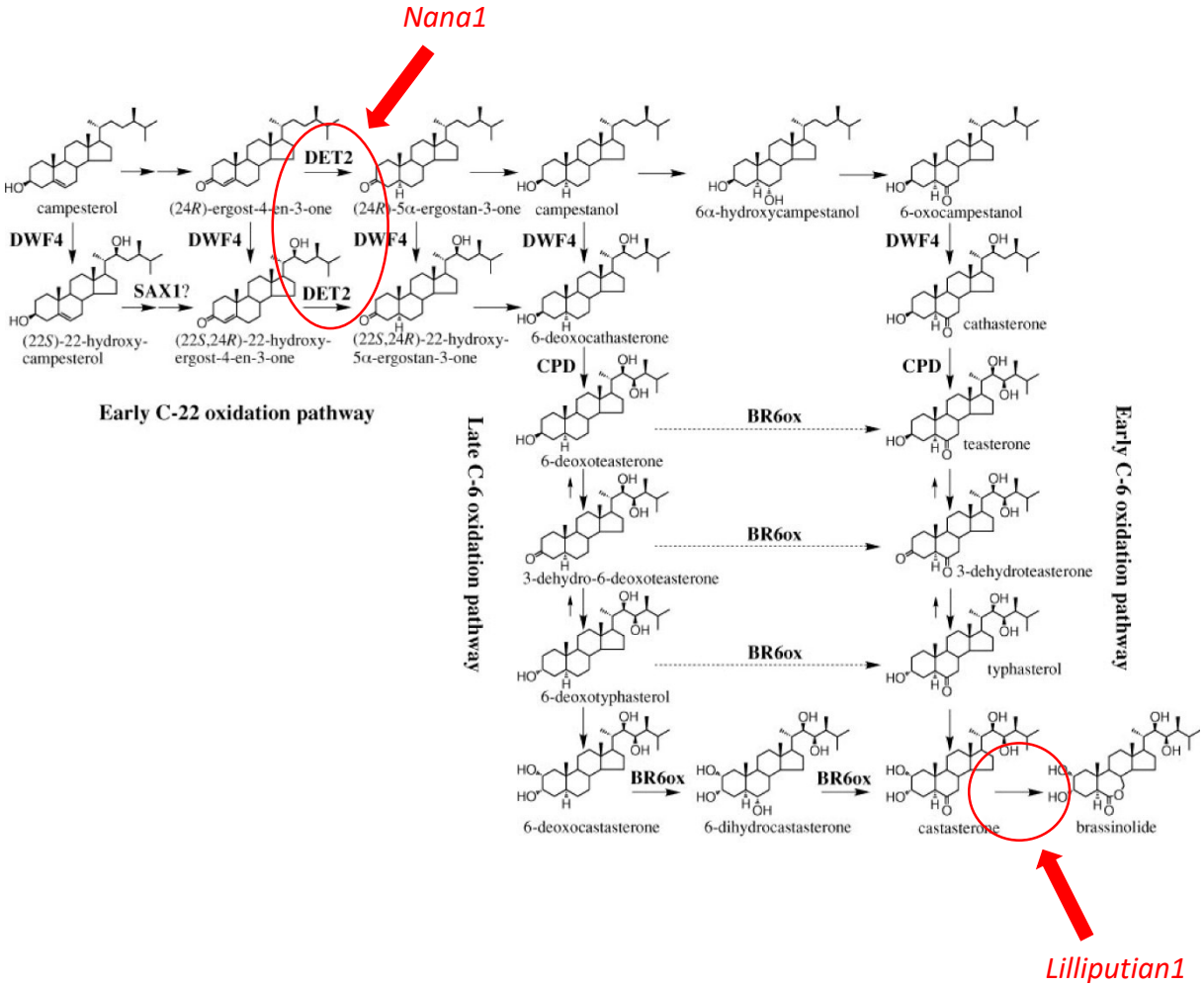

Figure 2. Brassinolide biosynthesis from campesterol. All the enzymes identified in Arabidopsis are shown. Image from: Fujioka, S., & Yokota, T. (2003). BIOSYNTHESIS AND METABOLISM OF BRASSINOSTEROIDS. Annual Review of Plant Biology, 54(1), 137–164. At the picture are been added a red circle in correspondence to the positions in the pathway of maize genes *Nana1* and *Lilliputian1*.

Both *na1-1* and *lil1-1* mutants are severely compromised in height, floral development and overall plant architecture (Hartwig *et al.* 2011b; Makarevitch *et al.* 2012).

na1-1 mutants, compared with wild type plants, shows a decrease in plant height due to a reduction of internode length. The number of internodes is the same of wild type plants. Overall, *na1-1* mutant plants reach approximately one-third in height compared with wild type. Mutant plants show also alterations in leaf size and morphology. The leaf width remained largely unaffected, but their length is about 60% of the wild type.

In addition, *na1-1* mutant leaves were positioned more erectly toward the stem and showed twisting around the midrib. Tassels of *na1-1* mutants were also often partly feminized (Hartwig *et al.* 2011b).

lil1-1 mutant seedlings show the same phenotype with a drastic reduction in the whole stature if compared with wild type siblings. In particular, mutant mesocotyl elongation appears blocked, and mutant coleoptile elongation reaches about 25% that of the wild type. Morphology is not altered in the mutant shoot apex, however leaf primordia appear more compressed, as evident in the analysis of longitudinal sections. Mutant leaves appear thicker than wild type leaves, exhibit altered shape and presence of supernumerary cell layers in the mesophyll region between the leaf vessels and the adaxial leaf epidermis. Comparison of adaxial mutant and wild type fourth and tenth leaf epidermis reveal that mutant cells have a square-shaped morphology that differs from the elongated shape of wild type cells.

Aim of the work

In this study, part of a wider work, we investigated the role of BRs in plant development and in plant-environment interactions, through the analysis of *lilliputian1-1* (*lil1-1*), a dwarf mutant impaired in the BR biosynthesis in maize.
In the first analysis, we investigated the involvement of BRs in the regulation of epicuticular waxes deposition and in plant leaves permeability.
Furthermore, we tried to clarify the structure of the BRs biosynthetic pathway, studying the interaction between *lil1-1* and *na1-1*.

MATERIAL AND METHODS

Plant material

The maize dwarf mutants analysed in this work are referred to two different alleles:

- *lilliputian1-1* (*lil1-1*): was originally isolated from the selfed progeny of the Mutator stock outcrossed to an unrelated stock. The *lil1-1* mutant was introgressed three times into B73 and one in A188, H99 and Rscm2 inbred lines. Due to the seedling lethality or impaired inflorescence development, the *lil1-1* mutant was maintained as heterozygous (Fig. 3).

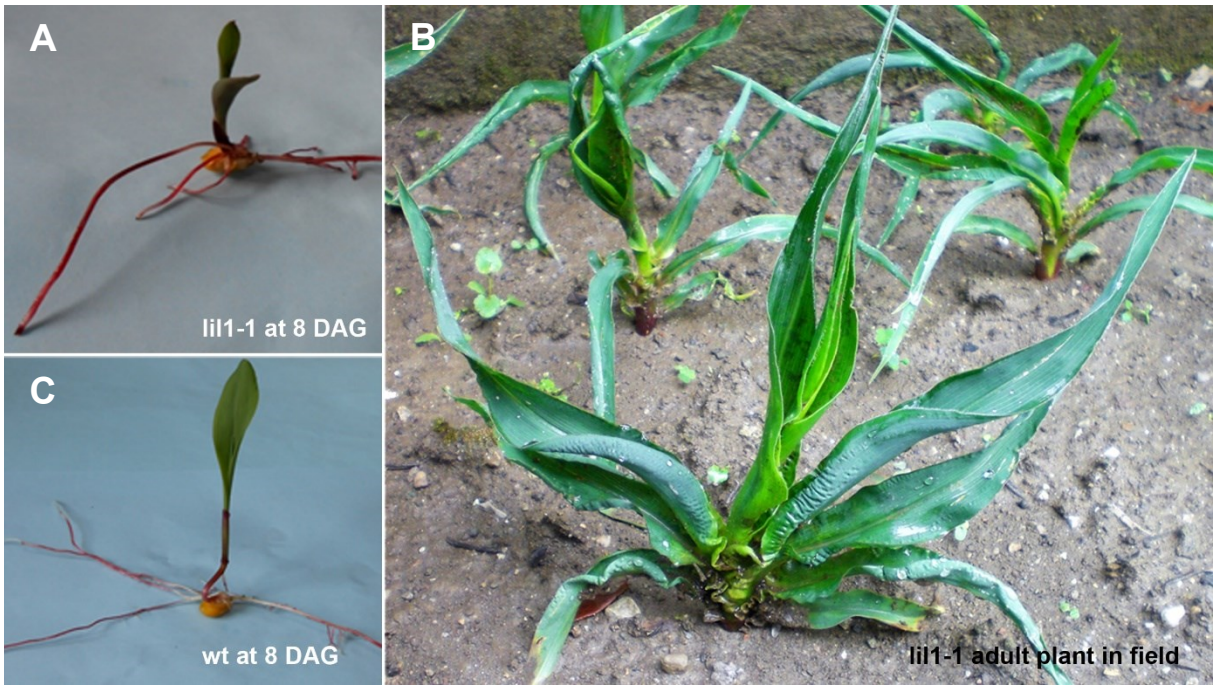

Figure 3. lil1-1 mutant plant seedling (A) compared with a wild type plant at the same age (B). Adult *lil1-1* plant in open field (C).

- *nana1-1* (*na1-1*): was obtained from the Maize Genetics Cooperation Stock Center (Maize COOP, Code 2011-754-3). The *na1-1* mutant was introgressed one time into the Mo17 inbred line. Due to the seedling lethality or impaired inflorescence development, the *na1-1* mutant was maintained as heterozygous (Fig. 4).

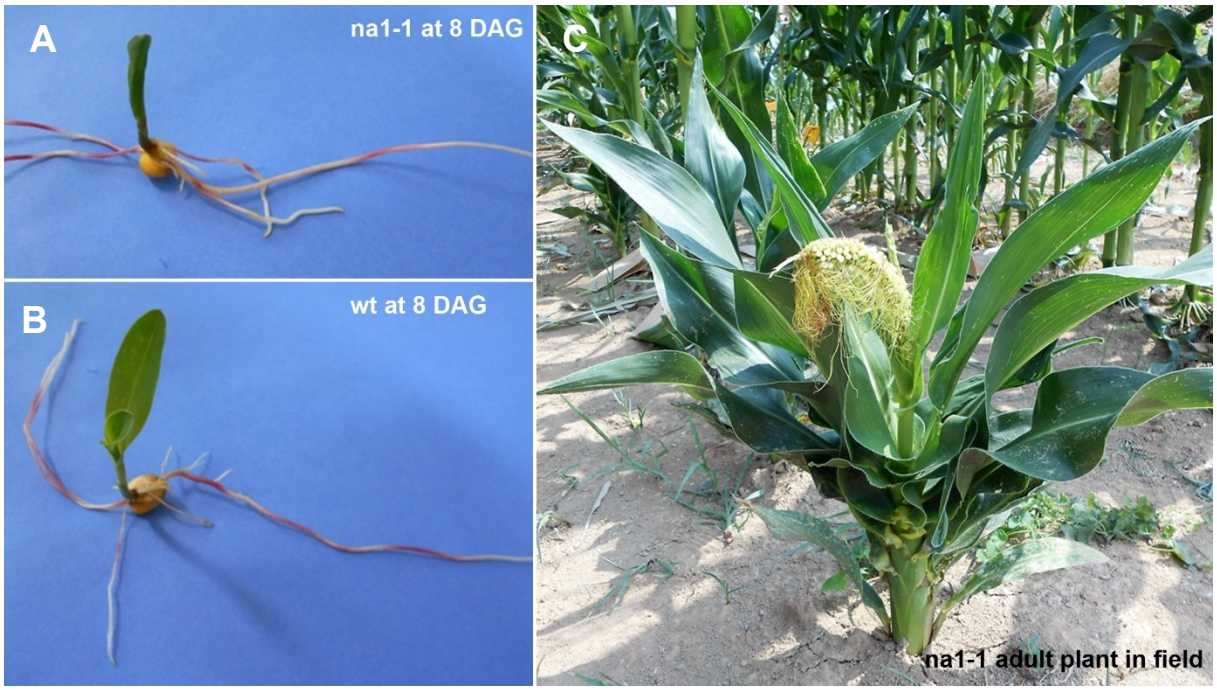

Figure 4. na1-1 mutant plant seedling (A) compared with a wild type plant at the same age (B). Adult *na1-1* plant in open field (C).

Plants for experiments at seedling stage were sown in growth chamber on wet paper or in soil. The conditions inside the chamber were: 25°C and a 16 h-light photoperiod.

Plants for crosses and experiment at adult stage were sown and growth directly in open field. The field was located in Verderio Superiore (LC), Italy. Plants were sown between April and May.

Seeds sterilization

Before the sowing in growth chamber, all the seeds were sterilized by keeping them in a solution of bleach/water 1:1 for 20 minutes. Then the seeds were washed with deionized water and immediately sown.

Genomic databases and in silico analysis

Gene sequences used in this work were obtained from online databases:

- NCBI Genbank (www.ncbi.nlm.nih.gov/genbank)
- MaizeGDB.org (www.maizegdb.org)
- Gramene.org (http://www.gramene.org)
- JGI Phytozome (phytozome.jgi.doe.gov)
- KEGG (http://www.genome.jp/kegg)

DNA extraction

DNA was extracted from plant with the procedure here described that employs ethanol precipitation for concentrating and de-salting nucleic acids preparations in aqueous solution.

- Put 20-40 mg of tissue in an 1.5 ml Eppendorf vial
- Add 300 µl of extraction buffer
- Grind the tissue
- Add 100 µl of SDS 2%
- Incubate at 60°C for a time between 30 min and 2 hours
- Spin at maximum speed for 15 min
- Transfer 150 µl of supernatant in another clean Eppendorf vial
- Add 150 µl of 5M ammonium acetate and 300 µl isopropanol. Mix gently
- Incubate at room temperature for 15 min
- Spin at 9000xg for 5 min.
- Waste the supernatant
- Wash the pellet with 500 µl of 70% ethanol (cooled at -20)
- Spin at 9000xg for 5 min
- Waste the supernatant
- Dry at the air or in vacuum condition
- Suspend gently in 50 µl TE pH8

- Incubate at 65°C for 5 min
- Store at -20°C

Extraction buffer: 2M NaCl, 200mM Tris-HCl pH8, 70mM EDTA pH8, 20mM Sodium metabisulfite

PCR analysis

PCR analyses were performed using "GoTaq® G2 Flexy DNA Polimerase" by Promega.
The reaction mix was prepared in a total volume of 10 µl, using the protocol reported in Table 1.

COMPONENT	VOLUME FOR 10 µl TOTAL	FINAL CONCENTRATION
H_2O	4.25 µl	
5X GoTaq® Flexi Buffer	2 µl	Na^+ 50 mM
$MgCl_2$ 25 mM	1 µl	2.5 mM
Betaine 5 M	0.9 µl	450 mM
dNTPs 10 mM	0.2 µl	0.2 mM
Forward primer 10 mM	0.3 µl	0.3 mM
Reverse primer 10 mM	0.3 µl	0.3 mM
Taq	0.05 µl	0.025 U/µl
DNA		Up to 100 ng/µl

Table 1. Protocol exploited for PCR analysis in this work. For every component are reported the volume used for 10 µl final volume, and the final working concentration.

Reactions were performed following the protocol provided by the manufacturer. Annealing temperatures (T_a) and extension times ($Time_{ext}$) were variables according to the pair of primers used.

Primers were designed using the NCBI "Primer blast" online software. All the primers used in this work are reported in Table 2. In Table 3 are reported the PCR condition for every primers couple used.

NAME	GENE NAME	GENE ID (NCBI)	ORGANISM	SEQUENCE (5' – 3')	T_M (°C)
Lil1F	*Lil1*	GRMZM2G103773	*Zea mays*	GGGAAAACAACACCGACTT	58
Lil3R				GCATGAAGGCGTCGATCT	56
Na1-F	*Nana1*	GRMZM2G449033		CAACTGAAGATGCCCGACCA	59
Na1-F2				ATCCCCAAACCCCAGAAAC	57
Na1-R				CCTGTAGGTAGGCGTTGAGG	61
Mu53s			*Mutator element*	GGATTCGACGAAATAGAGGC	60

Table 2. PCR primers used in this work. Primers are shown individually. For every primer is reported the melting temperature (T_m) calculated, the sequence and the correspondent gene.

PRIMERS COUPLE	GENE NAME	ORGANISM	T_A (°C)	PRODUCT LENGTH (BP) (GENOMIC/cDNA)	$TIME_{EXT}$ (S)
Lil1F – Lil3R	*Lil1*	*Zea mays*	56	443	30
Lil1F – Mu53s	*Lil1*	*Zea mays*	56	250	15
Na1-F2 – Na1-R	*Nana1*	*Zea mays*	56	451	30
Na1-F – Mu53s	*Nana1*	*Zea mays*	56	348	20

Table 3. Couple of PCR primers used in this work. Primers are shown associated in pairs, as they were used in PCR analysis. For every couple are reported the annealing temperature (T_a) used for reactions, the amplified region length, and the extension time ($Time_{ext}$).

Furthermore, for *Lil1* and *Na1*, the gene model is reported in Figure 5.

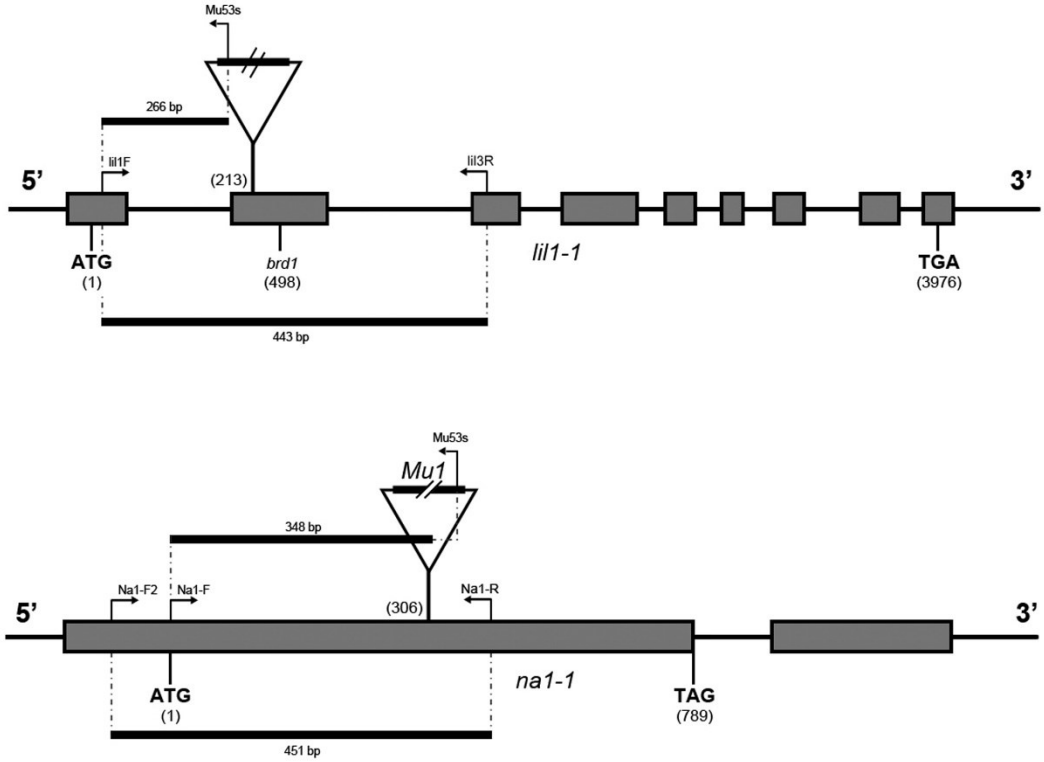

Figure 5. Gene models for *Lil1* and *Na1* genes. All the genes are oriented in 5' – 3' direction. Exons are represented in grey boxes, introns and untranslated parts are represented by a black line.

PCR products were separated by electrophoresis in 1% agarose gels stained with 0.5 µg/ml final concentration of ethidium bromide.

Microscopy analysis

For the analysis of epicuticular waxes, leaf pieces of wild type and *lil1-1* mutant were dried and processed according to La Rocca et al. (2015). The specimen surfaces were examined with the SEMLEO 1430 (Zeiss) scanning electron microscope (SEM).

Analysis of stomatal density and stomatal index

To measure stomatal density and stomatal index, leaves of the same age and from the same relative position were sampled from wild-type and mutant plants. A leaf surface imprint method was used. Briefly, a drop of glue was applied to the leaf surface, both the adaxial and abaxial side, and distributed with a brush. When the glue was completely dried, the thin layer was carefully removed with a tong and put on a glass slide for light microscope observation (Ortholux, Leitz, Germany). For statistical analysis of stomatal density, five leaf areas were sampled for each plant and for each side and seven plants were sampled for the wild-type and the mutants. Stomatal index (si) was determined as [number of stomata/(number of epidermal cells + number of stomata)] × 100 (Salisbury 1928).

Statistical analysis

All the data were subjected to statistical analysis and the means were tested by one-way analysis of variance (ANOVA) at 5% level of significance. All the statistical analyses were conducted using the statistical packages SPSS 21.0 and Graph Pad Prism 6.

Chlorophyll leaching analysis

For the chlorophyll leaching analysis fifth leaves from wild type, *na1-1* and *lil1-1* plants were used. Leaves were dissected into 8 cm length pieces, weighted, immersed in ethanol 80% and incubated at room temperature (Fig. 6). Every vial was carefully covered to protect the samples from light. A series of 1 ml aliquots were taken at 12, 24, 36, 48, 60 and 72 hours. Absorbance was measured at 647 and 664 nm with a spectrophotometer (Agilent Technologies Cary 60 UV-Vis) in order to quantify the chlorophyll released in the solution. The micro molar concentration of total chlorophyll per gram of fresh weight of tissue was calculated using the equation: Total micromoles chlorophyll = 7.93 x A_{664} + 19.53 x A_{647} (Lolle *et al.* 1997).

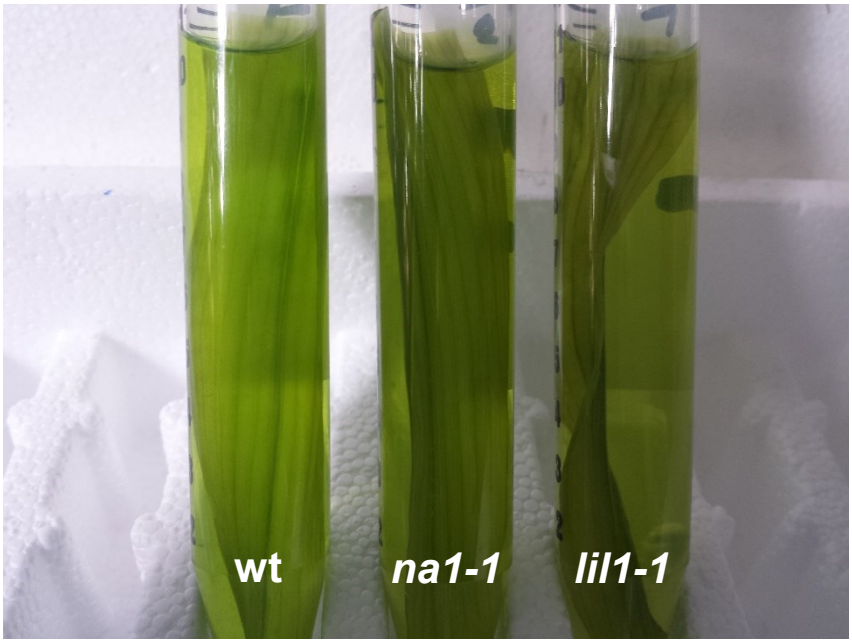

Figure 6. Leaves after 72 hours of immersion in ethanol 80%.

RESULTS

Epicuticular waxes and leaf permeability are altered in the *lil1-1* mutant

Previous observations demonstrated that in maize, *lil1-1* mutant shows a better tolerance against dehydration compared with wild type plants (Persico 2015). Furthermore, other works on *lil1-1* and *na1-1* mutants, both mutated in a gene involved in the brassinosteroids biosynthesis pathway, (Dolfini *et al.* 1999; Kir *et al.* 2015) have demonstrated that these two mutants show a thicker leaf epidermis compared with wild type plants.

To gain insight into the role of these genes in responding to water stress condition we performed two analyses.

A possible alteration in epicuticular waxes was inferred by a peculiarity observed for the *lil1-1* mutant leaves. Indeed, leaves retain water beads on their surface when they are misted with water (Fig. 7). For this reason, we first analysed epicuticular waxes.

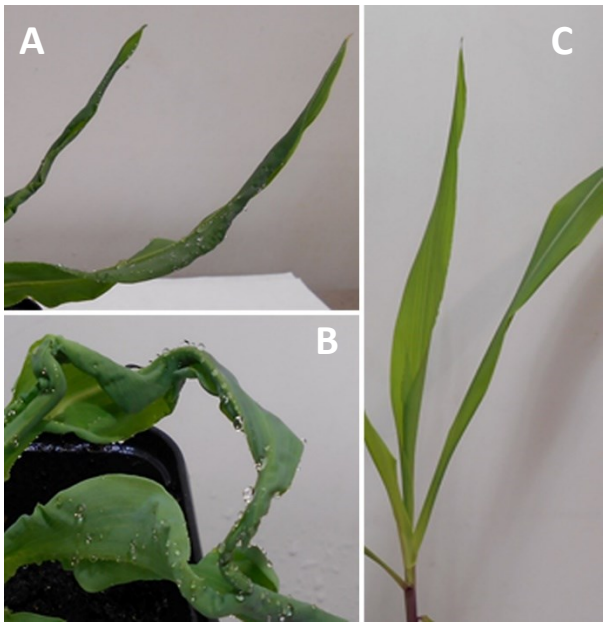

Figure 7. Representative leaves of mutant and wild type plants misted with water. In the photos are shown the fourth leaves of A,B) *lil1-1* mutant, and C) wild type plants. Is possible to see water droplets covering the surface of mutant leaves, whereas water flows on the leaves of the wild type plants, leaving them without drops on the surface.

Scansion electronic microscopy (SEM) analysis of the forth leaves surface of *lil1-1* mutant and wild type plants (Fig. 8) confirmed this observation.

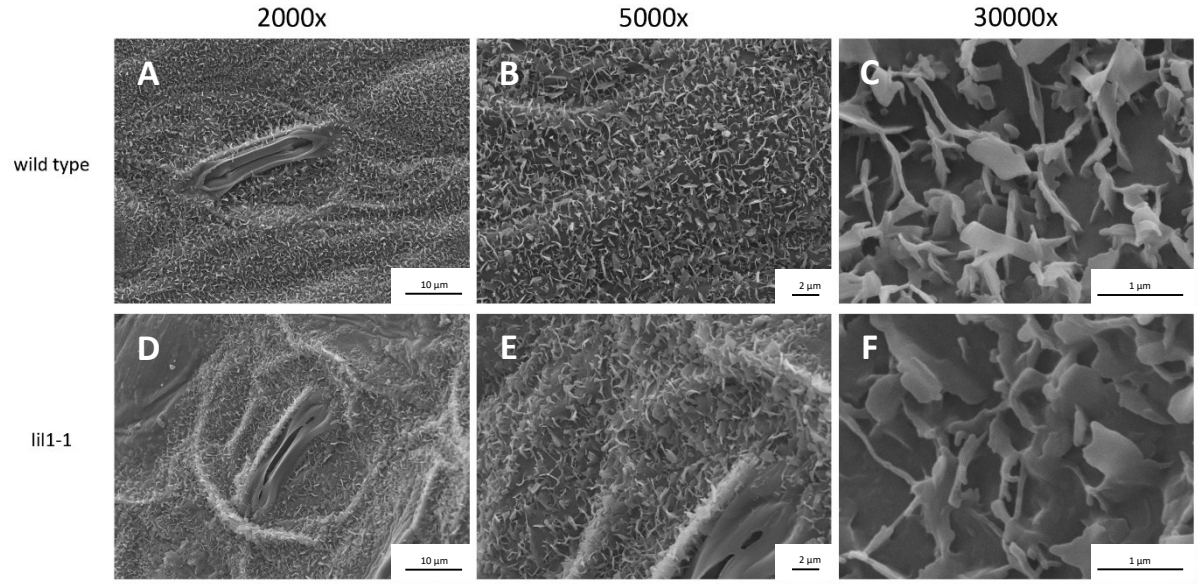

Figure 8. SEM photos of the surface of wild type (A, B, C) and *lil1-1* (D, E, F) leaves, the photos were taken in the same areas, at different magnifications (2000x, 5000x, 30000x).

SEM photos (pictures) clearly show differences in epicuticular waxes between wild type and mutant. Photos of wild type plants (A, B and C) show a regular distribution of wax crystalloids. Photos of *lil1-1* instead (D, E, F), show an irregular distribution of waxes, with areas abundant in waxes, forming crests, and areas completely lacking. Moreover, photos at 30000x magnification (C and F) show that *lil1-1* waxes are altered also in the shape of crystalloids, which appears less developed and partially melded between them.

We also assess if this alteration could have an effect on the leaf permeability, by performing a chlorophyll leaching analysis. To this aim, fifth leaf samples of wild type, *na1-1* and *lil1-1* were immersed in ethanol 80% and incubated at room temperature for 72 hours. Every 12 hours an aliquot of ethanol was taken from every sample and chlorophyll content measured. Results are shown in Fig. 9.

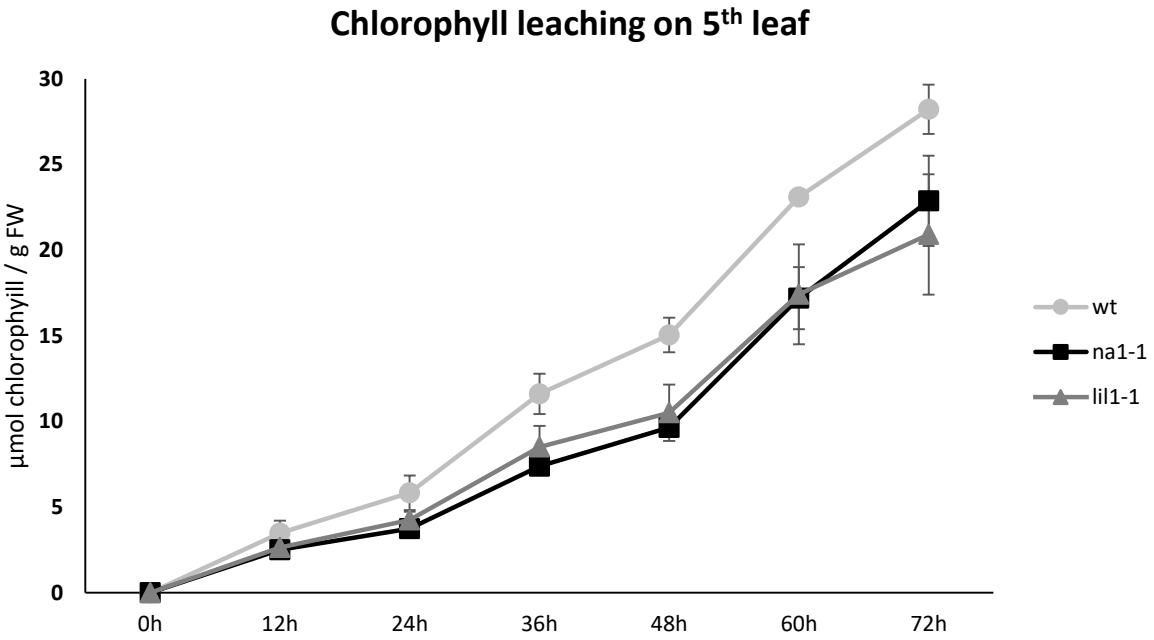

Figure 9. Amount (in micro moles) of total chlorophyll for gram of fresh weight leached by the fifth leaf of wild type, *na1-1* and *lil1-1* plants. Reads were performed every 12 hours, from 0 to 72. wt: wild type genotype. na1-1: homozygous *nana1-1* genotype. lil1-1: homozygous *lil1-1* genotype. Error bars show Standard Error.

The results of the experiment show that leaves of wild type plants release a significantly higher amount of chlorophyll compared with *lil1-1* and *na1-1.* The difference became evident after 36 hours of incubation, and slowly increases with the time. Concerning the mutants, *lil1-1* and *na1-1* keep a very similar trend throughout the experiment. The amount of chlorophyll leached remains almost the same until 72 hours of treatment.

Evaluation of the interaction between *lil1-1* and *na1-1* alleles

The *na1-1* (Hartwig et al., 2011) and *lil1-1* mutants are impaired in the earlier and the final steps of the BR biosynthesis, respectively. We observed that in homozygous *na1-1* (*na1-1/na1-1*) plants growth defects appeared less severe than in homozygous *lil1-1* (*lil1-1/lil1-1*) plants. Therefore, to compare their phenotypes as well as to analyse the genetic relationship between the two mutants, F_2 progenies were produced from selfing heterozygous *na1-1*/+ *lil1-1*/+ F_1 plants.

The genotype of the four F_1 progenies obtained was determined through PCR analysis.

All the four progenies of the F_1 were tested through PCR for *na1-1* allele (348 bp amplicon) (Fig. 10).

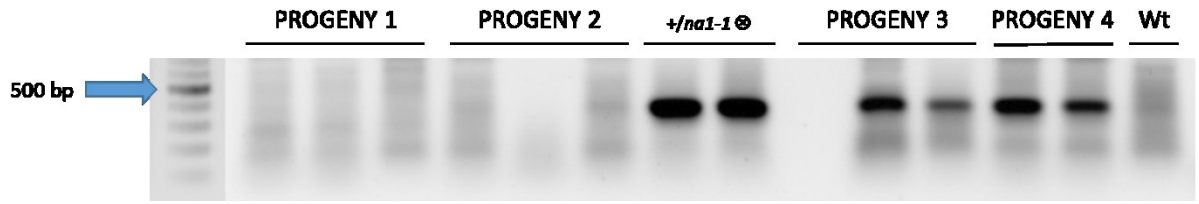

Figure 10. Genotyping for *na1-1* allele on the all 4 F1 progenies. The weight of expected amplicon is 348 bp. Sample +/*na1-1* was used as positive control.

Progenies 3 and 4, confirmed for *na1-1* allele were tested for *lil1-1* allele (250 bp amplicon) (Fig. 11).

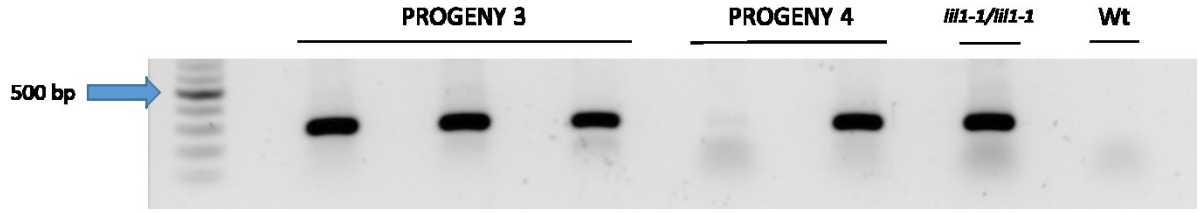

Figure 11. Genotyping for *lil1-1* allele on F1 progenies 3 and 4. The weight of expected amplicon is 250 bp. Sample *lil1-1/lil1-1* homozygous for *lil1-1* was used as positive control.

Plants from progenies 3 and 4 showed both *na1-1* and *lil1-1* alleles. These double heterozygous plants were self-crossed, to obtain an F_2 progeny, which are expected to contain a number of plants (1/16) homozygous for both *lil1-1* and *na1-1* alleles.

One of the F_2 progenies obtained (C970 (4) ⊗), was deeply analysed. We germinated on paper 200 seeds. At 9 days after germination (DAG), plants were visually evaluated for their phenotype, and shoot length of every plant was measured.

Four phenotypic classes were expected in the progenies, however, since it was not possible to recognize a clear double mutant phenotype in the progeny, plants were classified into three classes: wild type, *lil1-1* like mutant and *na1-1* like mutant (Fig. 12).

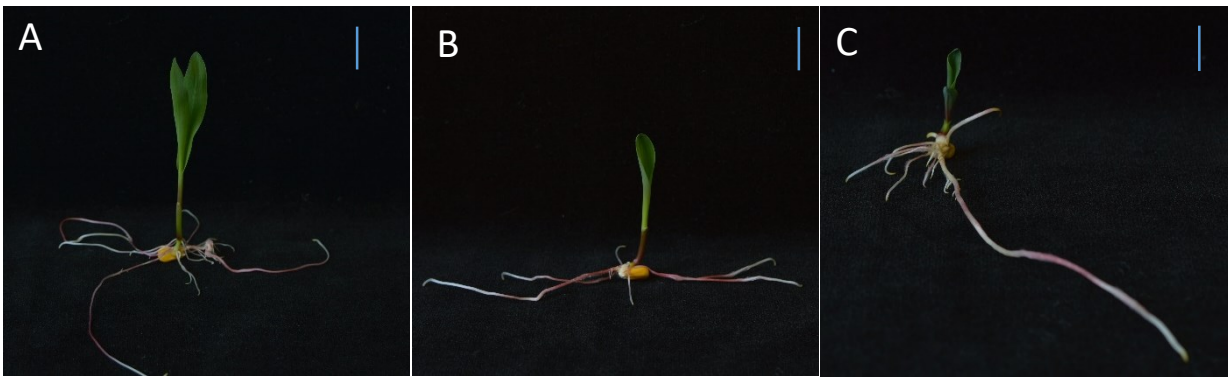

Figure 12. Representative photos of the three classes of seedlings after 9 DAG. A) wt, B) *nana1-1,* C) *lil1-1.* Scale bar: 2cm

The number of plants for every class is reported in Table 4.

	PHENOTYPIC CLASS			TOTAL PLANTS NUMBER
	Wild type	*na1-1*	*lil1-1*	
OBSERVED PLANTS	102	31	38	171

Table 4. Number of plants observed for every phenotypic class in C970 (4) ⊗ progeny analysed.

The X^2 test confirmed the hypothesis of a 9:4:3 Mendelian segregation (X^2 value: 0.91), in which presumably the double mutant plants are included inside the *lil1-1* class.

The genotype of all the plants was determined by PCR. Every DNA sample was tested for four different alleles: *Lil1, lil1, Na1, na1*, and the plants were classified into four genotypic classes:

1. Wild type class (wild type or heterozygous for either one or both *lil1-1* and *na1-1* alleles)
2. *na1-1* class (plants homozygous only for *na1-1* allele)
3. *lil1-1* class (plants homozygous only for *lil1-1* allele)
4. Double mutant class (plants homozygous for both *na1-1* and *lil1-1* alleles)

The number of plants for every class is reported in Table 5.

	GENOTYPIC CLASS			
	Wild type	*na1-1*	*lil1-1*	Double mutant
OBSERVED PLANTS	102	31	26	12

Table 5. Number of plants observed for every phenotypic class in C970 (4) ⊗ progeny analysed.

The X^2 test confirmed the hypothesis of a 9:3:3:1 Mendelian segregation (X^2 value: 1.69).

All the double mutant plants were previously included in the *lil1-1* like group, and their phenotype appeared identical to the *lil1-1* homozygous mutant plants.

A little number of plants for every genotypic class was growth inside a growth chamber for 70 days, in order to verify their adult phenotype (Fig. 13). Also at this age, the phenotypes of *lil1-1* and double mutant plants appear to be not distinguishable.

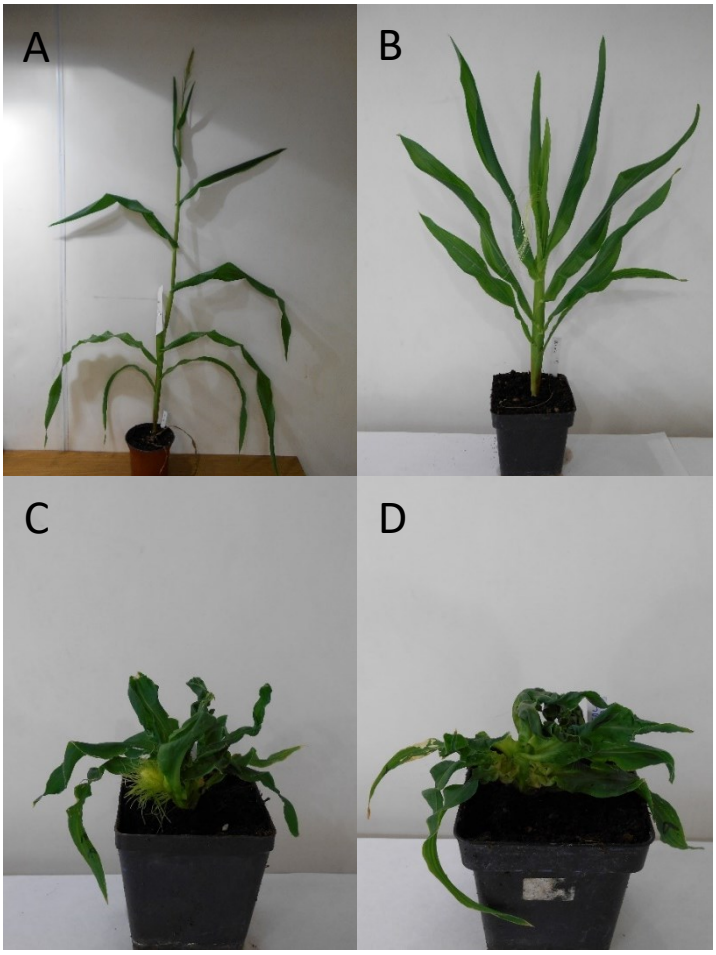

Figure 13. Representative plants at 70 days after germination, divided into the four genotypic classes. A) Wt, B) *na1-1*, C) *lil1-1*, D) double mutant.

Differences in morphology between wild type, *na1-1*, *lil1-1* and double mutants

Our experiment shows that wild type plants were clearly distinguishable from mutant plants. It also showed that the homozygous *na1-1* individuals were all included in the "na1–like" mutant class while both homozygous *lil1-1/lil1-1* and double homozygous (*na1-1/na1-1 lil1-1/lil1-1)* mutant plants belonged to the "lil1-like" category. For this reason, a deeper analysis of the plant morphology was performed, in order to observe if some differences can be detected between *lil1-1* homozygous plants and double homozygous (*na1-1/na1-1 lil1-1/lil1-1)* mutant plants.

Shoot length

The shoot length (9 DAG) of every plant, divided into the four genotypic classes, were plotted in order to visualize the length distribution (Fig 14). The shoot lengths appear clearly distributed in classes, with wild type and *na1-1* classes clearly different from all the others. Double mutant and *lil1-1* classes appear very similar to each other.

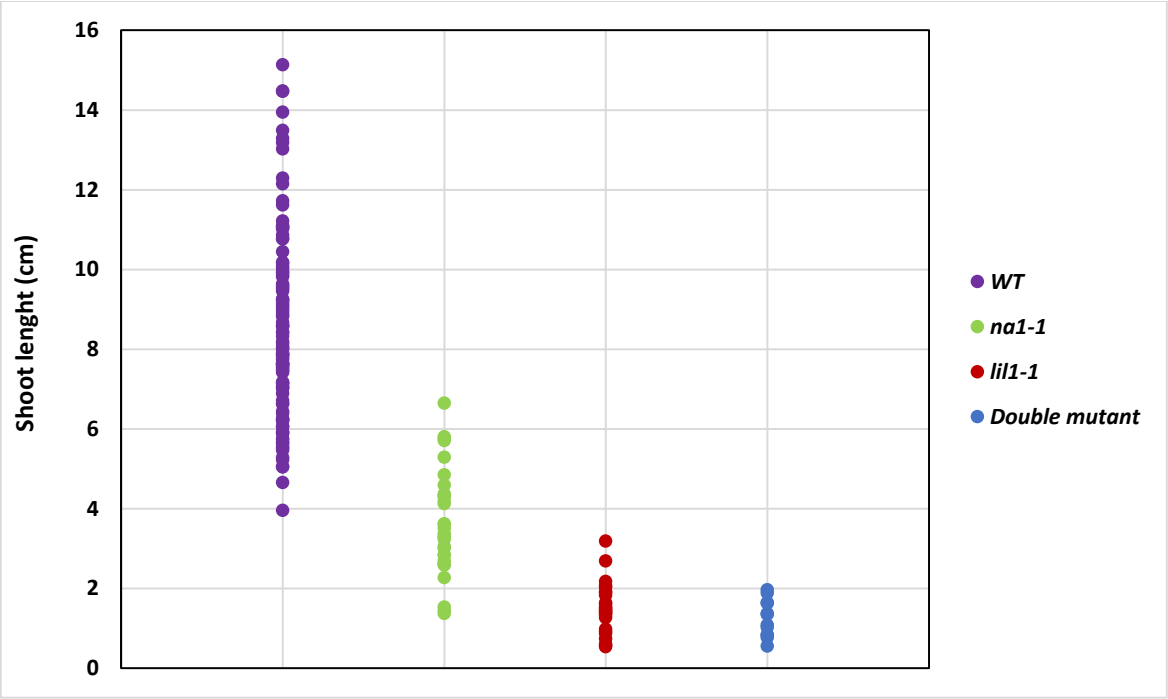

Figure 14. Dot plot of the plants shoot length, divided into the four genotypic classes recognized. Every dot represents a plant. WT: wild type genotype. *na1-1*: homozygous *nana1-1* genotype. *lil1-1*: homozygous *lil1-1* genotype. *Double mutant*: homozygous *na1-1/na1-1 lil1-1/lil1-1* genotype.

An ANOVA test was applied to the data, in order to found statistically significant differences between the shoot lengths of every genotypic class (Fig. 15).

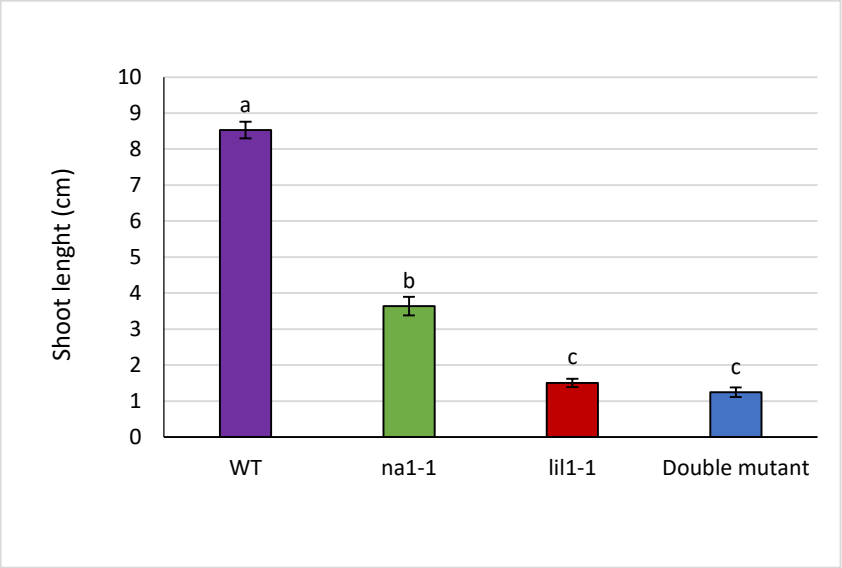

Figure 15. The plot shows the average shoot length of the plants in every genotypic class. WT: wild type genotype. *na1-1*: homozygous *nana1-1* genotype. *lil1-1*: homozygous *lil1-1* genotype. *Double mutant*: homozygous *na1-1*/*na1-1 lil1-1*/*lil1-1* genotype. Letters are referred to the result of the ANOVA test, which found no differences between *lil1-1* and double mutant classes. Error bars show Standard Error.

The test founds differences between wild type and all the other classes. The same result was obtained for *na1-1* class. Instead, no significant differences were found between *lil1-1* and double mutant classes, confirming the fact that these two genotypes appear to have the same average shoot length.

Stomatal index

The genetic relationship between *na1* and *lil1* was analysed also for epidermal traits in the median portion of fully expanded fourth and sixth leaves. A stomatal index analysis was performed on wild type, *lil1-1*, *na1-1* and double mutant leaves.

In Figure 16 are shown representative photos of the abaxial epidermis belonging to wild type, *lil1-1*, *na1-1* and double mutant 6th leaves.

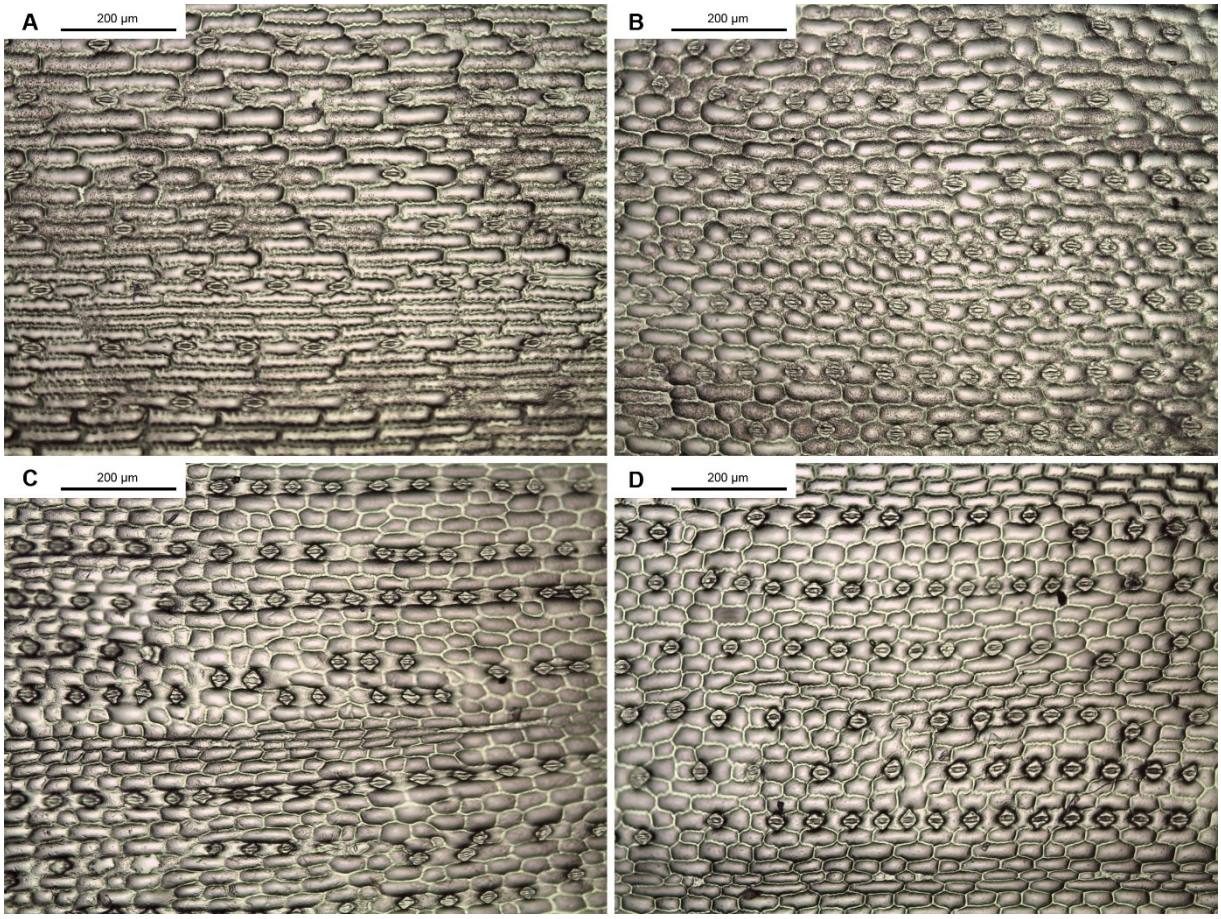

Figure 16. Representative photos of 6th leaf abaxial side, belonging to A) wild type, B) *Nana1-1*, C) *Lilliputian1-1*, D) Double mutant. In all the photos is possible to see stomata and pavement cells.

For every genotype was calculated the stomatal index, reported in Figure 17 and Figure 18.

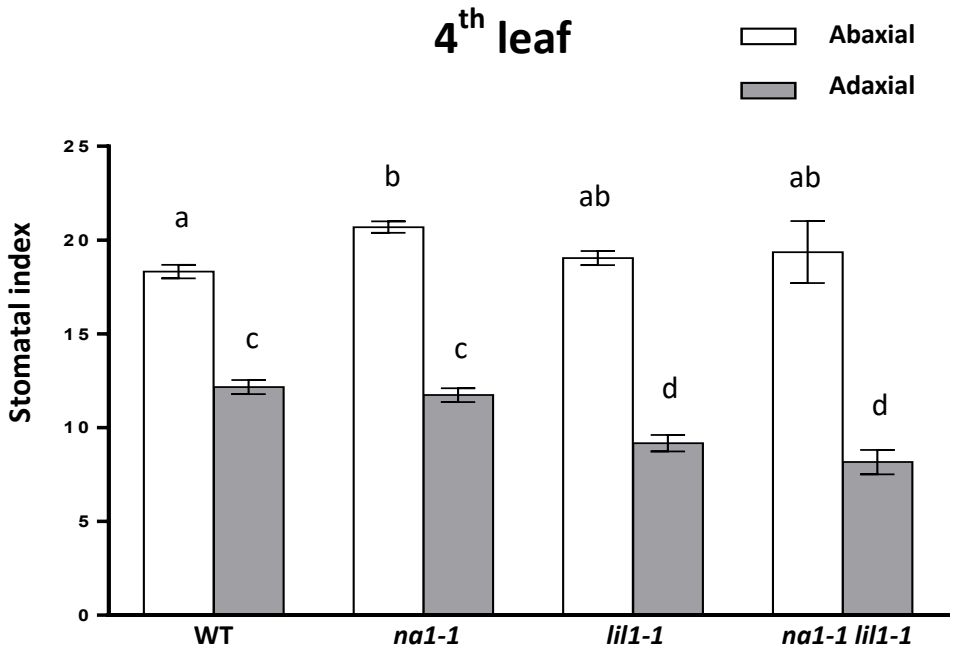

Figure 17. Stomatal index of the 4th leaf. Data for abaxial page is reported in white, adaxial page is reported in grey. WT: wild type genotype. *na1-1*: homozygous *nana1-1* genotype. *lil1-1*: homozygous *lil1-1* genotype. *na1-1 lil1-1*: homozygous *na1-1/na1-1 lil1-1/lil1-1* genotype. Bars indicate Standard Error, letters are referred to ANOVA test.

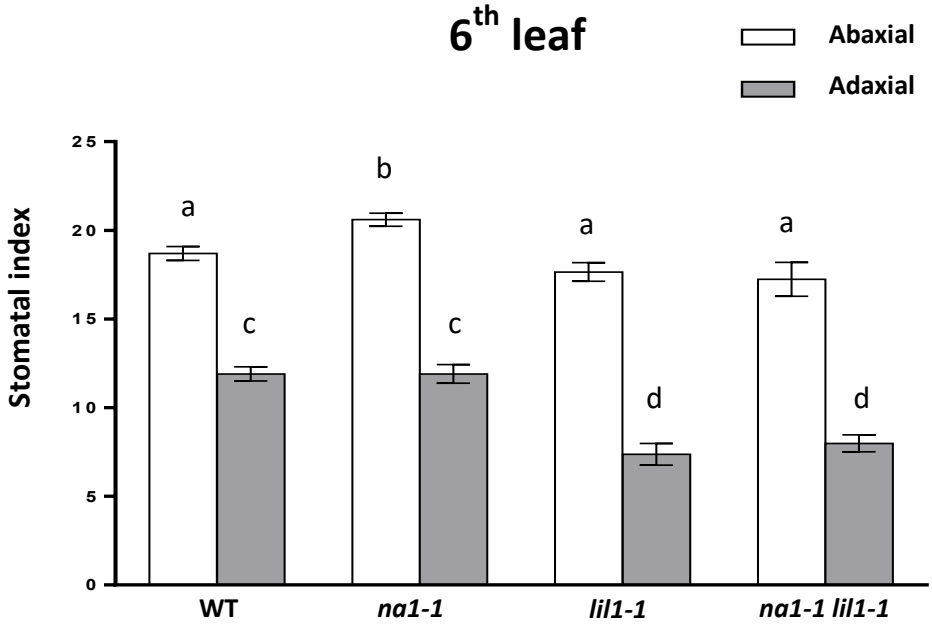

Figure 18. Stomata index of the 6th leaf. Data for abaxial page is reported in white, adaxial page is reported in grey. WT: wild type genotype. *na1-1*: homozygous *nana1-1* genotype. *lil1-1*: homozygous *lil1-1* genotype. *na1-1 lil1-1*: homozygous *na1-1/na1-1 lil1-1/lil1-1* genotype. Bars indicate Standard Error, letters are referred to ANOVA test.

Analysing the 4th leaf, there are little differences among genotypes on the abaxial page. On the adaxial page instead, differences are more relevant. As is possible to see, wild type and *nana1-1* plants were identical and also *lil1-1* and double mutants showed equal values between them but were different from the first two. A very similar situation is observable also in the 6th leaf.

For a deeper analysis, is possible to compare the cell density of pavement cells and guard cells for every genotype (Fig. 19 and Fig. 20).

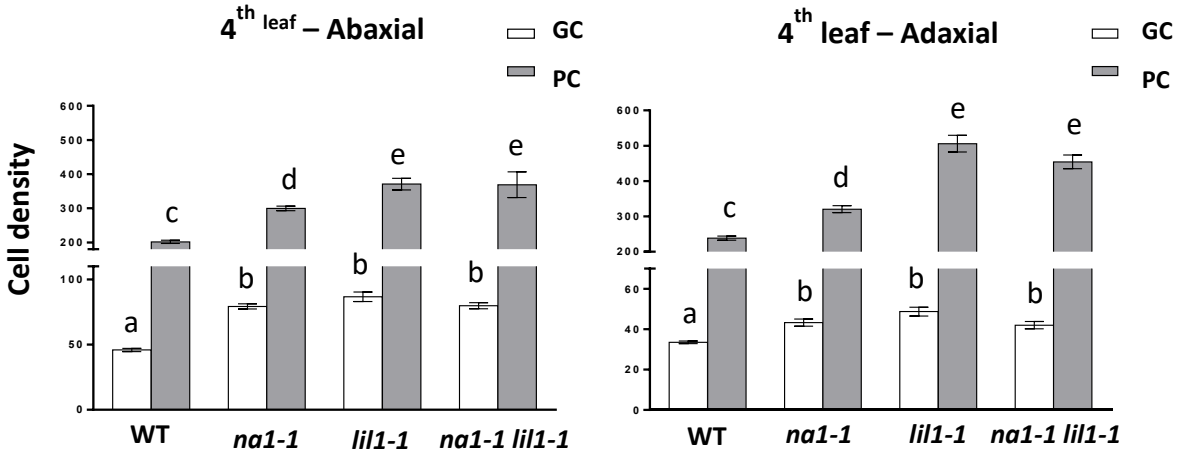

Figure 19. Cell density of guard cells (GC) and pavement cells (PC) in fourth leaves. Measurement were done on adaxial and abaxial pages. WT: wild type genotype. *na1-1*: homozygous *nana1-1* genotype. *lil1-1*: homozygous *lil1-1* genotype. *na1-1 lil1-1*: homozygous *na1-1*/*na1-1 lil1-1*/*lil1-1* genotype. Bars indicate Standard Error, letters are referred to ANOVA test.

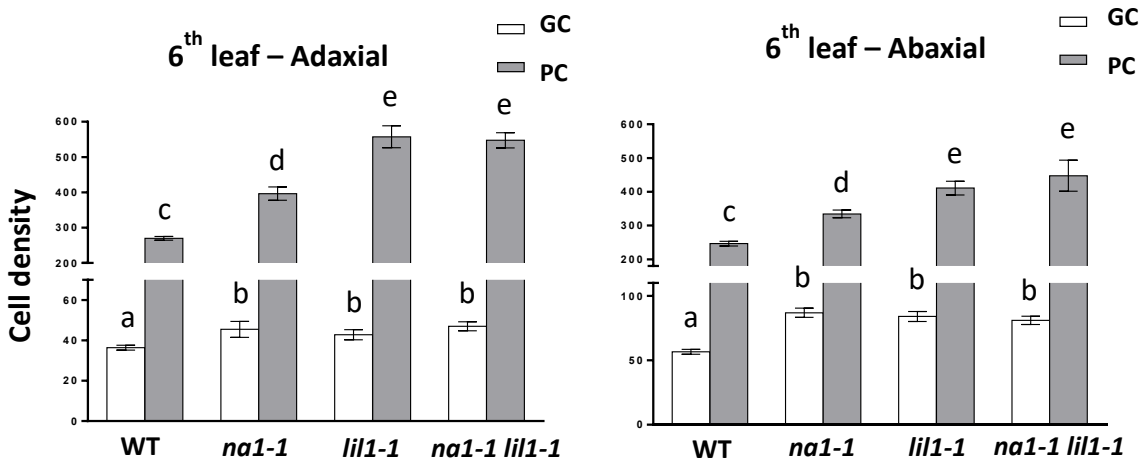

Figure 20. Cell density of guard cells (GC) and pavement cells (PC) in fifth leaves. Measurement were done on adaxial and abaxial pages. WT: wild type genotype. *na1-1*: homozygous *nana1-1* genotype. *lil1-1*: homozygous *lil1-1* genotype. *na1-1 lil1-1*: homozygous *na1-1*/*na1-1 lil1-1*/*lil1-1* genotype. Bars indicate Standard Error, letters are referred to ANOVA test.

Comparison of the cell density in the 4th leaf adaxial side among wild type, single and double mutant plants revealed that both *nana1-1* and *lil1-1* mutants have a higher number (density) of pavement cells (PC) compared with wild type. Analogously to seedling height (Fig. 15), *lil1-1* and double mutants showed a higher PC density compared with *nana1-1* but instead they were not statistically different between each other. With regards to the guard cells (GC) density, wild type resulted lower and significantly different from all single and double mutants. The adaxial side and the abaxial side of the 4th leaf presented the same trend, but in the first the PC density of the mutant plants showed a greater increment.

Also in this case, similarly to what was observed for the stomatal index, the situation in the 6th leaf appears very similar to that observed in the 4th leaf.

DISCUSSION AND CONCLUSION

This study provided further information on the role of the *lil1* gene during maize seedling development.

Previous observations obtained in our laboratory indicated that the *lil1-1* mutant shows better dehydration tolerance, which could be probably attributable to the presence of a thicker epidermis. Furthermore, the observation that water beads were retained on the leaves' surface suggested an alteration of epicuticular waxes.

Alterations of epicuticular waxes were confirmed by SEM analysis. Furthermore, a chlorophyll leaching experiment demonstrated that leaf epidermis of *lil1-1* shows a significantly lower permeability than wild type. The experiment also showed that *nana1-1* mutant leaves have the same property. In our hypothesis, the thicker epidermis observed both in *lil1-1* and in *nana1-1* compared with wild type, can explain the lower permeability and the better dehydration tolerance of these mutants.

The other experiments were done with the aim of clarifying the interaction between *lil1-1* and *nana1-1* mutants.

Brassinosteroids control several plant developmental processes in plants (Divi and Krishna, 2009). For this reason, BR mutants show a large number of alterations in their phenotype. The maize *lil1-1* mutant, shows severe alterations compared with wild type plants, such as extreme dwarfism, and thick and crinkly leaves. These alterations are also common in other BR mutants, like *nana1-1* (Hartwig *et al.,* 2011a). However, alterations showed by *lil1-1* appeared dramatically stronger compared with *nana1-1*.

Both *nana1* and *lil1* genes have a key role in the BR biosynthesis pathway, which has been reconstructed in recent years (Fujioka and Yokota, 2003). The product of *nana1* is involved in two parallel pathways, therefore lack of its action may lead to an interruption of both. The *lil1* gene product, however, is involved in the last steps of the pathway, leading to the formation of castasterone and brassinolide.

Mutation in either of the genes should completely interrupt the brassinolide biosynthesis, and cause a deficiency in the active molecules. However as previously mentioned, their

phenotypes are slightly different. The interaction between *lil1-1* and *nana1-1* mutations was therefore investigated through genetic analysis.

Our results show that the mutant plants homozygous both for *lil1-1* and for *nana1-1* (double mutants), appear to have the same phenotype as *lil1-1* mutants. Double mutants and *lil1-1* mutants did not appear significantly different in shoot length, stomatal index and cell density. Analysis of F_2 progenies segregating for both *lil1-1* and *nana1-1* mutants revealed that *lil1-1* is epistatic to *nana1-1*. Indeed, *lil1-1 nana1-1* double mutants show a phenotype identical to *lil1-1* mutants. This observation was confirmed both in seedling height and in stomatal index analysis.

The product of *nana1*, which is the maize orthologue of Arabidopsis *det2*, is a 5a-reductase located further upstream in the BR pathway, which catalyses multiple steps in different branches of the pathway that converge at Castasterone (CS) precursors.

The observation that the phenotype alterations showed by *lil1-1* mutant appear more dramatic than *na1-1* mutant, and the fact that *lil1* appears epistatic to *na1*, suggest the existence in the maize BR pathway of an additional *det2*-independent branch leading to the production of CS precursors.

BR biosynthesis is a complex pathway and, although it has been the subject of several studies in recent years, some aspects are still to be clarified. A complete understanding of BR biosynthesis and action could be very important in crop genetic improvement. A final challenge would be an effective modulation of the endogenous brassinosteroids levels that will lead to improved plant resistance to different environmental stresses without impairing plant growth.

BIBLIOGRAPHY

Anuradha S., Rao S., 2001 Effect of brassinosteroids on salinity stress induced inhibition of seed germination and seedling growth of rice (Oryza sativa L.). Plant Growth Regul.: 151–153.

Argueso C. T., Ferreira F. J., Kieber J. J., 2009 Environmental perception avenues: The interaction of cytokinin and environmental response pathways. Plant, Cell Environ. 32: 1147–1160.

Bajguz A., Tretyn A., 2003 The chemical characteristic and distribution of brassinosteroids in plants. Phytochemistry 62: 1027–1046.

Bishop G. J., Nomura T., Yokota T., Harrison K., Noguchi T., et al., 1999 The tomato DWARF enzyme catalyses C-6 oxidation in brassinosteroid biosynthesis. Proc. Natl. Acad. Sci. 96: 1761–1766.

Choe S., Tanaka A., Noguchi T., Fujioka S., Takatsuto S., et al., 2000 Lesions in the sterol ??7 reductase gene of Arabidopsis cause dwarfism due to a block in brassinosteroid biosynthesis. Plant J. 21: 431–443.

Choi Y. H., Fujioka S., Harada A., Yokota T., Takatsuto S., et al., 1996 A brassinolide biosynthetic pathway via 6-deoxocastasterone. Phytochemistry 43: 593–596.

Clouse S. D., 2011 Brassinosteroid Signal Transduction: From Receptor Kinase Activation to Transcriptional Networks Regulating Plant Development. Plant Cell 23: 1219–1230.

Cosgrove D. J., Sovonick-Dunford S. a, 1989 Mechanism of gibberellin-dependent stem elongation in peas. Plant Physiol. 89: 184–91.

Dhaubhadel Chaudhary S., Dobinson K.F., Krishna P. S., 1999 Treatment with 24-epibrassinololide, a brassinostreroid, increases the basic thermotolerance of Brassica napus and tomato seedling. Plant Mol. Biol. 40: 333–342.

Divi U. K., Krishna P., 2009 Brassinosteroid: a biotechnological target for enhancing crop yield and stress tolerance. N. Biotechnol. 26: 131–136.

Dolfini S., Landoni M., Consonni G., Rascio N., Vecchia F. D., et al., 1999 The maize lilliputian mutation is responsible for disrupted morphogenesis and minute stature. Plant J. 17: 11–17.

Farooq M., Wahid A., Lee D. J., Cheema S. A., Aziz T., 2010 Comparative time course action of the foliar applied glycinebetaine, salicylic acid, nitrous oxide, brassinosteroids and spermine in improving drought resistance of rice. J. Agron. Crop Sci. 196: 336–345.

Fujioka S., Yokota T., 2003 BIOSYNTHESIS AND METABOLISM OF BRASSINOSTEROIDS. Annu. Rev. Plant Biol. 54: 137–164.

Grove M. D., Spencer G. F., Rohwedder W. K., Mandava N., Worley J. F., et al., 1979 Brassinolide, a plant growth-promoting steroid isolated from Brassica napus pollen. Nature 281: 216–217.

Hartwig T., Chuck G. S., Fujioka S., Klempien a., Weizbauer R., et al., 2011 Brassinosteroid control of sex determination in maize. Proc. Natl. Acad. Sci. 108: 19814–19819.

Hedden P., Kamiya Y., 1997 GIBBERELLIN BIOSYNTHESIS: Enzymes, Genes and Their Regulation. Annu. Rev. Plant Physiol. Plant Mol. Biol. 48: 431–460.

Hong Z., Ueguchi-Tanaka M., Shimizu-Sato S., Inukai Y., Fujioka S., et al., 2002 Loss-of-function of a rice brassinosteroid biosynthetic enzyme, C-6 oxidase, prevents the organized arrangement and polar elongation of cells in the leaves and stem. Plant J. 32: 495–508.

Iino M., Yu R. S., Carr D. J., 1980 Improved Procedure for the Estimation of Nanogram Quantities of Indole-3-acetic Acid in Plant Extracts using the Indolo-a- pyrone Fluorescence Method. Plant Physiol. 66: 1099–1105.

Iino M., Carr D. J., 1982 Sources of Free IAA in the Mesocotyl of Etiolated Maize Seedlings. Plant Physiol. 69: 1109–12.

Kir G., Ye H., Nelissen H., Neelakandan A. K., Kusnandar A. S., et al., 2015 RNA Interference Knockdown of BRASSINOSTEROID INSENSITIVE1 in Maize Reveals Novel Functions for Brassinosteroid Signaling in Controlling Plant Architecture. Plant Physiol. 169: 826–39.

Krishna P., 2003 Brassinosteroid-Mediated Stress Responses. J. Plant Growth Regul. 22: 289–297.

Li J., Yang H., Peer W. A., Richter G., Blakeslee J. J., et al., 2005 Arabidopsis H+-PPase AVP1 Regulates Auxin Mediated Organ Development. Science (80-.). 310: 121–125.

Lolle S. J., Berlyn G. P., Engstrom E. M., Krolikowski K. A., Reiter W., et al., 1997 Developmental Regulation of Cell Interactions in the Arabidopsis fiddlehead-1 Mutant : A Role for the Epidermal Cell Wall and Cuticle. 321: 311–321.

Makarevitch I., Thompson A., Muehlbauer G. J., Springer N. M., 2012 Brd1 gene in maize encodes a brassinosteroid C-6 oxidase. PLoS One 7.

Messing S. A. J., Gabelli S. B., Echeverria I., Vogel J. T., Guan J. C., et al., 2010 Structural Insights into Maize Viviparous14, a Key Enzyme in the Biosynthesis of the Phytohormone Abscisic Acid. Plant Cell 22: 2970–2980.

Mitchell J. W., Mandava N. B., Worley J. F. P. J. R. and S. M. V., 1970 Brassins - a new family of plant hormones from Rape pollen. Nature 2251: 1065–1066.

Noguchi T., Fujioka S., Takatsuto S., Sakurai A., Yoshida S., et al., 1999 Arabidopsis det2 is defective in the conversion of (24R)-24-methylcholest-4-En-3-one to (24R)-24-methyl-5alpha-cholestan-3-one in brassinosteroid biosynthesis. Plant Physiol. 120: 833–839.

Nomura T., Nakayama M., Reid J. B., Takeuchi Y., Yokota T., 1997 Blockage of Brassinosteroid Biosynthesis and Sensitivity Causes Dwarfism in Garden Pea. Plant Physiol. 113: 31–37.

Nomura T., Kitasaka Y., Takatsuto S., Reid J., Fukami M., et al., 1999 Brassinosteroid/Sterol synthesis and plant growth as affected by lka and lkb mutations of Pea. Plant Physiol. 119: 1517–26.

Persico M., 2015 A forward genetic approach to study seed and seedling development in maize.

Pan X., Chen J., Yang Z., 2015 ScienceDirect Auxin regulation of cell polarity in plants. Curr. Opin. Plant Biol. 28: 144–153.

Salisbury E. ., 1928 On the causes and ecological significance of stomatal frequency, with special reference to the woodland flora. Philos. Trans. R. Soc. London 216: 1–65.

Santner A., Estelle M., 2009 Recent advances and emerging trends in plant hormone signalling. Nature 459: 1071–1078.

Schaller H., 2004 New aspects of sterol biosynthesis in growth and development of higher plants. Plant Physiol. Biochem. 42: 465–476.

Schultz L., Kerckhoffs L. H. J., Klahre U., Yokota T., Reid J. B., 2001 Molecular characterization of the brassinosteroid-deficient lkb mutant in pea. Plant Mol. Biol. 47: 491–498.

Shi Y. Y., Zhu S. S., Mao X. X., Feng J. J., Qin Y., et al., 2006 Transcriptome Profiling , Molecular Biological , and Physiological Studies Reveal a Major Role for Ethylene in Cotton Fiber Cell Elongation. Plant Cell 18: 651–664.

Vardhini B. V., Rao S. S. R., 2003 Amelioration of osmotic stress by brassinosteroids on seed germination and seedling growth of three varieties of sorghum. Plant Growth Regul. 41: 25–31.

Wahid A., Ghazanfar A., 2006 Possible involvement of some secondary metabolites in salt tolerance of sugarcane. J. Plant Physiol. 163: 723–730.

Wahid A., 2007 Physiological implications of metabolite biosynthesis for net assimilation and heat-stress tolerance of sugarcane (Saccharum officinarum) sprouts. J. Plant Res. 120: 219–228.

Wang L., Wang Z., Xu Y., Joo S. H., Kim S. K., et al., 2009 OsGSR1 is involved in crosstalk between gibberellins and brassinosteroids in rice. Plant J. 57: 498–510.

Yamamuro C., 2000 Loss of Function of a Rice brassinosteroid insensitive1 Homolog Prevents Internode Elongation and Bending of the Lamina Joint. Plant Cell Online 12: 1591–1606.

Yokota T., Sato T., Takeuchi Y., Nomura T., Uno K., et al., 2001 Roots and shoots of tomato produce 6-deoxo-28-norcathasterone, 6-deoxo-28-nortyphasterol and 6-deoxo-28-norcastasterone, possible precursors of 28-norcastasterone. Phytochemistry 58: 233–238.